SUITABILITY OF NUMERICAL MODELLING APPROACH OF AN INTEGRAL BRIDGE FOR STRENGTHENING OF RC PILE FOUNDATION USING SSI

A Thesis Submitted
in Partial Fulfilment of Requirements
for the Degree of
DOCTOR OF PHILOSOPHY

by

Sreya Dhar

DEPARTMENT OF CIVIL ENGINEERING
INDIAN INSTITUTE OF TECHNOLOGY GUWAHATI
GUWAHATI-781039, INDIA
June 2018

To my grandparents and loving sister..

CERTIFICATE

This is to certify that the work contained in the thesis entitled "***Suitability of Numerical Modelling Approach of an Integral Bridge for Strengthening of RC Pile Foundation Using SSI***" by **Ms. Sreya Dhar** has been carried out under my supervision and this work has not been submitted elsewhere for a degree.

Kaustubh Dasgupta

(Dr. Kaustubh Dasgupta)
Thesis Supervisor
Department of Civil Engineering,
Indian Institute of Technology Guwahati

Dated: 4 June 2018
Place: Guwahati

Abstract

Integral Abutment Bridges (IABs) have become widely popular in the recent years due to the absence of bearings at the junction of bridge deck and bridge abutment. That leads to a reduction in the overall maintenance cost of the bridge. However, the monolithic action of deck-abutment junction changes the behaviour of the overall bridge under temperature loading and earthquake shaking. In an integral abutment bridge, bearings may be absent at the locations of the piers also. Then, the bridge is known as a fully integral bridge. In such a bridge, the behaviour of the bridge tends to follow frame-type action with all the junctions of the deck and the vertical members acting as monolithic units. Although, past studies have been carried out on behaviour under temperature variation for both the types of bridges, detailed investigations of seismic behaviour of the bridge with different modelling approaches of soil-structure interaction, have not been carried out. Also, the pile foundations below bridges have been observed to undergo failure during past earthquakes and this necessitates further investigations. All these provide the motivation for the current study.

In the present study, a multi-span RC integral bridge on RC pile foundation is first modelled using an open source program, *OpenSees*, with stratified foundation soil. For modelling Soil-Structure Interaction (SSI), two approaches are implemented separately, namely (a) soil domain approach in which the soil is modelled as a continuum, and (b) spring-dashpot approach in which the lateral strength and stiffness of the soil are modelled considering Beam on Dynamic Winkler Foundation concept. Based on the site details (the real bridge site is located in California, USA, from which the bridge characteristics have been taken), seven ground motions are selected from a strong ground motion database by matching of mean displacement spectrum for all the ground motions with a target spectrum. Under the selected site-specific ground motions,

nonlinear time history analyses are carried out for different models with changes in boundary conditions at the bottom of the piers, presence or absence of backfill soil and the two different SSI modelling approaches. The variations in the deformation at bridge deck level and section level response of the piers are observed. As compared to the soil domain approach, the spring-dashpot approach is observed to provide conservative estimates of forces and moments, and possibly can be recommended for implementation in seismic design.

For an integral bridge, the overall length of the bridge tends to play a major role in the response under temperature loading. The same parameter is expected to significantly influence the overall bridge response during earthquake shaking. In the second part of the study, the overall length of the same integral bridge is changed and nonlinear time history analysis is carried out under site specific ground motions using the spring-dashpot model for different types of foundation soil. With increase in overall length, inelasticity is observed in the response of pier and pile foundation for certain soils. Consequently, one of the retrofitting methods for pile foundation, i.e., through installation of new piles encased in jet grout, is implemented on the pile groups below abutments and the piers in two separate stages. The numerical modelling of the encasement method is carried out using suitable spring-dashpots to model the soil and the grout around the new piles. For certain soils, the response of the bridge gets significantly improved through reduction of nonlinear behaviour of the components, after applying the retrofitting method.

In a summary, the present thesis tends to provide insight into the seismic behaviour of an integral bridge with RC pile foundation from the aspects of different numerical modelling approaches, influence of overall length and improvement in the response of pile foundation through encasement method of retrofitting.

Acknowledgement

Part of this research was carried out while the author of thesis (S. Dhar) was visiting Politecnico di Milano (PoliMi) Italy, under INTERWEAVE Project, Erasmus Mundus Program during 2014-2017. The author would like to thank Ministry of Human Resources (MHRD) for the scholarship during PhD work.

I express my sincere gratitude to my advisors *Prof. Kaustubh Dasgupta* and *Prof. Roberto Paolucci* for their enthusiastic guidance, continued support and encouragement throughout the course of the dissertation. I want to thank *Prof. Lorenza Petrini* for her immense help during my thesis work. Her motivations and many fruitful discussions are greatly appreciated. I have learnt many things from my mentor *Dr. Ali Günay Özcebe*, post-doctoral scholar in PoliMi, in academic and non-academic aspects, which I will try to reflect in my future career. I want to thank my doctoral committee members, *Prof. Sudip Talukdar*, *Prof. Hemant B. Kaushik* and *Prof. Pankaj Biswas* for their fruitful comments on my thesis.

I am deeply indebted to my *grandparents* for their love and affection from my childhood. I want to thank my motherly sister who have guided me in thick and thin. I dedicate my thesis to all of them . . .

My deepest thanks go to my parents, for their warm support and unparalleled affection. I want to thank my husband *Swarnava* and my parents in law for their immense support. My personal gratitude and respects to *Prof. Hemant B. Kaushik, Dr. Snehal* and *Benazir* for their warm support and care.

I thank *Dr. Geetimukta* for her help during my PhD. I also thank *Sophia, Dr. Isha, Anjaly, Thianswemong* for their warm friendship.

Table of Contents

List of Figures

List of Tables

List of Symbols

A : A factor account for cyclic loading in sand

A_p : Area of pile

As : Area of steel

$A_{s,\,pro}$: Area of steel provide

A_{sw} : Area of the stirrups or ties in one direction of confinement

A_w : Equivalent are of pile row

C_1, C_2, C_3 : Coefficient as function of ϕ

CL : Very stiff clay

D : Pile diameter

D_b : Diameter of longitudinal bar

E_1, E_2, E_3 : Stiffness of pile 1st, 2nd, and 3rd pile rows

E_{eq} : Equivalent elastic modulus

H : Depth below soil surface

J : Dimensionless empirical constant

M_w : Moment of magnitude

N_{ed} : Design value of applied axial force

OL/SM : Loose sandy silt

R : Fault to site distance

S_a : Spectral acceleration

S_L : Spacing of hoops or spiral

SP : Very dense sand

SP/SM : Medium dense silty sand

X : Depth below soil surface

X_R : Depth below soil surface to bottom of reduced resistance zone

a : The distance of CG of the concentrated load from nearest support

b_1 : Breadth of concentrated area of load

b_{ef} : Effective width of the slab perpendicular to span

b_w : Width Of the slab

c : Cohesion

epsc0 : Strain at compressive strength of concrete

fpcU : Crushing strength of concrete

epsU : Strain at crushing strength

fpc : Compressive strength of concrete

f_{yd} :Design yield strength of reinforcement

l_0: Effective span of main girder

p : Perimeter of pile

p_u : Ultimate resistance

α : A constant having the following value depending on width of slab and l_0

γ : Unit weight of soil

ε_c: Strain at which half of maximum stress is occurring

δ : Soil-wall internal friction

η_k : Normalised axial force

ρ_ω : Volumetric ratio of transverse reinforcement

ϕ : Angle of internal friction

$\omega_{\omega d}$: Required confining reinforcement ratio

$\omega_{\omega d, pro}$: Provided confining reinforcement ratio

Chapter 1

Introduction

1.1 Introduction

In conventional bridges, different types of bearings or supports are provided at the locations of piers and abutments to accommodate movement arising from temperature effects, creep and shrinkage of the bridge superstructure. In recent years, many bridges are being constructed with monolithic action of the abutment and the superstructure. Those bridges are known as integral abutment bridges (Fig. 1.1). The monolithic construction of abutment and superstructure eliminates the requirement of bearings and leads to reduction in the maintenance cost. However, the piers may support the superstructure by means of bearings or get integrally connected with the deck (Burke, 2009). In an Integral Abutment Bridge (IAB), the abutment may rest on shallow footing or pile foundation depending on the type of soil.

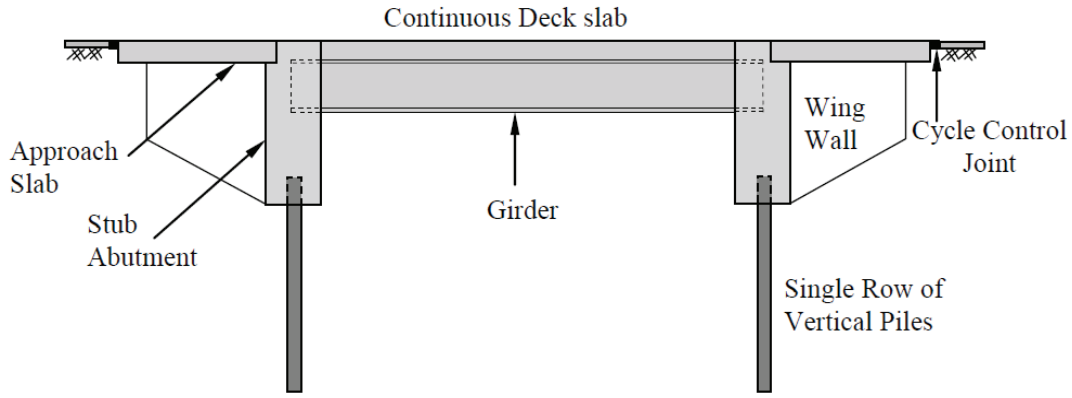

Fig. 1.1 A typical single span jointless bridge

Generally, the superstructure of an IAB is constructed of structural steel or reinforced concrete (cast-in-situ) or prestressed concrete. Prestressed concrete and steel superstructure integral abutments (Conboy and Stoothoff, 2005; Weakley, 2005; Maberry

and Camp, 2005; Lampe and Azizinamini, 2000; Arockiasamy *et al*., 2004) have been constructed extensively in the past, however the design and construction details have varied from place to place (Maruri and Petro, 2005; White *et al.*, 2010). Several modifications have been made in RC integral abutment and foundation design (Yannotti *et al*., 2005). For integral abutment bridges, three types of construction are possible, namely (a) Full Integral Abutment (FIA) (Fig. 1.2), (b) Semi Integral Abutment (SIA) (Fig. 1.3) and (c) deck extension (Weakley, 2005; Perkun and Michael, 2005; Maberry and Camp, 2005) (Fig. 1.4). In SIA bridges, there may be partial force and moment transfer but in FIA bridges, full transfer of moment and forces occurs from deck to abutment. A detailed procedure to achieve complete rigid deck girder-abutment connection has been developed in Itani and Pekcan (2011). In an IAB, the abutments and the foundation need to be designed to accommodate both temperature effects and the effect of earthquake shaking. Thus, Soil-Structure Interaction (SSI) plays a major role in the overall behaviour of the IAB for the different combinations of loadings.

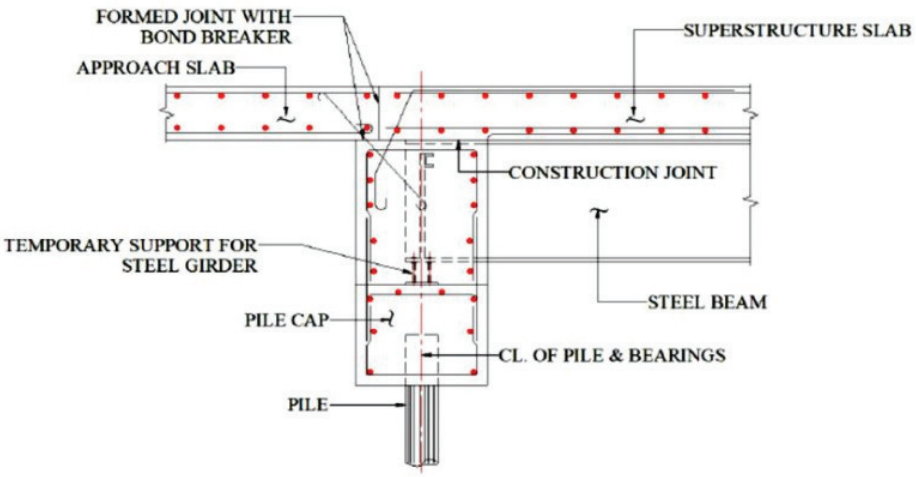

Fig. 1.2 Fully integral abutment bridge (Yannotii *et al*., 2005)

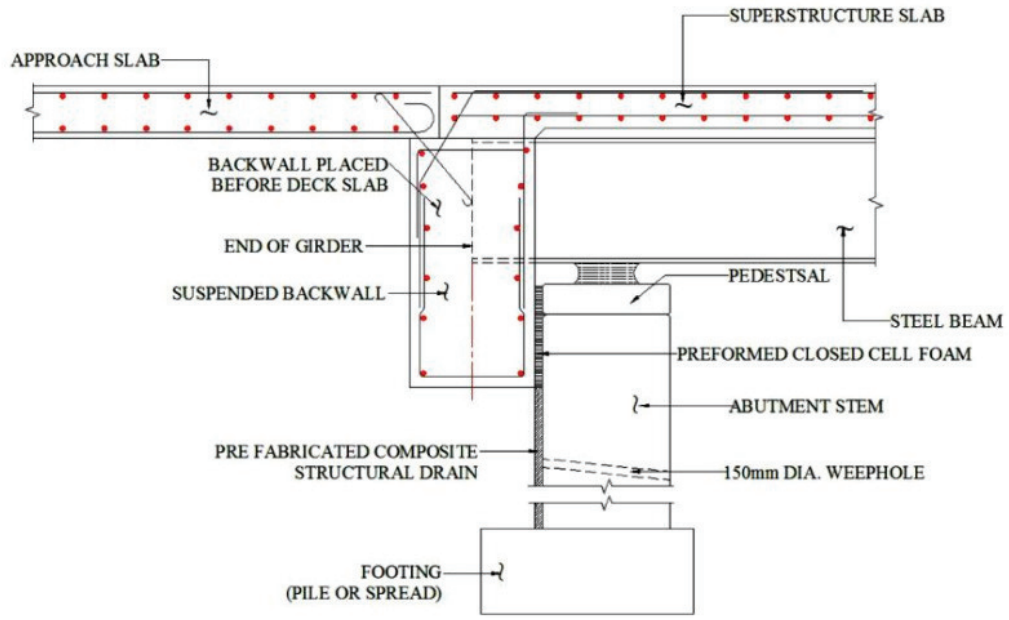

Fig. 1.3 Semi-integral abutment bridge (Yannotti *et al*., 2005)

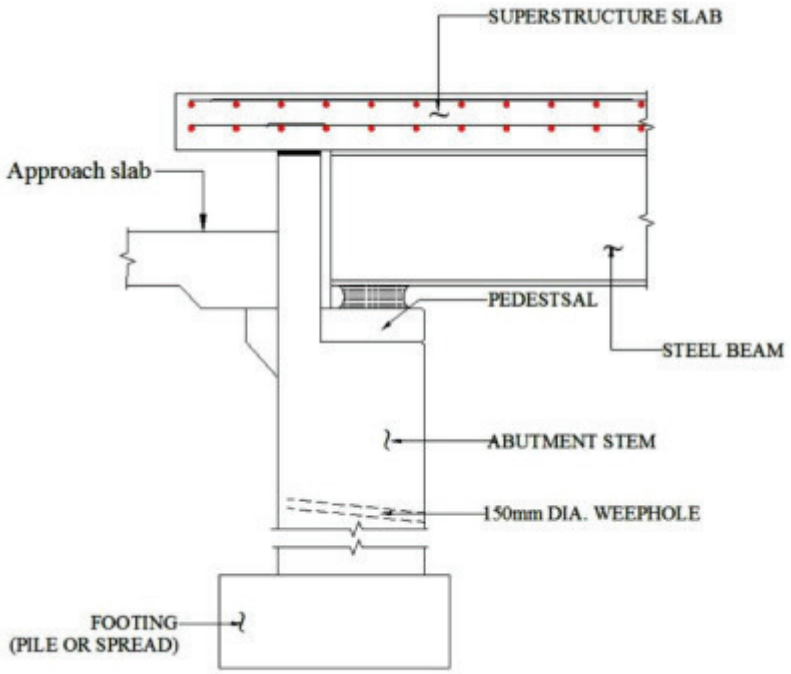

Fig. 1.4 Deck extension abutment (Yannotti *et al*., 2005)

1.2 Seismic Soil Structure Interaction

When the seismic wave propagation is not influenced by the presence of any structure, foundation or any other hindrance, the resulting ground motion is known as free field

motion (Kramer, 1996). If a structure is founded on solid rock then due to the extremely high stiffness of the rock, the rock motion resembles the free field motion very closely. Structures founded on rock are considered as fixed-base structure as the possible translations and rotations at the base of the structure are completely restrained during earthquake shaking. On the other hand, the same structure may respond differently when supported on soft foundation soil. Under free field motions, the foundation will not be able to deform, thus, the motion at the base of the structure tends to deviate from the free field motion. Then, the dynamic response of the structure itself will induce deformation of the supporting soil. This process, in which the dynamic response of the soil influences the possible motion of the structure and then, the dynamic response of the structure influences the possible motion of the soil, is referred to as Soil Structure Interaction (SSI). Seismic waves propagate through the soil strata and finally reach the foundation of the structure, causing it to move, as a result of which the superstructure also starts to vibrate (JSCE, 1985). The dynamic characteristics of ground motion at the base of structure depend on the modification of bedrock motion while propagating through the soil strata (Dutta, 2010). Thus, it is important to know how the seismic waves propagate through the soil medium to understand the modification of ground motion due to variation in the soil properties. Also, the vibration characteristics of the soil medium are required to carry out numerical modelling of wave propagation through the semi-infinite soil medium.

1.3 Major Concern and the Motivation of the Study

In an integral bridge on pile foundation, the abutments, bridge deck and the piers act like a combined single unit due to the monolithic nature of construction. During earthquake shaking, the seismic response of the integral bridge-foundation system depends on the abutment-backfill interaction and soil-pile interaction. Thus, soil structure interaction

(SSI) needs to be considered while investigating the seismic behaviour of an integral bridge on pile foundation. Although the SSI effects have been considered for analysing the behaviour of an integral bridge under temperature loading in past research (Efretuei, 2013; Laman and Kim, 2010; Far *et al*., 2015), the influence of the modelling approaches incorporating SSI on the seismic behaviour of the integral bridge has not been studied. A few parametric studies have also been carried out in the past (Erhan and Dicleli, 2017; Kong *et al*., 2016; Huang *et al*., 2008; Civjan *et al*., 2007) involving the effects of different structural and geotechnical parameters on the seismic response of an integral bridge. However, the seismic response of integral bridge with RC pile foundation needs to be investigated in detail to prescribe seismic design guidelines for such bridges.

Also, in past earthquakes, pile foundations in several bridges have been observed to undergo significant damages (San Fernando, 1971; Tangshan, China, 1976; Hyogoken Nanbu, Kobe, 1995; Izimit, Turkey, 1999; Jiji, Taiwan, 1999; Athens, Greece, 1999). In an integral bridge with pile foundation, the seismic demand on the piles below the abutments and the piers can significantly increase with the overall length of the bridge. It can also vary with the different types of underlying soil. Detailed investigations and identification of such possible failures of abutment piles and pier piles are also required as part of assessment of seismic vulnerability of the bridge. Subsequently, appropriate retrofitting measures of pile foundations need to be studied for possible remedy. All these provide the motivation for the present study.

1.4 Objectives of the Study

The objectives of the thesis are as follows:

- The influence of different modelling approaches on the seismic response of an integral bridge on RC pile foundation, considering soil-structure interaction and site-specific ground motions, is to be investigated.
- The influence of overall length of an integral bridge with RC pile foundation on its seismic response will be studied for different types of foundation soils.
- The effectiveness of one of the retrofitting methods of pile foundation below the abutments and the piers, by using new piles encased in jet grout, is to be studied through numerical modelling.

1.5 Outline of the Thesis

The organization of the contents of the thesis is discussed below:

1. Chapter 1: In this chapter, an overview of integral abutment bridge and the background for the present study, are discussed. Finally, the objectives of the present study and the organization of the thesis are presented.

2. Chapter 2: Past research work and technical guidelines on IABs are discussed in this chapter. Based on the past studies, the gap areas are identified and the scope of the work is mentioned.

3. Chapter 3: In this chapter, the modelling of the integral bridge-foundation-backfill system using continuum soil domain approach in *OpenSees* program, is discussed in detail. The corresponding material properties are also elaborated. Further, the details of the alternative spring-dashpot modelling, using Beam on Dynamic Winkler Foundation (BDWF) approach, are also discussed.

4. Chapter 4: In this chapter, a two-dimensional site response analysis is carried out on a free field soil column using *OpenSees*, STRATA and DEEPSOIL programs and the

results are compared. For further detailed studies, site specific ground motions are selected using REXEL-DISP tool for a target site specific displacement spectrum.

5. Chapter 5: In this chapter, the behaviour of superstructure and substructure of an integral bridge is determined using different modelling approaches (with and without the SSI effects), and the comparative results are discussed in detail.

6. Chapter 6: As the overall length of an integral bridge is expected to increase the forces and the moments in the bridge components, the influence of overall length on the seismic behaviour of an integral bridge under site specific ground motions is studied in this chapter.

7. Chapter 7: In this chapter, the retrofitting method for abutment and pier pile foundations, using new piles encased in jet grout, is first discussed. The retrofitting technique is implemented on the integral bridge with maximum overall length, as discussed in Chapter 6, through numerical modelling in the SAP2000 program. Further, the effectiveness of the retrofitting method is discussed considering the response of piers and the piles for different types of foundation soils.
8. Chapter 8: In this chapter, conclusions from the present study are drawn and the possible future scope of work is mentioned at the end.

★★★

भारतीय प्रौद्योगिकी संस्थान गुवाहाटी
Indian Institute of Technology Guwahati

Chapter 2

Literature Review

2.1 Introduction

In an Integral Abutment Bridge (IAB), the superstructure and the abutment are constructed monolithically at their junction without the presence of any bearing or expansion joint. This leads to a significant reduction in the maintenance cost of the bridge. However, integral connection at the deck-abutment junction causes a significant change in the bridge behaviour under thermal loading and earthquake shaking as the superstructure (along with bridge deck and girders), abutment with foundation, wing wall and the approach slab may act like a single unit. Different countries and the respective Highway Agencies have adopted different guidelines for design and construction of IABs. In the present chapter, the past research involving studies on soil-structure interaction and design guidelines on integral abutment bridges are reviewed.

The major parameters of an IAB required for its design, namely the overall length, skewness and loadings on the bridge are discussed first. Next, the behaviour of the abutment including abutment-backfill interaction, and the possible numerical modelling techniques are reviewed. Among the different types of foundation, only the pile foundation is considered in the present study. So, past studies on soil-pile interaction and its modelling are discussed in detail. Although, most of the bridge design guidelines in different countries do not include provisions on soil-structure interactions, the available prescriptions are reviewed. Finally, a few retrofitting methods for pile foundation are discussed along with identification of gap areas and scope of the present work.

2.2 Characteristics of IAB

2.2.1 Length

The length of an IAB depends on pile capacity, soil type and abutment displacement due to temperature variation and seismic excitation (Greimann *et al*., 1984). According to temperature variation, construction methods and geological conditions, the limiting length of IAB varies across different regions. In US, most of the states have relatively low maximum span lengths for steel beam within 60 m and concrete beams upto 45 m (Baptiste *et al*., 2011). Using pile supported stub type abutment, prestressed girder bridges upto 244 m length and steel bridges upto 122 m length are routinely constructed (Dicleli and Albhaisi, 2003). The maximum recommended length of bridges in cold climates is 190 m with concrete girders and 100 m with steel girders. In moderate climates, the limits are increased to 240 m and160 m with concrete and steel girders respectively. Barr *et al.* (2013) have observed that an increasing in span by a factor of two can lead to an increase of bending moment by 60% for weak axis bending of the bridge abutment (Appendix A). Although, long span IABs may have total span to be more than 300 m (e.g., Happy Hollow Creek Bridge with a length of 358 m (Comisu, 2005)), currently, researches are continuing in the direction of increasing the length of IABs considering optimisation approach for pile shape design (Lan, 2012). As imposed seismic forces on an integral bridge tend to increase with its overall length, proper measures should be taken before constructing long span IBs depending on proper geological investigation and site specific characteristics.

2.2.2 Skew angle

Skewness and curvature in IABs play a crucial role to elevate the time dependent load on backfill soil. The maximum permitted skew angle varies according to the guidelines of different countries, and is prescribed as (a) 30° for UK, Finland and Australia (Gibbens, 2011; White, 2007) and (b) 30°-60° in different states of USA and European countries (Greimann *et al*., 1983; Puzey, 2012; Barr *et al*., 2013; Quinn and Civjan, 2016). In

Canada, detailed investigations are required while designing IABs with skew angle more than 20°. However, countries like Germany do not permit construction of skewed IABs due to possible increase of backfill earth pressure for skewed bridges (Civjan *et al*., 2013). The same practice is followed in Japan due to possibility of frequent earthquake shaking.

2.2.3 Loadings on IAB

In addition to the primary load effects (dead load and live load), integral bridges are subjected to secondary load effects due to (a) creep and shrinkage, (b) thermal gradients, (c) Abutment-Backfill Interaction (ABI) and (d) Soil-Pile Interaction (SPI) (Arockiasamy *et al*., 2004). Although, creep and shrinkage effects have been ignored by many designers (Maruri and Petro, 2005), those effects can contribute significantly to the overall loading on an IAB.

For pretensioned or posttensioned concrete bridges, creep, shrinkage and elastic shortening account for changes in the internal behaviour (Liu *et al*., 2005; Bazant and Panula 1980). Shrinkage of the concrete deck slab tends to impose compressive stresses in the top flange of the girder and tensile stresses in the bottom flange (Wetmore and Peterson, 2005). Additional shear force and bending moment arise in the superstructure due to shrinkage of deck on the hardened superstructure girder (Arockiasamy and Sivakumar, 2005). Most of creep and shrinkage deformations in the precast girders get completed by the time the girders are made continuous at the time of deck slab casting. Measurements indicate a significant shortening of the deck associated with creep and shrinkage of the prestressed beams (Barker and Carder, 2001). But shortening tends to get reduced after a few years of construction (Lawver *et al*., 2000); thus, it is not considered to have a significant effect. Differential deck slab and girder shrinkage, inherently shortens the superstructure and directly affects the integral abutment system.

Creep coefficients of high performance concrete tend to be less as compared to the traditional concrete mixes (Knickerbocke *et al*., 2005; Roller *et al*., 1995).

Changes in temperature may cause significant changes in the length of bridge deck girders. Unlike the conventional bridges, an IB does not have any expansion joint or bearing between superstructure and abutment. Bridge displacement is affected by both seasonal and diurnal temperature changes. Extreme temperature changes during summer days and winter nights control the extreme displacements of an IAB (Shah *et al*., 2008). Based on experimental and analytical data (BA 42/96, 2003; England *et al*., 2000), a limit of seasonal movement of ±20mm for short span IABs has been prescribed for temperature induced pressure on different types of integral abutments. Far *et al*., (2015) have prescribed that during negative temperature changes, seismic force should be combined with temperature load as contraction of IABs is more critical and it is unsafe for the bridges, particularly located in cold earthquake prone regions.

The response due to temperature load are governed by many factors, such as type of abutment backfill, season of backfill construction (Efretuei, 2013), abutment displacements including translations and rotations, the type of pile and its orientation. The effective temperature which governs the overall longitudinal movement of the bridge depends on shade temperature, solar radiation, wind speed, material properties, surface characteristics and section geometry. In several past studies, two major parameters, namely (a) maximum and (b) minimum shade temperatures have been correlated with effective bridge temperature (Volz, 2005; Emerson, 1976; BSI, 1978; Imbsen *et al*., 1985; AASHTO, 1989; Girton*et al*., 1991). It was postulated that the thermal expansion of a bridge deck could be accommodated to a certain extent by cambering of the deck rather than causing the deck to undergo hogging action (Darley and Alderman, 1995). Laman

and Kim (2010) developed temperature gradient based on axial load and bending strains from AASHTO gradient profile.

Studies have been carried out to determine the longitudinal thermal expansion of bridge deck, enforcing a longitudinal strain equilibrium and compatibility by collection of bridge deck segments (Volz, 2005; ACI, 1982; Girton *et al*., 1991). Although the distribution of temperature across the depth of girder is non-uniform, code provisions (IRC:6, 2017) prescribe expressions to estimate variation of temperature considering the same. Comparisons from various proposed thermal gradients with data accumulated from field test indicate that the temperature gradients in AASHTO (2012) and Volz (2005) provide reasonable upper bounds to solar radiation differentials (Abendroth *et al*., 2007). The bending moment arising from thermal expansion can significantly influence the axial capacity of the pile (Abendroth *et al*., 1989). During earthquake shaking, inertia forces generated at the deck level are transmitted to the backfill through integral abutments as well as to the soil through foundation. The deck-abutment joints are thus subjected to high stresses under seismic loading. Dicleli and Albhaisi (2003) suggested that ABI effect need not be considered for an IAB under negative thermal variation due to very small displacement. However, it is strongly dependent on the type or geometry of the abutment and do not hold good for extreme cold weather. Most of the countries in Europe and USA prefer to consider full passive pressure behind the abutment. The intensity of the backfill pressure behind the abutment depends on the magnitude of the bridge displacement towards the backfill soil and strain 'racheting' effect of backfill due to thermal variation.

2.3 Abutment Behaviour

The total earth pressure on the abutment during an earthquake is contributed by three components, namely (1) the static pressure due to gravity loads, (2) pressure induced due

to displacement of the wall towards the backfill from inertial loading and (3) temperature or earthquake induced lateral pressures due to ABI (Matthewson *et al*., 1980). For the analysis of integral abutment-foundation system, three different stiffness contributions are considered, namely (a) longitudinal or translational stiffness of abutment, (b) rotational stiffness of the abutment wall-backfill system and (c) stiffness of underlying foundation, as shown in Fig. 2.1. By lumping various components of stiffness at different locations in the structural model, the expressions for abutment stiffness have been derived (Petursson and Kerokoski, 2011). Active earth pressure tends to get mobilized at a very small lateral displacement when the abutment moves away from the backfill (Barker *et al*., 1991). For practical purposes, the variation of passive earth pressure coefficient with lateral displacement of integral abutment towards backfill can be assumed to be linear with effect of thermal variation (Dicleli, 2000).

2.3.1 Foundation type

Usually, fixed head steel H-piles are very commonly used as foundation for the abutments. Other than H-piles, different types of abutment foundation (Dunker and Liu, 2007) include steel pipe piles, precast concrete piles, timber piles (Kamel *et al*., 1996), sheet piles (England *et al*., 2000) and spread footing. X-shaped (cross shaped) piles are also used for abutment foundation below IABs in some countries of Europe (White *et al*., 2010). Spread footing should be avoided for multi-span IABs due to differential settlement. Use of batter piles for skewed IABs is not suggested in construction practice (Hassiotis *et al*., 2006).

When an IAB is supported by flexible or hinged pile heads, all lateral forces are taken by abutment backfill, bridge deck and to some extent by the flexible abutment piles. A pinned abutment-pile connection is observed to increase the overall displacement of the bridge significantly due to increased translation and rotation of the abutment (Dicleli

and Albhaisi, 2003) but it reduces the force transferred from superstructure to substructure significantly (Arsoy*et al*., 2002).Usage of carpet wrap at pile head of abutment piles is not sufficient to allow rotation at pile head (Abendroth *et al*., 2007).

The abutment supported by a single row of piles provides higher flexibility along longitudinal direction by weak axis bending (Burke, 1993; Arockiasamy *et al*., 2004; Wasserman and Walker, 1996; Nielsen and Schmeckpeper, 2001; Arsoy *et al*., 2002; Quinn and Civjan, 2016; BSDC, 2017), but that also tends to increase the stresses in piles leading to the possibility of plastic hinge formation near the pile head. This results in a desirable behaviour for the abutment-pile system with avoidance of concrete cracking even for skewed bridge and H-piles under thermal variation. Although H-piles are not suggested to be oriented to mobilize strong axis bending (Abendroth and Greimann, 2005), combination of strong axis bending and stiff foundation soil reduces stresses in piles and increase forces in concrete deck girders (Huang *et al*., 2008). Bahjat (2014) observed that abutment rotation or displacement may not depend on pile orientation in skewed IAB subjected to thermal variation. So, pile design and orientation should be based on specific bridge situation. The design and orientation of abutment piles should be based on specific bridge characteristics, temperature variation and the type of abutment backfill.

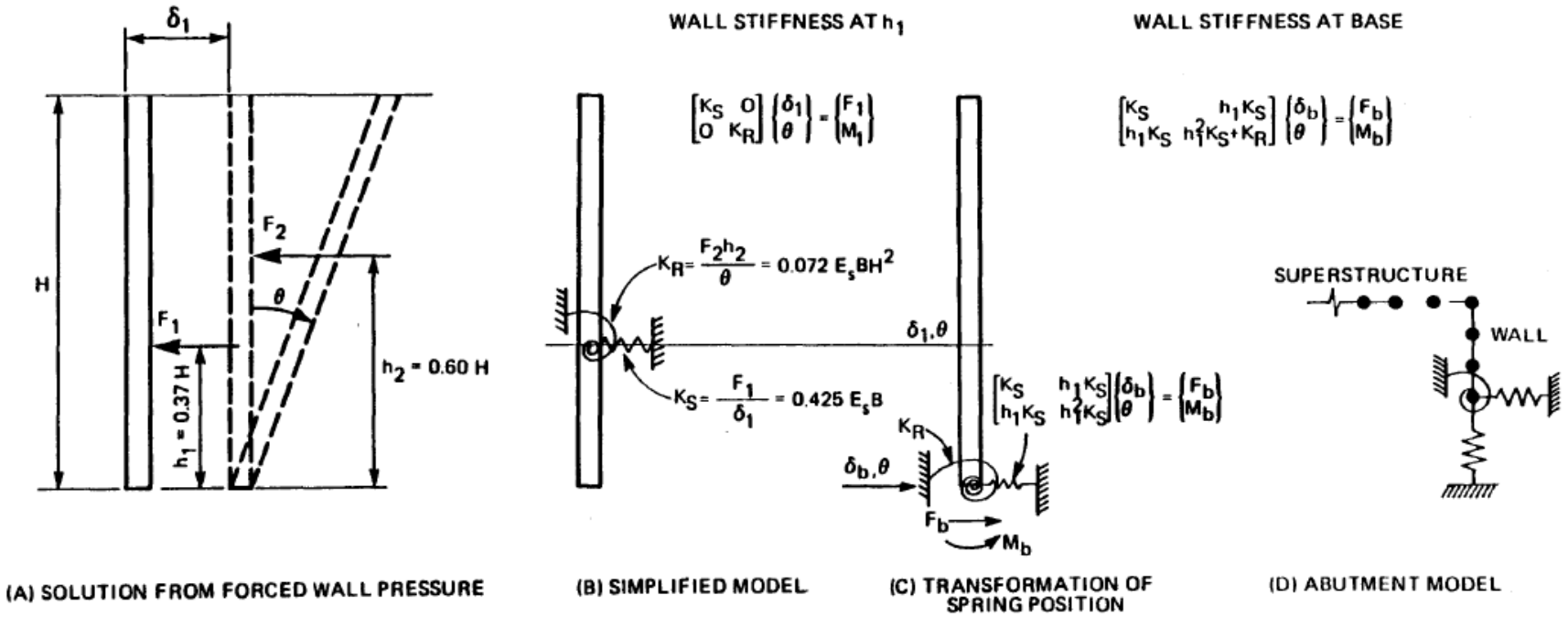

NOTE:

F_1 = FORCE AT HEIGHT h_1 ABOVE BASE OF WALL
F_2 = FORCE AT HEIGHT h_2 ABOVE BASE OF WALL
F_b = FORCE AT BASE OF WALL
M_1 = MOMENT AT HEIGHT h_1 ABOVE BASE OF WALL
M_b = MOMENT AT BASE OF WALL
B = WIDTH OF ABUTMENT WALL

Fig 2.1 Modelling of wall contribution in the stiffness of abutment (Lam and Martin, 1986).

2.3.2 Abutment backfill interaction

Abutment backfill soil should not be susceptible to get drained way during rainfall, be frozen in winters and free from roots, sods or perishable materials. Most US states prefer well compacted granular materials as backfill. The level of compaction behind the abutment affects the overall response of the IAB. Earthquake-induced lateral loading can mobilize passive soil pressure resistance through sliding or horizontal displacement of abutment towards backfill. For walls of low heights (upto 1.5 m) it is expected that the inertial effect under earthquake shaking should be small, thus the passive resistance is computed using static pressure distribution (SCDOT, 2010). The Mononobe Okabe (MO) method of determining seismic passive pressure coefficients for abutments is not recommended due to its various limitations. Considering wall friction and soil surface failure, seismic passive earth pressure coefficients have been suggested in past studies (Shamsabadi, 2006; Shamsabadi *et al*., 2007; Anderson *et al*., 2008). When superstructure inertia forces are transmitted into the backfill through abutment, adequate passive resistance must be available to avoid translation and rotation of the abutment. It is recommended that abutments should be designed to restrict lateral displacements upto approximately 91mm in order to avoid severe failure during strong earthquake shaking (AASHTO, 2002). Damping arising from ABI is significant in several experimental studies for relatively short IABs (upto 60 m length) (Douglas and Reid, 1984).

The variation of the backfill pressure as a function of the abutment displacement towards the backfill can be calculated from the studies carried out by Claugh and Duncan (1991), and Petursson and Kerokoski (2011). John and Faraji (1998) compared the design curves given in Canadian Foundation Engineering Manual (CFEM) (2006) and NCHRP (1991) with experimental results for translation and rotation of the abutment wall. For dense soil, design curves given in CFEM are recommended for ABI while for loose and

medium soils, the curves given in NCHRP are suitable. The equations to calculate the coefficient of passive earth pressure which suit the NCHRP design curves has been given by Bonczar *et al*. (2005). Acceptable comparisons are achieved from design curves for dense and medium soils given in CFEM and NCHRP with the suggested expressions from past researchers for modelling of integral abutment (Kumar, 2008). Comparison of different design curves is given in Fig. 2.2. Caltrans (2004) has recommended the estimation of seismic passive soil resistance behind bridge abutments based on full scale experimental results. An approximate quasi-linear relationship between seismic passive earth pressure and wall movement has also been established (Arsoy*et al*., 1999; Dicleli and Albhaisi, 2004).

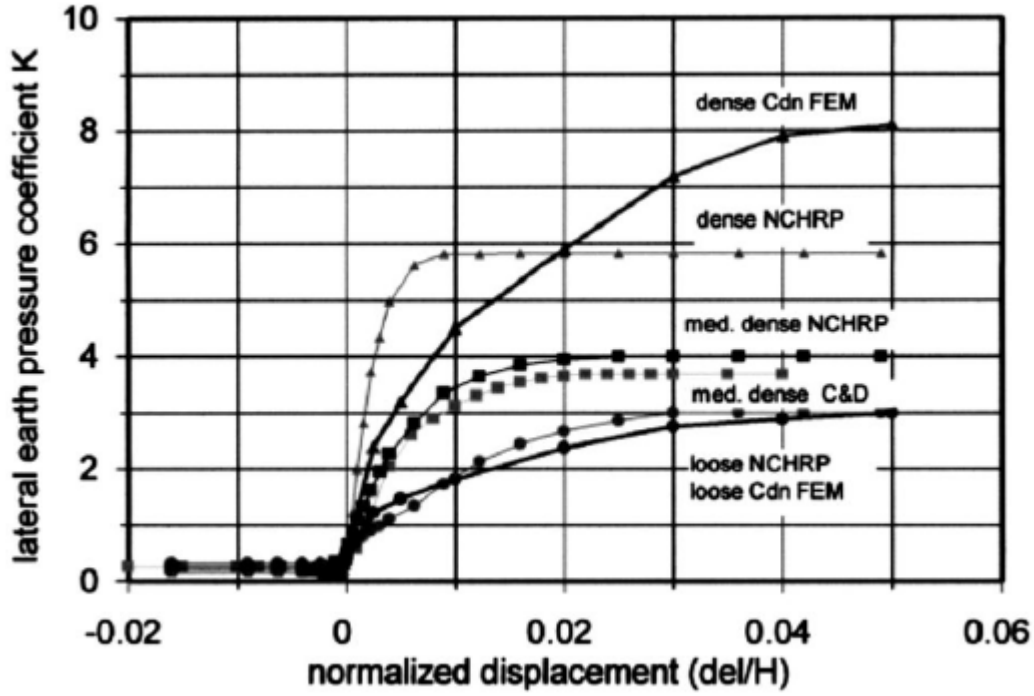

Fig. 2.2 Comparison of design curves given in different manual (Faraji *et al*., 1998)

'Log-spiral' Hyperbolic Load Deflection (HLD) curves (Fig.2.3) for seismic passive pressure have been proposed to represent the nonlinear ABI for monotonic

pushover analysis (Shamsabadi *et al*., 2007; Duncan and Mokwa, 2001; API, 2000). In the figure, F_{ult} is the maximum abutment force (kips) for the entire wall defined as

$$F_{ult} = f_{ult} \times b_{wall} \tag{2.1}$$

The maximum abutment force per unit width of wall (kips per foot of wall width) is computed as,

$$f_{ult} = p_{wall} \times h_{wall}\,, \tag{2.2}$$

where, f_{ult} is mobilized at a maximum displacement y_{max} (in inches), b_{wall} is the width of abutment wall (in feet), p_{wall} is the maximum uniform wall pressure (in ksf) developed at y_{max}, and h_{wall} is the height of abutment wall (in feet).

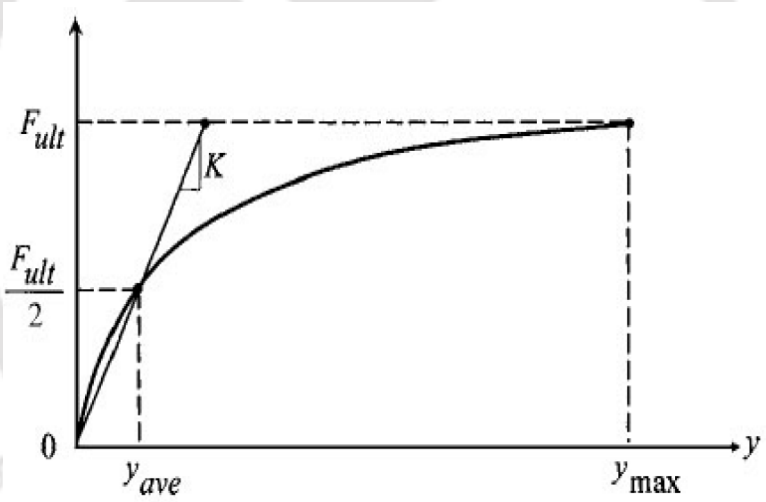

Fig. 2.3 Hyperbolic force-displacement formulation for abutment-backfill interaction (Shamsabadi *et al*., 2007).

Later on, from extended HFD curves (Shamsabadi *et al*., 2010), generalised HFD curves are obtained for passive backfill resistance (Khalili-Tehrani *et al*., 2016). A direct displacement based design is introduced to evaluate the stiffness and damping properties of deck-abutments-backfill system under dynamic loading by Mitoulis *et al*., (2015). Based on experimental and analytical data BA 42/96 (2003) provides different equations

to calculate earth pressure on different types of integral abutments. The framed abutment supports the vertical loads from the bridge and acts as a retaining wall for embankment earth pressure. The magnitude of the passive pressure acting on the wall is significant. The pressure coefficient K^* for that abutment shown in Fig. 2.4, where K_o is earth pressure coefficient at rest and H is the height of the abutment. The distribution of passive and active earth pressures as per Claugh and Duncan (1991) are shown in Fig. 2.5.

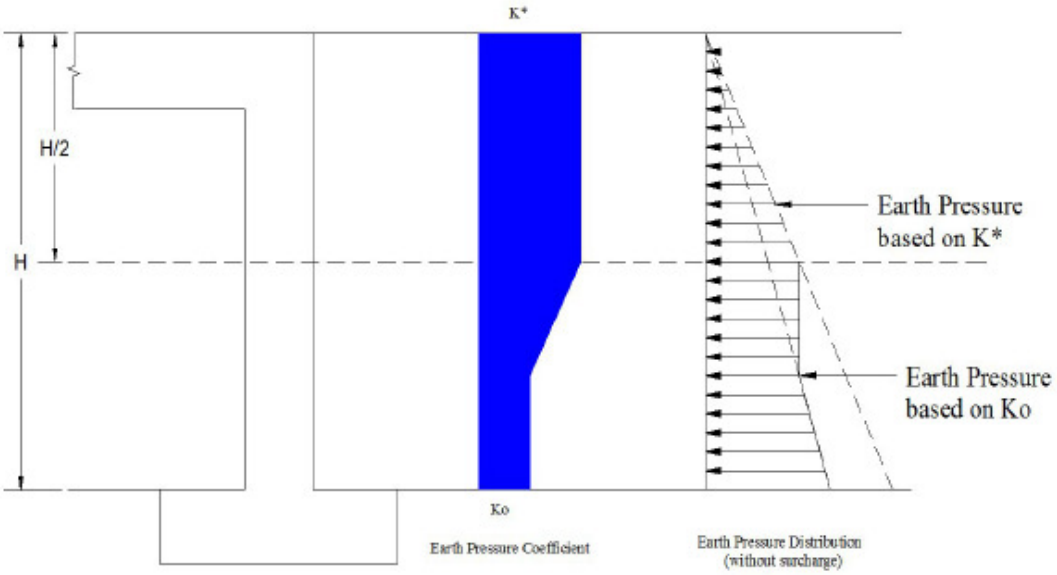

Fig. 2.4 Earth pressure distributions on framed abutments (BA 42/96, 2003)

Researches have produced relatively simple and cost-effective design solutions for reduction of irreversible movements of IAB and strain ratcheting of backfill under thermal loading (Hassiotis *et al*., 2005). Additive lateral earth pressures on abutments can be reduced by using a variety of modern design approaches, for example use of geosynthetic reinforcement or geogrid in backfill soil (Zornberg, 2007; Tatsuoka *et al*., 2014), rubber-soil mixture or reused tyre aggregates at backfill (Argyroudis *et al*., 2016; Mitoulis *et al*., 2016; Mitoulis, 2016), buried approach slab (Wendner and Strauss, 2014), using polyethylene sheets below approach slab to reduce friction with backfill soil(Mistry, 2005), different ground-improvement methods (Horvath, 2000; Horvath,

2005) and updating retrofitting techniques from jointed bridge to IABs (Xue, 2013; Jayaraman *et al*., 2001). Use of rubberish material with backfill soil reduces abutment top displacement, 'ratcheting effect', gap between backfill and abutment and'bump-at-the-end-of-bridge', as stresses and forces on overall bridge structure get reduced.

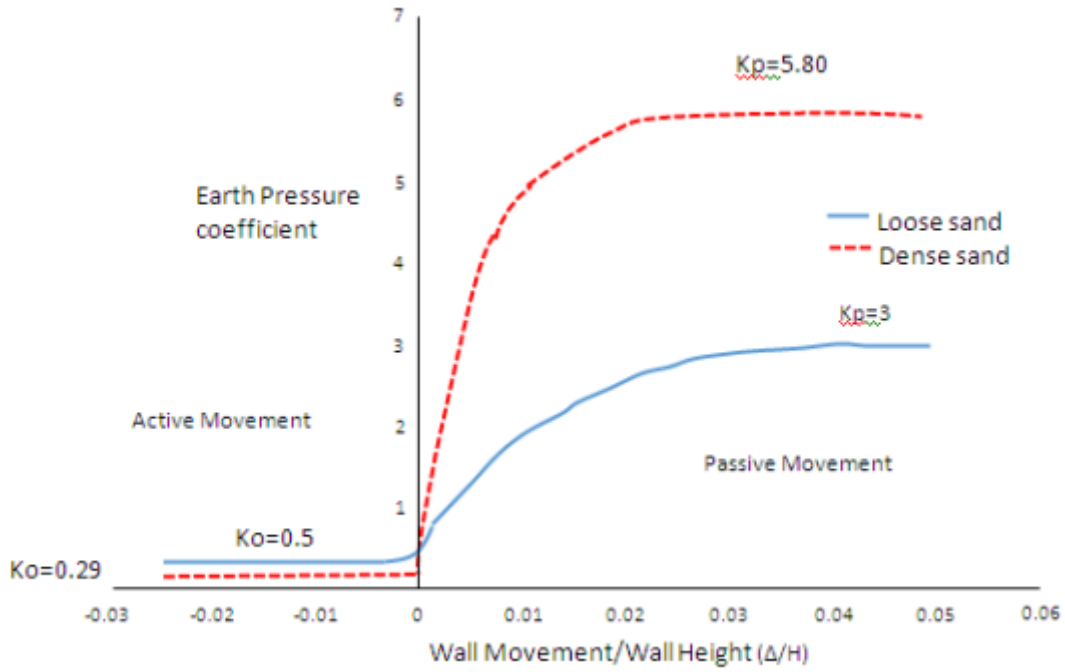

Fig. 2.5 Variation of passive earth pressure with the lateral displacement of abutment wall (Claugh and Duncan, 1991)

For bridges, proper provisions for drainage of backfill behind the abutment need to be provided in order to minimize the build-up of fluid pressure on abutment. In general, a series of vertical drains is recommended rather than a single continuous drainage to increase the efficiency of the system (Gibbens, 2011). Pipe under drains must be provided to drain the fill from backfill and wing wall. For mechanically stabilised wall, impermeable membrane is required surrounding the steel straps (drains) to avoid soil contamination. Poor drainage control during construction can cause settlement of approach slab due to erosion during rainfall, around and under the abutment and wing walls (SBDC, 2017).

2.4 Soil Pile Interaction

In IABs, the forces coming from primary and secondary loads are resisted by ABI and SPI. In this section, SPI for both abutment and pier piles will be discussed. Piles in IAB are designed to carry forces coming from substructure and superstructure. Also, the piles should be flexible enough to accommodate lateral movements without failure. The basic assumptions of a three-dimensional spring-dashpot system to model SPI were initially proposed by Greimann *et al.* (1986). Lateral displacement of the pile affects the lateral load capacity of the pile to transfer load to the ground. However, lateral displacement does not affect the end bearing resistance of flexible piles. The shaft capacity of the pile gets mobilised at a lower displacement like 2% of the pile diameter in vertical direction (Fleming *et al*., 1992). The lateral displacement capacity is reached when either the plastic hinge is formed in the piles or the abutment fails in shear or flexure. Pile bearing resistance should be verified in field during installation using static load tests and dynamic tests (AASHTO, 2012). A design procedure is proposed where the depth to bedrock is also considered to evaluate the effective length of piles (DeLano, 2002). Plastic design of steel H-piles for IAB has also been suggested by LFD method (Huckabee, 2005).

Soil characteristics in the SPI can be described by three types of force displacement curves in piles (API, 2000), namely, (a) variation of horizontal lateral force with lateral displacement (p–y), (b) variation of vertical skin friction with vertical displacement (f–z) and (c) variation of end bearing capacity with pile tip displacement (q–t). Axial and lateral force effects have been considered uncoupled and the concept was first developed by McClelland and Focht (1958). Based on extensive field tests on piles, Matlock (1970) has proposed p-y curves for piles in soft clay. Later, Reese *et al*. (1975) have proposed a family of p-y curves for stiff clay and sand based on experimental field

testing of piles. Afterwards, a unified curve for both soft and stiff clays has been defined by Sullivan *et al*. (1979). Several other methods like Hansen's theory (1963), 'Broms' method (1964), have also been proposed for estimation of lateral pile resistance for the same soil conditions (Fan and Long, 2005; Shia, 2005). The most commonly used API (2000) method has been implemented for soft clay (Matlock, 1970), stiff clay (Reese *et al*., 1975) and sand (Murchison, 1983).

A thorough discussion for the determination of *p-y* curves is given by Wang and Reese (1993). COM624Psoftware can beused for analysis of SPI (Wasserman and Walker, 1996; Wasserman, 2001). This procedure is confirmed by research at University of Tennessee (Burdette *et al*., 2004). The effective length of the pile is determined from identification of the points of zero moment at several depths of pile and the longest of these distances is used in subsequent nonlinear calculations. Previously, field tests have been performed on driven piles to compare the ultimate strength to that computed, using AASHTO (1996) and AISC (1996) column design equations. The results from the field study have shown that the prescribed equations predicted overly conservative values for the ultimate lateral bearing capacity of the piles (Ingram *et al*., 2003) because considering piles as unsupported between inflection points does not take into account the influence and support by the surrounding soil. So, measures should be taken during lateral design of different types of concrete piles which are partially included in the current code version (AASHTO, 2012). Prebored holes filled with flexible material and sleeve piles can be used to prevent downdrag of piles (IDOT, 2006; Hassiotis *et al*., 2005).

The abutment and wing-wall may not behave as a rigid block even if abutment is supported on flexible piles (Mourad and Tabsh, 1998).As expected, reducing the number of piles under the abutment greatly affects the axial load on piles but it does not significantly change the tension force in piles under the wing-walls. The axial stresses in

the piles are not affected by the type of wing-wall and fixed or hinged abutment-pile joint. In USA, guidelines recommend not to build piles under wing wall as it would restrict the rotation of integral abutment system which may further induce additional forces on the structure (White, 2008). Cantilever wing wall in the perpendicular direction of traffic and integrally founded with abutment, can increase the forces on girders during thermal expansion as it resists the expansion of the bridge superstructure (Paraschos, 2016; Huang *et al*., 2008). The axial forces and bending moments in the deck increase and peak moments in the piles decrease when the backfill soil is varied from loose to dense nature. However, for H-piles, the bending moment demand increases once the foundation soil changes from loose to dense (Faraji *et al*., 2000; Zhao *et al*., 2011). Very little work concerning the capabilities of integral abutments founded on short piles has been carried out. Existing design procedures preclude the use of piles below effective length because of the assumptions which are generally based on or validated for longer piles only (DeLano, 2002). Stresses in a pile may increase due to several reasons like, long bridge span, stiff soil, deep girders and weak axis bending. The spatial extent of the bridge-foundation system is large which necessitates an appropriate finite-element mesh to provide adequate modelling resolution. So, pre-processing and output visualization in 3D finite element (FE) analysis of the entire bridge-ground system can be quite tedious and time consuming (Elgamal *et al*., 2008).

Beam on Dynamic Winkler Foundation model (BDWF) (Makris and Gazetas, 1992) has been established for SPI which states that each subdivided layer of soil should be represented by a series of independent, discrete springs in the vertical and the horizontal directions. The soil surrounding the pile is considered to be divided into two zones (Hutchinson *et al*., 2004), namely (a) near field and (b) far field zones, as shown in Fig. 2.6. Strong material nonlinearity is expected in the near field zone while soil

behaviour would be primarily linear elastic in the far field zone. If viscous dashpots are modelled in parallel configuration with the nonlinear spring element (to capture hysteresis in soil for the near-field zone) for capturing the effects of radiation damping, it is referred as parallel radiation damping soil-modelling method (Kagawa and Kraft, 1980a, b; Badoni and Makris, 1996). If nonlinear hysteretic spring-dashpot is placed in series with the linear visco-elastic spring-dashpot (radiation damping), it is termed as series radiation damping of soil modelling (Novak and Sheta, 1980). Series radiation damping method ismore realistic as compared to the parallel radiation damping method as it avoids the possibility of unrealistically large damping forces in the near field zone (Wang *et al*., 1998). Radiation damping in the far-field soil domain of bridges occurs due to SSI and energy dissipation of waves radiating out into soil away from the bridge foundation (Gazetas and Dobry, 1984).

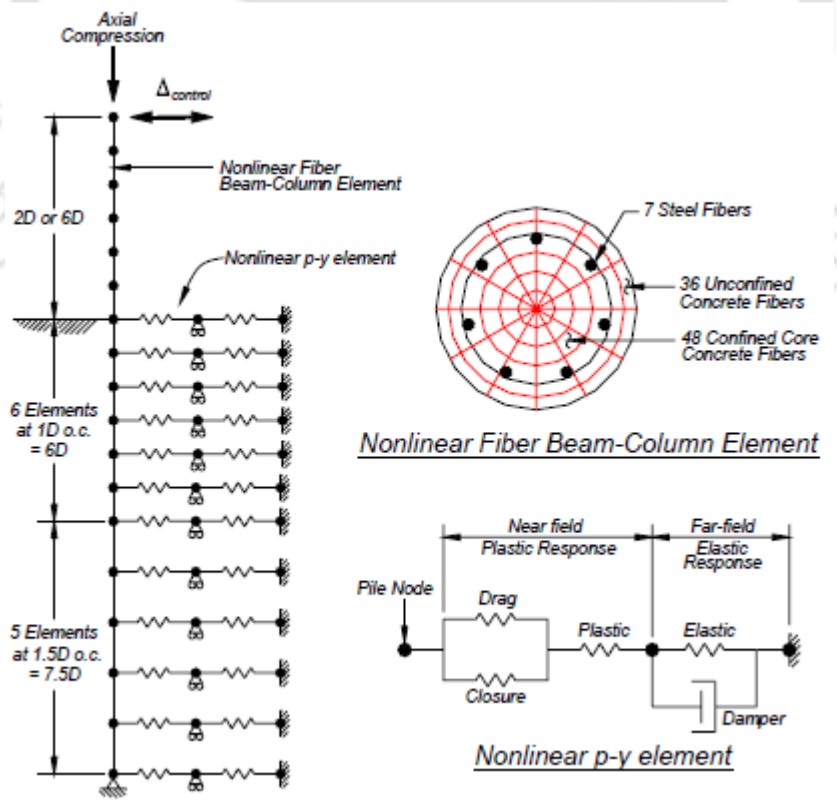

Fig. 2.6 General schematic of the finite element (FE) model used for the BNWF analyses using the nonlinear fiber beam-column element and the nonlinear p-y element (Hutchinson *et al*., 2004).

2.4.1 Computational approach

Many finite element softwares have been developed to analyse the two-dimensional (2D) or three dimensional (3D) SPI like *OpenSeesPL* (Lu *et al*., 2011), IAB2D, IAB2D (McBride, 2005), ANSYS (2013), CSiBRIDGE (CSI, 2016), *OpenSees* (Mazzoni *et al*., 2007), ABAQUS (Hibbitt *et al*., 2014), ADINA (2017), MIDAS (2017) and LUSAS (2014) which can incorporate the SPI aspect in the analyses in different ways. Proper parametric values, incorporated in the numerical programs, can produce results close to those obtained from the experimental tests (Greimann *et al*., 1986). The near or far field soil can be modelled as a linear or a nonlinear spring-dashpot element in series or parallel configuration to each other in simplistic way (Fig. 2.7(a)). To this end, continuous soil domain (Fig. 2.7(b)) can be modelled for analytical purposes with realistic soil properties (Dhar *et al*., 2016; Elgamal*et al*., 2008; Zhang *et al*., 2008). Different types of geotechnical domain modelling for dynamic analysis with proper boundary conditions have been illustrated in Kontoe (2006).

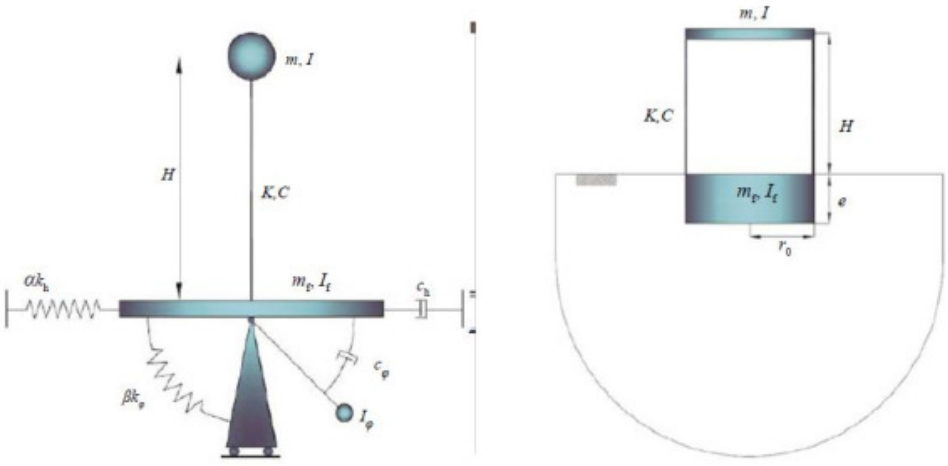

(a) (b)

Fig. 2.7 (a) Proposed discrete lumped mass with spring-dashpot model (Khodabhakhshi *et al*., 2011) and (b) generic soil-structure foundation system.

Numerical methods for analysis of soil-structure interaction can be divided into two main categories, namely (a) Direct methods and (b) Multistep methods. In the direct method, the entire soil-foundation-structure system is modeled and analyzed in a single step. Free field input motions are specified along the base and sides of the model, the resulting response of the interacting system is computed (for the finite element model) from the equation of motion. Multistep methods use the principle of superposition to isolate the two primary causes of soil structure interaction, namely (a) the inability of the foundation to match the free-field deformation and (b) the effect of the dynamic response of the structure-foundation system on the movement of supporting soil.Two types of interactions are observed, namely (a) kinematic and (b) inertial interactions. In kinematic interaction, earthquake shaking will cause soil displacements along both the horizontal and the vertical directions. If a foundation on the surface of, or embedded in, a soil deposit is so stiff that it cannot follow the free-field deformation pattern, its motion will be influenced by kinematic interaction, even in the absence of any mass. Kinematic interaction will occur whenever the stiffness of the foundation system impedes the development of the free-field motions. Kinematic interaction can also induce different modes of vibration in a structure. In inertial interaction, the masses of the structure and the foundation are considered which play a major role in the dynamic response. If the supporting soil is compliant, the forces transmitted to it by the foundation will produce foundation movement that would not occur in a fixed-base structure. The effects of soil compliance on the resulting response are due to inertial interaction.

In direct method, FE discretisation is carried out to model the structure and a portion of the underlying soil to artificial boundary. Various such artificial boundaries have been developed to simulate radiation of spurious waves away from the soil domain. Kausel and Tassoulas (1981) have categorised the possible boundaries into three major

groups, namely (a) elementary boundaries, (b) local boundaries and (c) consistent (nonlocal) boundaries. In elementary boundaries, either zero displacements are specified by fixing the nodes lying at the boundary or zero surface tractions are enclosed at the boundaries. It works well when damping is present and boundary is chosen at a sufficient distance from structure. Ghosh and Wilson (1969) have suggested that if the boundary is kept at a distance of *3r* to *4r* in horizontal and *2r* to *3r* in vertical direction, then satisfactory results can be obtained, where *r* is the radius of foundation. In local boundaries, the degrees of freedom lying at the boundary are not coupled to each other and are thus local in nature (Fig. 2.8(a)). The most widely used local boundary is the *standard viscous boundary* suggested by Lysmer and Kulhemeyer (1969). Consistent boundaries can transmit both types of waves, for any angle of incidence resulting in no reflection (Fig. 2.8(b)). All the DOF lying at the boundaries are coupled, along with frequency dependent properties of springs and dashpots. These can transmit all the waves from the soil boundary. The only restraint imposed is that the frequency dependent properties may not be suitable for the dynamic time-domain analysis.

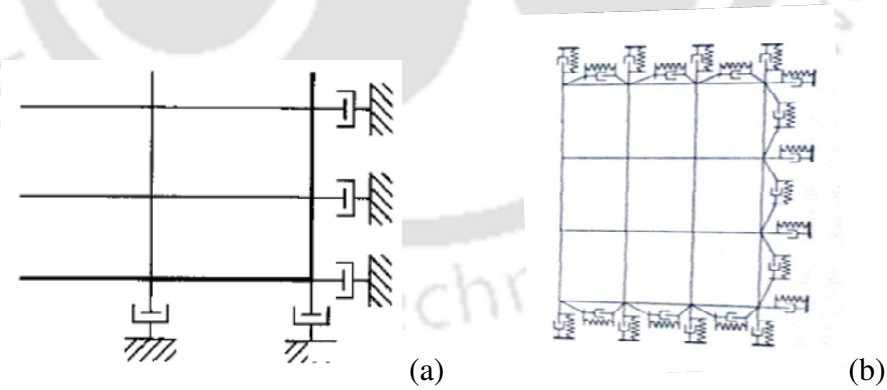

(a) (b)

Fig.2.8 (a) Lysmer Viscous Boundary and (b) Consistent Boundary

In case of 2D modelling method, continuum soil domain is generally modelled with quadrilateral or triangular FE mesh with suitable constitutive properties of soil. FE analysis indicated that SIA offer benefits over FIA, such as reducing the pile stresses,

particularly during contraction of the bridge. In addition, interaction between the approach fill and the foundation soil creates favourable conditions with pile stresses (Duncan and Arsoy, 2003). FE programs also account for the gap formation at the soil-pile and abutment-pile interfaces by introducing gap element or contact element. Zero-thickness interface elements can be used to model soil-pile and abutment-backfill interactions to allow slip at those interfaces (Zhang *et al*., 2008). Modelling of contact or interface elements has been discussed in past studies (Hibbitt, 2014; Zhang *et al*., 2008; Kolay, 2009; Gentela and Dasgupta, 2012).

Three-dimensional (3D) finite element models of IAB increase the level of complexity in the analysis, as well as the computational requirements. However, unlike 2D models, 3D models can account for the skew effects (Deng *et al*., 2015) and effects of eccentric loading. 3D soil continuum can be modelled by 8 or 20-noded brick element in FE softwares. Discrete Element Method (DEM) can be used for numerical analysis to model interaction between different rubber-soil mixtures and abutment (Cui and Mitoulis, 2015).

2.5 Field Studies

IABs equipped with instrumentation provide valuable insight into the behaviour of integral piles due to loading from traffic, earth pressure forces and temperature changes. Recently in several countries, short span old conventional bridges are updated to IABs for better performance. Measures are taken for IABs to relieve the earth pressure on the piles and the abutments to permit sufficient longitudinal movements. The void space created behind the abutment can be filled with corrugated metal supported by specifically thickened pressure relief compressible strips (Jorgenson, 1983). The piles which are rigidly connected to the bottom of the abutment tend to bend in double curvature. To

eliminate the bending action, integral abutment and pile connection can be provided as hinged. A schematic diagram of pile-to-cap hinged connection developed by Anastasopoulos *et al*. (2008) for dynamic analysis of pile under strong earthquake shaking (not fault related) is shown in Fig. 2.9.

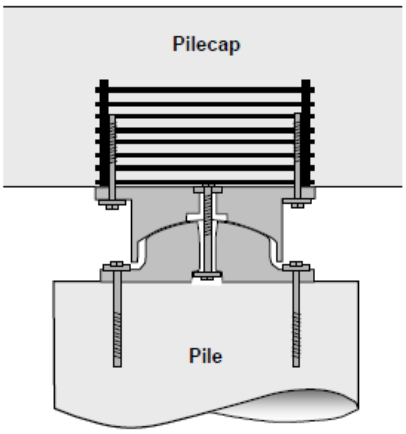

Fig 2.9 Schematic of Pile-to-Cap Hinged Connection

In full IAB, internal piers may be capable of lateral movements, if not, then some base isolation system should be arranged in between superstructure and internal piers (Frosch*et al*., 2005). Semi-integral abutment bridge can be constructed as hinged at the top and bottom of abutment by neoprene bearing strip transferring the force by padded dowel (Arsoy *et al*., 2004) and should be used where rigid soil and long span bridges are necessary (Burke, 2009). In typical Australian practice for IABs, link slab at intermediate piers joints is introduced (Connal, 2004). In New Zealand, full IABs and semi IABs are permitted if rotational stiffness component is taken into consideration (Jamieson, 2009) for bridges more than 60 m length. Highway overpasses less than 60 m length are suitable for construction as IABs (Torricelli *et al*., 2012).

Other than proper backfill compaction, dynamic response of the bridge structure is also governed by nonlinear inelastic response of the underlying soil during earthquake shaking. The plastic soil deformations impose large residual displacements on the IAB

after strong earthquakes (Zhang *et al*., 2008; Elgamal *et al*., 2008). Moments in piles has been calculated conservatively using simple beam theory and indicated that yielding of piles have not been occurred during long term thermal variation (Brena, 2007). Experimental results (Springman *et al*., 1996) suggest that loosely placed backfill should not be used, regardless of whether or not an approach slab is used; although loose backfill reduces the force coming on bridge during dynamic or thermal loading. To prevent settlement of approach slab, US guidelines recommend use of drag plates or buried approach slab with repairable special connection between slab and abutment (Frangi *et al*., 2011) which is easily repairable. The strain in approach slabs does not depend on whether the approach slab is a precast or cast-in-situ type (Phares *et al*., 2013). During extreme temperature, the expansion or contraction can be accommodated at approach slab-pavement joint in jointless bridges (Husain and Bagnariol, 2000; Mistry, 2005; BSDCH, 2017). Sometimes, the measured earth pressures on the bridge abutments may be quite high because of well compacted backfill (Kerokoski and Laaksonen, 2005). For highway bridges, the optimum friction angle of the backfill soil is recommended to be limited to 45° (BA 42/96, 2003). The density and stiffness of the backfill may increase or decrease over the yearly cycle of expansion and contraction of integral abutments (Darley *et al*., 1998). A special type of steel-concrete composite joint is proposed for IABs by Briseghella and Zordan (2015) which is easy to construct and have shown satisfactory response under cyclic loading. Field studies have been carried out with analytical verifications for skewed bridges to understand detailed behaviour of skewed IABs (Deng *et al*., 2015; Wright *et al*., 2015; Olson*et al*., 2013; Quinn, 2016). Based on comparisons of the finite element models with field studies, it can be concluded that finite element models do provide an excellent method to approximate the behaviour of an actual integral bridge structure.

2.6 Code Provisions

As the AASHTO (2012) specifications have not specifically addressed the design of piles for IABs, many state transportation agencies use in-house methods based on experiences and empirical formulae (DeLano, 2002). So far the research on integral abutment pile design has been aimed at simplified structural models or computational analysis to account for stresses and displacements in piles and superstructure due to thermal variation and dynamic forces. In past studies (Abendroth and Greimann, 1988; Abendroth, Greimann, and Ebner, 1989; Greimann and Wolde-Tinsae, 1988), the piles have been considered as equivalent cantilevers (Greimann *et al*., 1987) based on the stiffness of the soil and pile. The same method was presented considering three capacity criteria mentioned in AASHTO (1996), which are the capacity of the pile as a structural member, capacity of the pile to transfer load to the ground and capacity of the ground to withstand the load. The first assumption is a conventional elastic approach (Eurocode-8, 2005), while the second is an inelastic approach that considers redistribution of forces. In the elastic approach, the pile is considered as an equivalent cantilever thus, the moment, buckling load and horizontal stiffness can be calculated with respect to the effective length of pile during thermal expansion of superstructure.

The current AASHTO (2012) provisions do not support this assumption any more. In the other method, piles have been considered as inelastic and redistribution of forces due to the formation of plastic hinges can occur. The damping of integral bridges that occurs due to the inelastic behaviour of the backfill (Caltrans, 2013) has not been recognised by Eurocode8 (2005). Later on Mitoulis (2016) have found that damping ratios prescribed in Eurocode8 underestimated the realistic damping values. Neglecting the thermally induced pile stresses justifies the first-order plastic theory involving small displacements. However, for this case to be valid, local buckling needs to be prevented.

AASHTO (2012) does not allow combination of seismic and temperature loadings. Other than temperature variation for controlling the overall bridge movement, no specific guideline for IAB is mentioned in Australian Bridge Design Code (Austroads, 2004). A case study to perform static (service loads, creep and shrinkage) and dynamic analyses (displacement based) with design of IAB is given in Wood *et al*. (2015) and Wood (2015) according to NZTA (2014). According to JRA (2012), drainage layer should be provided in the approach embankment to prevent separation and corrosion of construction joints in presence of water. Soil susceptible to lateral spreading or liquefaction after high intensity of earthquake is highly discouraged as backfill material. In Canada, different states' research manuals (Husain and Bagnariol, 2000; BSDC, 2017) provide the supplement to the requirement of CSA (2014) for design and behaviour of IABs.

2.7 Retrofitting of Pile Foundation

The failure mechanism of an RC pile is typically manifested through four possible mechanisms, namely (a) crushing of concrete, (b) yielding of steel, (c) punching failure at the pile cap, and (d) failure of the pile due to pull-out forces. In the past, laboratory testing and computer modelling have been performed for analysing the causes of the failures (Chung *et al*., 2006; Li *et al*., 2005). Generally, fracture of piles is observed to occur along with loss of lateral support from the surrounding soil or by soil layers of different stiffness. This type of failure in pile is very common in liquefied sand due to large lateral displacements. The punching failure at the pile cap may occur due to insufficient thickness of the pile cap. Pile failure due to pull out forces occurs due to lack of adequate anchorage detailing between the pile head and the pile cap reinforcement. The reinforcing steel in the concrete pile may get pulled out from the pile cap or the pile shaft, causing significant deformation in pile foundation (Wang, 2015).

Improving seismic resistance and strengthening of the foundation is generally time consuming and cost ineffective because of various restrictions including space limitation and installation of additional protections. Keeping in mind, the growing necessity to revise disaster prevention specifications and designs for existing bridges situated at high intensified earthquake zones, development of easy and cost efficient techniques for seismic retrofit of the foundations of existing structures needs special attentions. For a pile foundation retrofit, additional piles are driven around the perimeter, widening the plan dimension of existing pile cap when the piles are examined for lack of tension and compression capacity. The newly installed piles are encased together in the pile cap to work in tension and compression so that the foundation can act as a single unit. This conventional method becomes problematic when the construction site has limited clearance and working space. Insufficient vertical clearance below the existing pile foundation also complicates the mentioned retrofitting method.

One of the retrofitting procedures adopted in case of pile foundation is the "encasement" method, a derivative form of "incremental capacity method". The encasement method was first adopted by Japanese engineers in severe seismic zones (earthquake level II) with comparatively softer soil (Fukada *et al.*, 2005; Wang, 2015). It is a hybrid method for the seismic strengthening of existing pile foundation by modification of the existing foundation substrate. Originally, in this retrofitting technique, steel sheet piles are installed surrounding the existing pile cap upto a design target depth. Then, the soil underneath the pile cap or surrounding the pile cap is replaced by engineered grout through high pressure jet grouting. Once the substrate is solidified, the sheet pile and injected grout act as a monolithic unit. This method increases the unsupported length of piles and provides lateral stability to the pile group foundation by adding passive soil pressure during earthquake shaking. The steel sheet piling at the

perimeter offers resistance to the possible overturning moment through soil-sheet pile friction mobilized during earthquake shaking. The mentioned retrofitting technique is easy to repair at the later stage of failure and suggest a cost-effective solution for seismic retrofitting.

Instead of sheet piles, precast RC piles can be embedded into jet grout surrounding the pile or pile cap upto a target design depth to strengthen the lateral load carrying capacity of existing pile foundation (Wang, 2015). The schematic diagram of the pile embedded into jet grouting is shown in Fig. 2.10 (modified after He *et al*. (2016)).

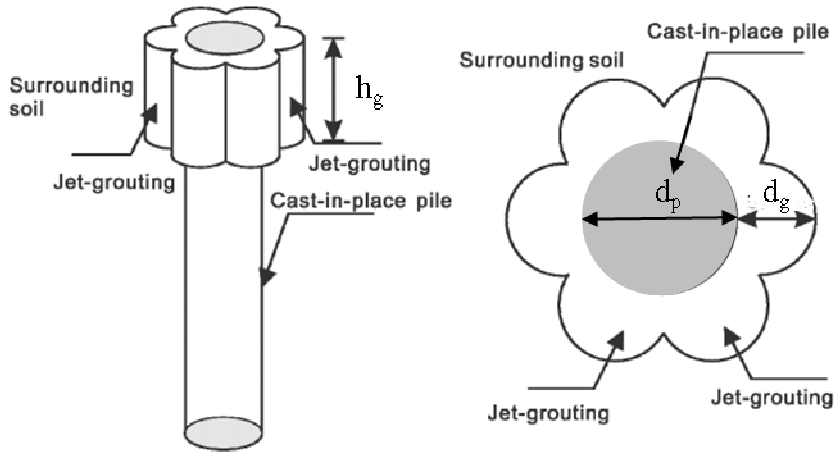

Fig. 2.10 Schematic of jet-grouting reinforced pile (He *et al*., 2016); where, h_g = height of jet grout, d_p = diameter of pile and d_g = diameter of grout.

2.8 Summary

The salient aspects from the review of the past studies are summarized below:

- Highway overpasses and short span foot bridges (upto 60m span) should be constructed as IABs and can be retrofitted from jointed bridges to jointless bridges easily. Most of the countries (except earthquake-prone countries like Japan) permit skew angle of 30° in IABs to construct unlike USA, where some states have permitted a skewness of 45°-60° for jointless bridges.

- Most conventional approach even in cold weather is weak axis bending of H-piles in concrete bridges. In moderate climate, strong axis bending of H-piles in concrete or steel bridge is permissible within stiff soil.
- Series radiation damping method for BDWF can be appropriate for carrying out numerical studies considering soil-pile interaction. Based on comparisons of the finite element models with field experiments, it can be concluded that finite elements models do provide uncompromising results to approximate the behaviour of an actual bridge structure.
- To mitigate the stress and forces in the overall integral 'abutment-backfill-deck-foundation' system during earthquake shaking, rubber-soil mixtures or 'mechanically stabilised' geosynthetic reinforced soil as backfill can be used. Backfill should be well compacted and should not get drained away during rainfall and should be free from frozen soil, roots, sods or other decomposable material. Apart from deck drains, a series of vertical drainage should be better than one continuous drainage because fill pressure could directly communicate with the abutment structure.
- Backfill and foundation soil density have different influence on the structural behaviour of an IAB. The forces and moments in the deck increase and peak moments in the piles get reduced when the compaction is varied from loose to dense backfill soil. However, the bending moment demand in HP-piles tends to increase once the nature of foundation soil changes from loose to dense.
- Approach slab-pavement joint and wing wall parallel to traffic could be used to reduce passive pressures by accommodating sufficient movement of integral abutment. Best results on their behaviour and design should be obtained by monitoring of completed projects in the past.

- Comparisons of various proposed thermal gradients with data accumulated from the test girders indicated that the temperature gradients in AASHTO LRFD (2012) provide reasonable upper bound to thermal variation.

2.9 Gap Areas

Based on the literature review, the possible gap areas are identified below:

- Latest codes like AASHTO (2012) prescribe adoption of 'Broms' Method (1964) for design of piles under lateral loading. Special design criteria for piles below abutments of IABs have not been prescribed anywhere and mandate detailed investigations with reference to the different geological conditions. More studies should be carried out on the influence of thermal and seismic load combinations on the behaviour of an IAB.
- Most of the IABs have been constructed on H-pile foundation. Seismic behaviour of an integral bridge on RC pile foundation has not been investigated previously. Comparison of bridge behaviour on RC pile and H-pile foundation is still required to be carried out with proper geotechnical investigation.
- The seismic behaviours of an IB incorporating simplistic spring-dashpots and soil continuum, have not been compared in any past study. Though, the simplistic model is easy to analyse and more conventional to build, still the analysis of an integral bridge on detailed soil domain-foundation system is expected to give detailed insight on the effects of SSI on structural response.
- Though researches are going on to increase the limiting length of IBs, but the effect of overall length on the seismic behaviour of IB has not been carried out.
- Abutment-pile foundation-backfill system plays a key role in load transfer and energy dissipation. From the field studies, it has been seen either the failure of piles or the

failure of backfill soil may lead to the failure of the entire integrated system, thus, detailed numerical studies are required for ABI.

- The performance of possible retrofitting techniques for RC pile foundation need to be investigated through extensive field studies and numerical modelling.
- The possibility of pile foundation of an integral bridge sustaining large displacement and forces during SSI, needs to be investigated.

2.10 Scope of Present Work

The scope of the present study is mentioned as follows:

- Influence of different approaches of numerical modelling, considering soil structure interaction, on the seismic behaviour of an integral bridge with RC pile foundation.
- Investigation on the effect of overall length of an integral bridge with RC pile foundation on its seismic behaviour in different types of foundation soil.
- Comparison of seismic behaviour of an integral bridge on RC pile foundation using spring-dashpot modelling approach and the detailed soil domain modelling approach.
- To study the influence of "in-cap encasement" method of retrofitting, using numerical modelling, on the seismic behaviour of pile foundation below an integral bridge.

★★★

Chapter 3

Modelling

3.1 Introduction

It is generally accepted in earthquake engineering practice that dynamic soil-structure interaction plays a beneficial role in the seismic response of structures by reducing the seismic demand on the structure. For this reason, seismic analysis of structures is often carried out either without considering the effect of the underlying soil, i.e., considering an infinitely rigid foundation soil, or with simplified soil-foundation-structure interaction using spring dashpot systems (e.g., Gazetas, 1991). Only in very special cases, the nonlinear response at the soil-foundation-structure interaction is considered, although it was proven in past studies to affect significantly the overall structural response (e.g., Boulanger *et al*., 1999; Figini and Paolucci, 2017).

Creation of fully coupled models including soil, foundation and structure, properly accounting for their nonlinear behaviour, requires significant attention and expertise; further the numerical simulations are often computationally costly. Therefore, the practice on this fully coupled approach is limited and commonly used only for important structures such as dams (Chuhan *et al*., 1998) and bridges (Shamsabadi *et al*., 2007). Besides, the impact of different modelling assumptions of the soil-structure interaction on the overall structural response, encompassing the nonlinearities of the soil response and of the soil-foundation interaction, still deserves additional clarification. In the present study, the different modelling approaches are investigated for a benchmark case of a bridge model which is “inspired” by the Humboldt Bay Middle Channel (HBMC) Bridge, California, USA. The seismic response of the original HBMC bridge has been already discussed in the past studies (Zhang *et al*., 2008; Elgamal *et al*., 2008);

thus it's not the intent of the present study. In this chapter, the details of the material modelling, namely for concrete, steel reinforcement and soil, are discussed.

3.2 Modelling

3.2.1 Modelling of bridge structure

As illustrated in detail in Zhang *et al*. (2008), the Humboldt Bay Middle Channel Bridge is located near Eureka in California. The bridge is 330 m long, 10 m wide, and 12 m in height (average height over mean water level). The bridge superstructure consists of nine spans with four precast prestressed concrete I-girders and cast-in-place concrete slabs. The bridge deck is supported by two seat-type abutments and eight bents with each bent consisting of a single column and hammer head cap beam. The third and sixth bents of original bridge have nonlinear shear keys for energy dissipation. However, the shear leys are not modelled for the present study. Pile caps of 1m thickness are supported on deep pile foundations consisting of five driven precast prestressed concrete piles (each of diameter 1.372 m) in a pile group where each pile is of 5.2 m long. Abutments are supported by a single row of 12 piles (each having diameter of 0.356 m). Pier piles and abutment piles are designed for axial compression of 500 kN and 400 kN, respectively.

Two finite element (FE) models of the bridge are considered, namely (a) a linear one with elastic beam-column elements for both the superstructure and the piers and (b) a nonlinear in which piers are modelled with fiber elements. In both the cases, the shear keys are not considered. Linear properties of structural elements are taken from Zhang *et al*. (2008), which are given in Table 3.1.

Table 3.1 Linear properties of bridge superstructure and substructure

Members	Area (m^2)	Young's Modulus (MPa)	Moment of inertia (m^4)
Abutments	12	28000	1.44
Beams	4.562	28000	3.212
Piers	3.4	28000	0.8188

In the present study, the bridge has been analysed for loading along longitudinal direction or along traffic direction. For Linear Time History Analysis (LTHA), all the components of bridge-foundation-soil system are assigned linear elastic material properties. For Nonlinear Time History Analysis (NTHA), only the bridge piers and the soil elements are assigned nonlinear material properties. The other components, namely pile foundation, abutments and the bridge superstructure are assigned linear elastic material properties for NTHA. Kent-Park-Scott (Scott *et al*., 1982) model (Fig. 3.1(a)) has been used for assigning the stress-strain curves of unconfined and confined concrete (Concrete01 material in *OpenSees*) with degraded unloading and reloading stiffness. No tensile strength has been considered in concrete. For the stress-strain curve of steel reinforcement (Steel02 material in *OpenSees*), Giuffre-Menegotto-Pinto (Filippou *et al*., 1983) model (Fig. 3.1(b)) has been used with isotropic strain hardening specified as 0.8%. The detailed parametric values for the two material models are specified in Tables 3.2 and 3.3, respectively. Load calculation for the bridge pier is performed according IRC: 6 (2010) shown in Appendix A. The ductile detailing of piers for seismic analysis has been done per IRC: 112 (2011), shown in Appendix B. 24 numbers of 28 mm diameter longitudinal bars constitute the main longitudinal reinforcement in piers and 8 mm diameter circular ties are used as shear reinforcement with a spacing of 140 mm. Piers are modelled using force based element discretized into five or ten integration points. Fiber based distributed nonlinearity is considered in those elements for carrying out NTHA in *OpenSees.* In a typical cross-section, the pier response is monitored at the steel, cover concrete and core concrete fibers for comparing results in the different cases (Fig

3.1(c)). The length and the centre-to-centre spacing of the piles are 5.2 m and 2 m, respectively. Piers are supported on 7m×7m×1m sized pile caps.

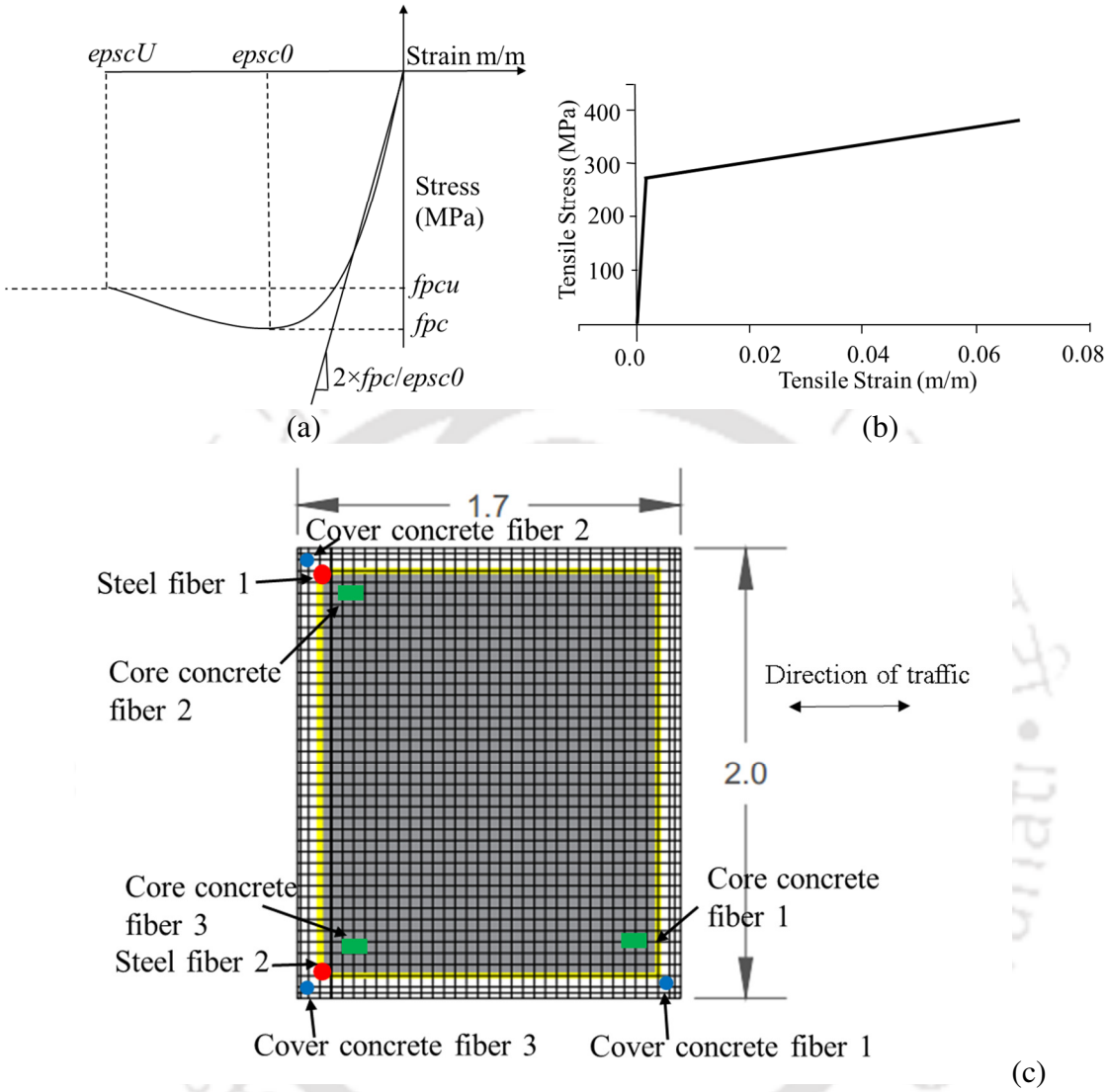

Fig: 3.1(a) Backbone curve of Concrete01 material for core and cover, (b) backbone curve of Steel02 material in tension for reinforcement and (c) Locations of monitored fiber locations in a pier cross section (all dimensions are in m).

Table 3.2 Concrete compressive strength parameters used in present study (after Zhang *et al.*, 2008)

Member	Concrete material	Compressive Strength, *fpc* (MPa)	Strain at compressive strength, *epsc0*	Crushing strength, *fpcU* (MPa)	Strain at crushing strength, *epscU*
Piers	Confined	34.485	0.002	0	0.006
	Unconfined	27.588	0.002	0	0.005

Table 3.3 Steel properties for reinforcement used in study (after Zhang *et al.*, 2008)

Properties	Elastic modulus (GPa)	Yield Strength (MPa)	Strain hardening ratio (%)
Values	200	276	0.8

3.2.2 Modelling of soil and foundation

Two-dimensional soil modelling has been carried out in *OpenSees* (McKenna, 2008). Soil domain is 1500 m wide (evaluated through iterations) and 220 m in depth (Fig. 3.2). The soil domain consists of 4 different layers, as shown in the 1D soil column in Fig. 3.2 (a), having the static and dynamic properties summarized in Table 3.4. Modelling parameters have been taken from Zhang *et al*. (2008). Pressure independent multi-yield material has been used to describe the soil behaviour through a formulation based on the multi-surface plasticity concept with associative flow rule, inbuilt in *OpenSees*. The yield surfaces are of the Von Mises type (Prevost, 1985). Since total stress analyses have been carried out, any direct consequence of significant excess pore water pressure generation has been naturally neglected in the present study. For nonlinearities in soil domain, variations of shear modulus degradation and damping ratio with shear strain curves are adopted as per the proposition of Darendeli (2001), which are shown in Figs. 3.2(b) and 3.2(c), respectively. The lateral boundary conditions of the soil domain have been implemented by tied degrees of freedom (TDOF) (Elgamal *et al*., 2008; Kontoe *et al*., 2007) at the two lateral ends of the domain. This implies that the soil domain follows the behaviour of a 2D shear beam constraints, in which the horizontal response is predominant than the vertical response. At the base level, classical Lysmer and Kuhlemeyer (1969) type absorbing boundary conditions are applied in the horizontal direction by properly calibrating the dashpot coefficients along with the classical vertical displacement has been restrained. The base input motion has been given in the horizontal direction to study the horizontal response of soil-structure system. Pile group stiffness has been analysed from Mokwa and Duncun (2000) and modelled as an equivalent pile group (Appendix C). Abutment backfill soil's dynamic properties have been kept the same as loose silty sand (OL/SM). To model the abutment-backfill interaction, no gap or interface elements

is considered at the abutment-backfill interface. A complete soil-foundation-bridge model with abutment backfill has been shown in Fig. 3.2(d).

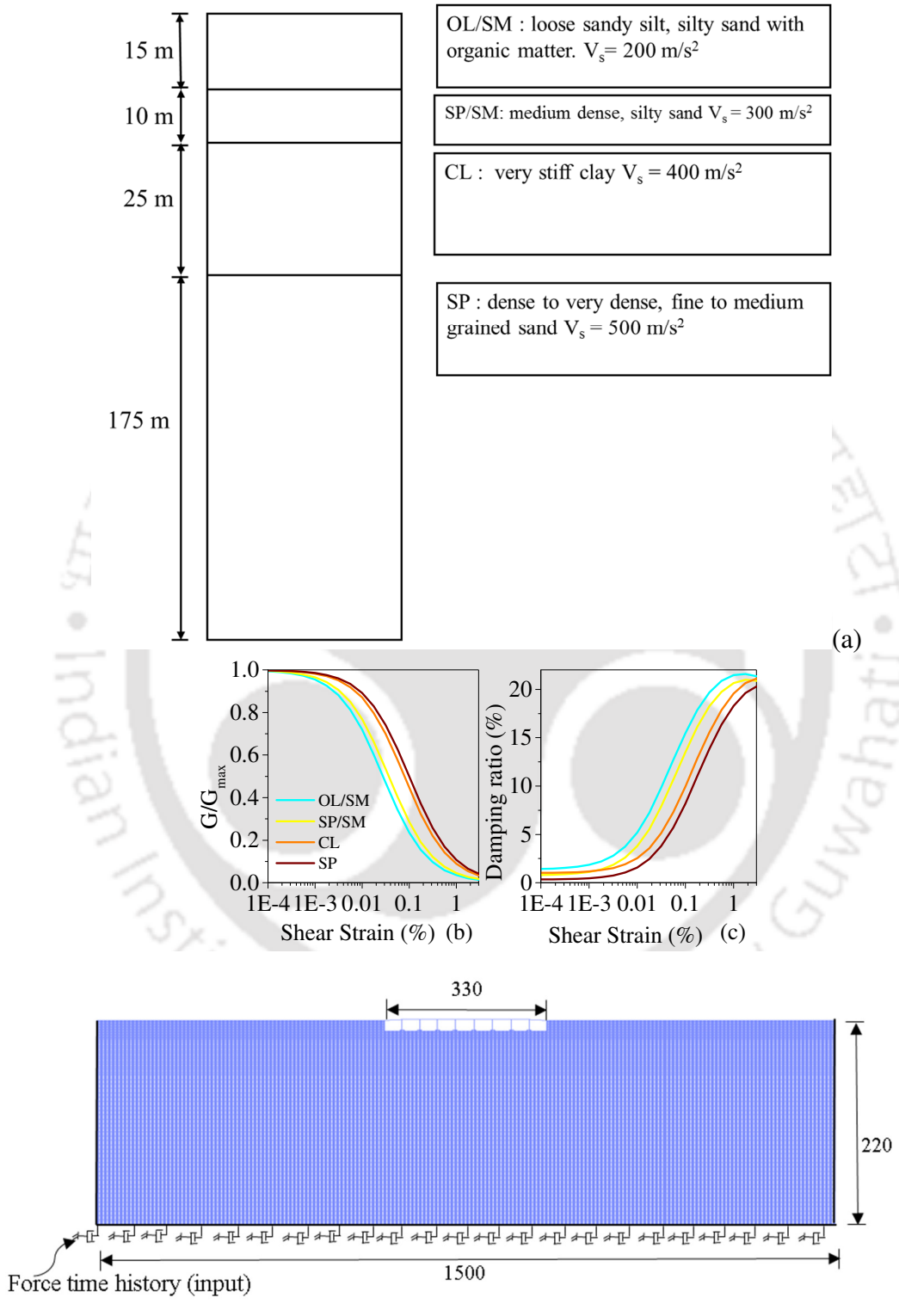

Fig. 3.2 (a) Modified 1D Soil column with soil classification (Zhang et al., 2008), (b) variation of shear modulus with shear strain for different soil layers, (c) variation of damping ratio with shear strain for different soil layers (Darendeli, 2001) and (d) complete soil-foundation-bridge model with abutment backfill (all dimensions are in m)

Table 3.4 Parametric values of soil characteristics used in the present study (Zhang *et al.*, 2008)

Soil layer	Elastic properties			Nonlinear properties		
	Maximum shear modulus (MPa)	Poisson's ratio	Total unit weight (t/m^3)	Undrained strength, (MPa)	Shear modulus ratio (Figs. 3.3(b) and (c))	Plasticity Index
OL/SM	76	0.45	1.9	0.030	Cyan Line	10
SP/SM	171	0.45	1.9	0.012	Yellow Line	0
CL	288	0.45	1.8	0.100	Orange Line	30
SP	525	0.45	2.1	0.053	Brown Line	0

3.2.3 Modelling of spring-dashpot system

For the spring-dashpot model, the soil domain below the foundation is replaced by suitable springs for modelling the behaviour of the foundation soil. The force-displacement curves for the nonlinear springs in the near-field zone are assigned to represent lateral load bearing capacity, vertical skin friction and pile tip axial load carrying capacity (API rp2a, 2000). . To incorporate soil-pile interaction, spring-dashpots have been modelled to represent the near-field and the far field effects of the soil domain. In the near field soil, nonlinear damping has been taken care by hysteresis damping. The springs in the lateral and the vertical directions are modelled in parallel configuration to represent lateral load bearing capacity and skin friction of pile surface respectively. Although soil mass has not been considered in the spring-dashpot model, far field soil stiffness and radiation damping have been modelled from the coefficients provided in Gazetas and Dobry (1984). Far field spring-dashpots have been modelled in series with near field nonlinear spring-dashpots (Fig. 3.3(a)). Far field spring and dashpots are modelled in parallel configuration. At the end of far field spring-dashpots, free field motions have been applied at the corresponding depth of piles. Abutment backfill interaction (ABI) is modelled by assigning nonlinear springs (Fig. 3.3(b)) behind the abutment wall. The abutment has been considered as 'frame type' and the corresponding

springs are modelled at a spacing of 1m along the height of the abutment. The nonlinear force-deformation curves of the springs are obtained from BA 42/96 (2003). In the analysis, Rayleigh damping is considered as 5% at the frequencies of 0.5Hz and 5.0Hz (Fig. 3.3(c)). From past studies (Granas, 2016; Brødbæk *et al*., 2009; Monkul, 2008), it has been proven that API force-displacement curves overestimate the soil stiffness. So, implementing API curves in bridge with spring-dashpot model tends to enhance the imposed forces on the piles and other bridge members, leading to a conservative estimate of the response. Thus, to reduce this error, 10% Rayleigh damping has been used in spring-dashpot models. In Fig. 3.4, at different depth of piles and abutment backwall, force-displacement curves are plotted to implement SPI and ABI in the spring-dashpot models built in *OpenSees*. The outer pile and the middle pile from the intermediate pile group are denoted as Pile_1 and Pile_2, respectively.

Under a suitable set of input ground motions from past earthquake records, the impact is studied on the overall structural response of the following modelling assumptions: (i) free field input at the base of fixed base bridge (*only B_FF*); (ii) SSI input at the base of fixed base bridge (*only B_SSI*); (iii) full scale SSI model which includes soil domain, foundation and bridge with and without backfill soil (*full SSI with BA* model and *full SSI no BA* model, respectively) and (iv) bridge model with foundation and spring–dashpots elements to represent soil with and without backfill (*FB_SD with BA* model and *FB_SD no BA* model, respectively). In Table 3.5, all the modelling assumptions with proper specifications are given for different types of models considered for this study.

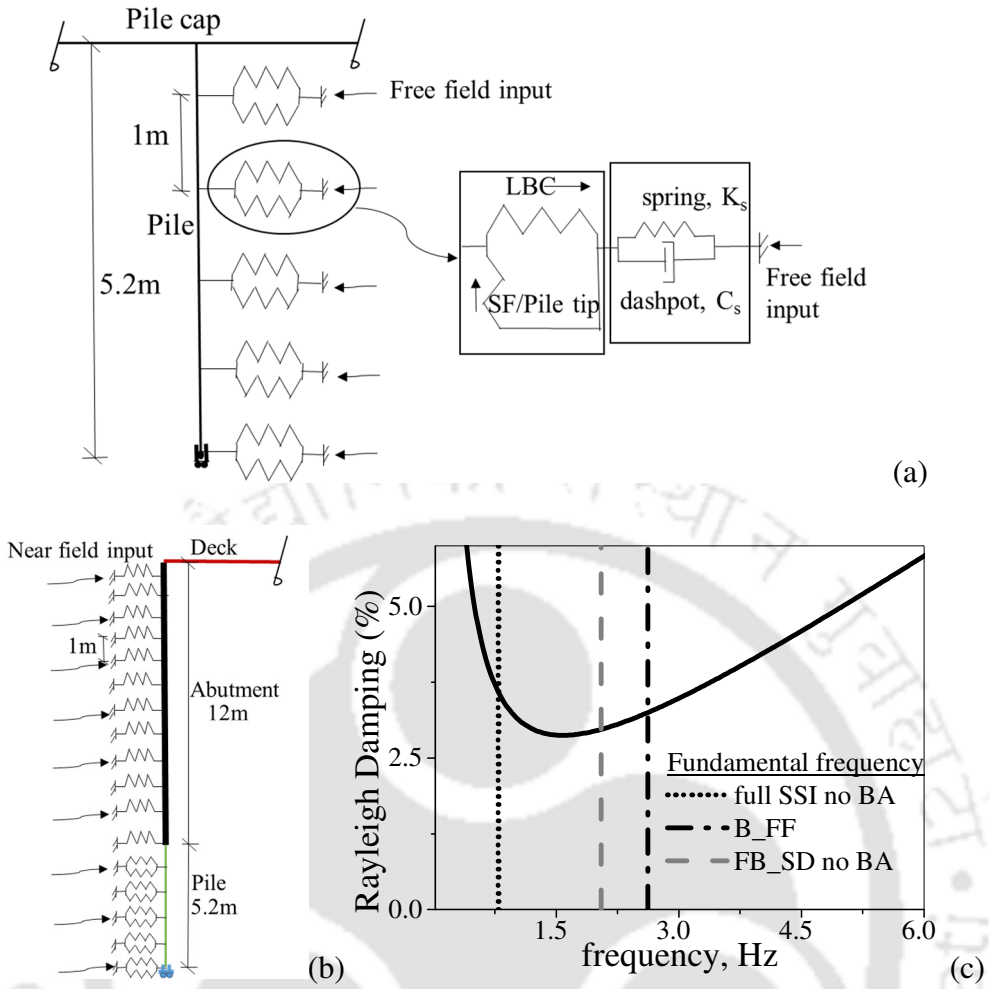

Fig. 3.3 Schematic diagram of (a) soil-pile interaction , (b) abutment-backfill interaction and (c) Rayleigh damping considered for analysis (For the notations refer to Table 5.1).

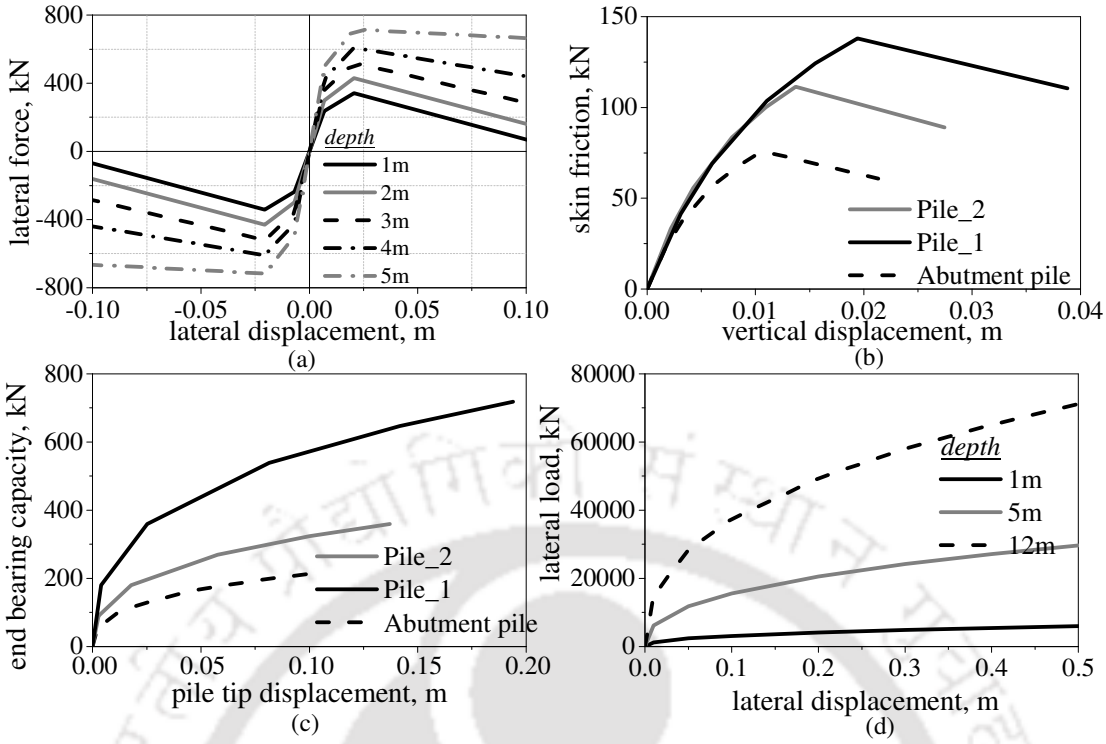

Fig. 3.4 Variation of (a) lateral force with lateral displacement for Pile_2, (b) skin friction with vertical displacement at the depth of 5.2 m, (c) pile tip end bearing load with vertical displacement at the depth of 5.2 m and (d) the lateral force with lateral displacemnt at abutment-backfill interface for different depths.

Table 3.5 Comparison between different modelling approaches

Model	Boundary conditions (BC) of vertical members	Soil	Abutment backfill	Input Motion
only B_FF	Base of the bridge's vertical members are fixed	No soil	Not present	Free field soil surface motion at the base of piers
only B_SSI	Base of the bridge's vertical members are fixed in translation and rotation	No soil	Not present	Input motion at base of piers from the base of piers of SSI model
full SSI no BA	Base of the bridge's vertical members have same BC in horizontal and vertical direction to pile cap connecting node	Linear or nonlinear continuum soil domain	Not present	Rock outcrop motion at the base of soil domain
full SSI with BA	Base of the bridge's vertical members have same BC in horizontal and vertical direction to pile cap connecting node	Linear or nonlinear continuum soil domain	Continuum backfill soil	Rock outcrop motion at the base of soil domain
lin str+nl soil no BA model	Same as *full SSI no BA model* (piers are linear)	nonlinear continuum soil domain	Not present	Rock outcrop motion at the base of soil domain
nl str+lin soil no BA model	Same as *full SSI no BA model* (piers are nonlinear)	Linear continuum soil domain	Not present	Rock outcrop motion at the base of soil domain
FB_SD no BA	Base of vertical members have no restraints (piers are nonlinear)	Soil stiffness and damping represented by equivalent nonlinear/linear springs and dashpots	Not present	Free field input motion at different depth of piles
FB_SD with BA	Base of vertical members have no restraints (piers are nonlinear)	Soil stiffness and damping represented by equivalent nonlinear/linear springs and dashpots	Equivalent springs represent backfill soil	Free field input motion at different depth of piles and abutment backwall

★★★

Chapter 4

Site Response Analysis and Selection of Ground Motions

4.1 Introduction

The seismic response of a structure depends on the site-specific characteristics of the underlying founding medium and the sets of possible site-specific ground motions of that area. In the present chapter, the response of a soil column for the particular bridge site, mentioned in Chapter 3, is determined under a Ricker wavelet applied at the bedrock level. Further, the selection of site specific ground motions from REXEL-DISP tool for time history analysis (THA) for the bridge-foundation-soil system is also discussed.

4.2. Site Response Analysis (SRA)

Before performing time history analysis, a Site Response Analysis (SRA) is carried out for the bridge site. A 1D soil column of 220 m depth (Fig. 3.2 (a)) with proper linear and nonlinear soil properties (Table 3.4) is modelled. Under various strong ground motions, local site effects have been established as an important factor (Caballero *et al*., 2012). In probabilistic seismic hazard analysis, ground motion data are collected over specific geographical area and the local site condition is one of the dominant factors influencing the seismic wave propagation and evaluation of the site-specific seismic hazard for a particular earthquake. The open source computational programs STRATA (Kotke *et al*., 2013) and DEEPSOIL (Hashash *et al*., 2016) are used to compare the site response performed in *OpenSees*. Three types of SRA have been performed, namely (a) linear site response analysis (LSRA), (b) equivalent linear site response analysis (ELSRA) and (c) nonlinear sire response analysis (NSRA). In ELSRA, linear elastic properties of the soil layers are used and these elastic properties are updated through iterative procedure depending on the amount of computed shear deformation. The final iteration step is still

fully linear elastic with *equivalent* elastic parameters which approximates the nonlinear response for that specific soil layer. In the NSRA, the dynamic wave equation with nonlinear stress-strain relationship is solved directly. LSRA and ELSRA have been carried out in frequency domain in STRATA. It computes the response for vertically propagating, horizontally polarized shear waves through horizontal soil layers. *OpenSees* performs the analysis using implicit Newmark beta method. The computer program DEEPSOIL *v*5.0 has been used to compare *OpenSees* response for 1D linear and nonlinear analyses in time domain. The two codes differ in the nonlinear modelling of soil column, i.e., *OpenSees* considers nested plasticity concept (Figs. 4.1(a) and 4.1(b)), while in DEEPSOIL a backbone curve is accompanied with unloading and reloading curves (Fig. 4.2 (c)). Variations of the hyperbolic model are adopted to represent the backbone curve of the soil along with the extended unloading-reloading Masing rules (Masing, 1926) to model hysteretic behaviour (Hashash *et al*., 2016) in DEEPSOIL. Masing rules and extended Masing rules (Pyke, 1979; Vucetic, 1990) are used in conjunction with the backbone curve to describe the energy dissipation characteristics (i.e., damping ratio) and cyclic degradation behaviour of soil. The Rayleigh damping (RD) is prescribed as 2% at 0.2 Hz and 20 Hz, in *OpenSees* and DEEPSOIL for linear and nonlinear SRA as low strain material damping. A Ricker wavelet of PGA as 0.2 g (with f_{max} = 2 Hz and maximum amplitude at t_0 = 1 sec) has been applied as bedrock input motion.

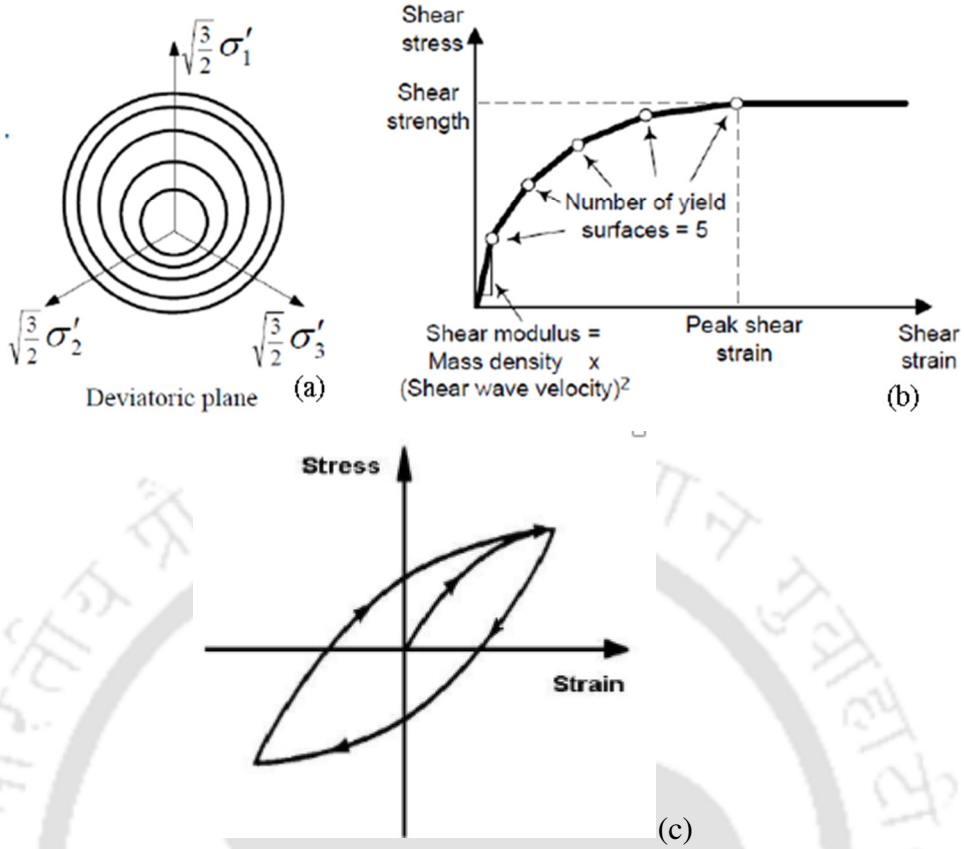

Fig. 4.1 (a) Nested plasticity theory and (b) octahedral shear stress–strain curve in *OpenSees* (McKenna, 2008), (c) a typical loading-unloading behaviour for material of Masing type (Rocha and Lopez, 2008).

The horizontal acceleration time histories (ATHs), maximum horizontal acceleration and strain profiles are shown in Figs. 4.2 and 4.3 for the linear and nonlinear analyses at 5 m from base and at ground surface. A good match is obtained for LSRA among all the codes. On the other hand, it is shown that a reasonable agreement is found for NSRA in *OpenSees* and DEEPSOIL. In LSRA, seismic motion is getting amplified at ground level and results in higher acceleration. But in NSRA, amplification of seismic waves depends on nonlinearity of soil material at that specific depth of the soil column. This effect may get reduced by mesh refining (Shiojiri *et al*., 2004) where the nonlinearity is predominant and post-process the output time histories with a proper zero-phase filter. The response of free field soil column for ELSRA varies predominantly from NSRA under 0.2 g PGA of Ricker pulse.

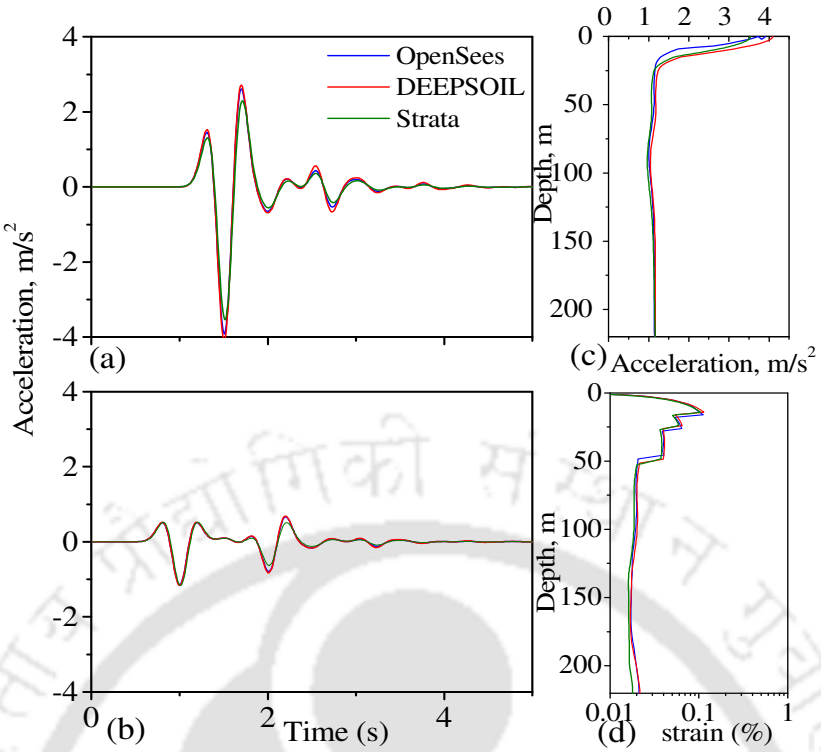

Fig. 4.2 Linear soil column analyses: (a) horizontal acceleration time history (HATHs) of soil column at surface, (b) HATHs of soil column at 5 m from the base, profiles of (c) maximum horizontal acceleration and (d) maximum shear strain along the depth of column.

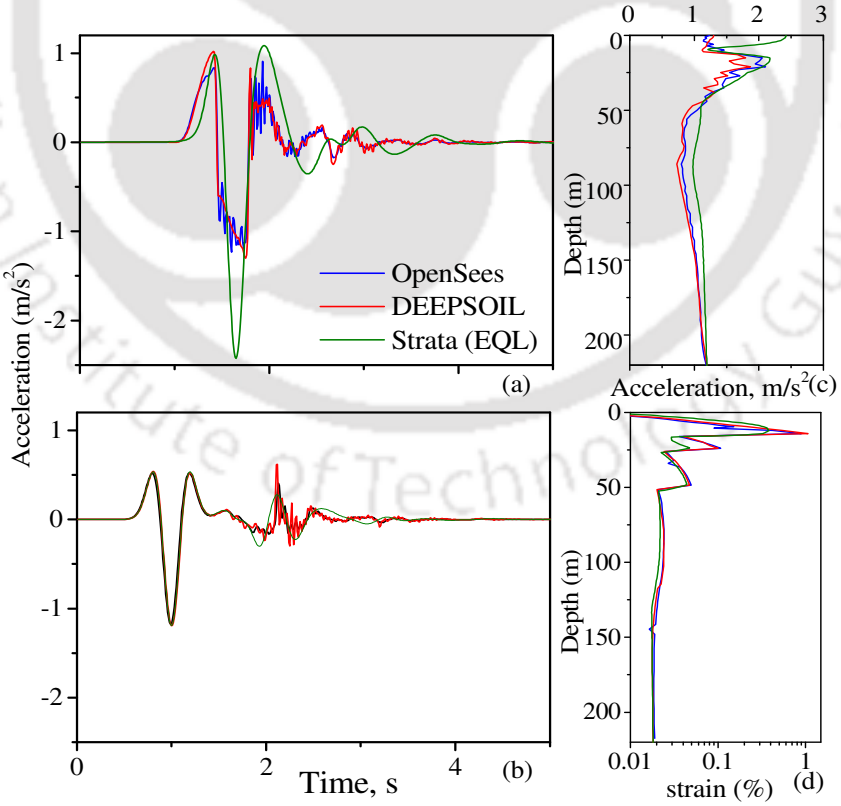

Fig. 4.3 Nonlinear soil column analyses: (a) HATHs of soil column at surface, (b) HATHS of soil column at 5 m from the base, profiles of (c) maximum horizontal acceleration and (d) maximum shear strain along the depth of column.

4.3 Selection of Ground Motions

A bedrock Uniform Hazard Response Spectrum (UHRS) is used to select input motions for the analyses (Dhar *et al*., 2016). The UHRS is developed from the 2008 United States Geological Survey (Petersen *et al.*, 2008) national seismic hazard maps for the Humboldt Bay area for rock outcrop motion assuming $V_{S,\ 30m}$ = 800 m/s (according to NEHRP (Holzer *et al*., 2005), site class B). The corresponding 5% damped elastic displacement response spectrum has been given as target spectrum to REXEL-DISP (Smerzini *et al*., 2012) to select the ground motions for dynamic analysis from strong ground motion database SIMBAD (Smerzini *et al*., 2014). Elastic displacement spectrum has been used over conventional acceleration target spectrum because it ensures spectrum matching over broad range of vibration period. The input parameters in REXEL-DISP to find the ground motions are: (a) moment magnitude, M_w = 5.5-7.5, (b) fault to site distance, R = 0–30 km, (c) spectrum matching tolerance = ±20%, (d) spectrum matching period = 0.2–5 s, (e) site specification = EC8 site class A and (f) probability of exceedance = 10% in 50 years, representing a return period of 475 years. If a minimum of seven time histories are used for each component of ground motion, the design actions can be considered as the mean response calculated for each principal direction (AASHTO, 2012). In the present study, the principal direction and the component of ground motion is along the length of the bridge. Although design level response is not determined in the present study, still the same principle is applied for the time history analyses of the bridge-foundation-soil system. So, seven ground motions recorded in horizontal direction during past earthquakes, are first selected (Table 4.1). Then, around the period of interest, i.e., in the same range of 0.2–5 s, the response spectra are scaled in such a way that the mean spectral response matches with the given target spectrum within the limits of the specified tolerance (Fig. 4.4). The two ground motions, recorded during South Iceland earthquake,

are selected for carrying out time history analyses in the next chapter. The Velocity Time Histories (VTHs) of all the ground motions are shown in Fig. 4.5.

Table 4.1 Different parameters of selected ground motions (Dhar *et al.*, 2016).

Station ID	Earthquake Name	Date	M_w	Fault Mechanism	Epicentral Distance, km	PGA, m/s^2	Scale Factor	Scaled PGA, m/s^2
ALT	Irpinia	23 Nov 1980	6.9	Normal	23.77	0.54	6.31	3.46
ST_106	South Iceland	17 Jun 2000	6.5	strike-slip	5.25	3.39	0.90	3.06
ST_112	Olfus	29 May 2008	6.3	strike-slip	8.25	3.28	1.67	5.47
ST_101	Olfus	29 May 2008	6.3	strike-slip	7.97	5.00	1.41	7.06
BSC	Irpinia	23 Nov 1980	6.9	Normal	28.29	0.95	0.72	0.68
ST_106	South Iceland	21 Jun 2000	6.4	strike-slip	21.96	0.51	1.42	0.73
LPCC	Christchurch	21 Feb 2011	6.2	Reverse	1.48	9.16	1.38	12.64
	mean values:		6.5		13.85	3.26	1.98	4.73

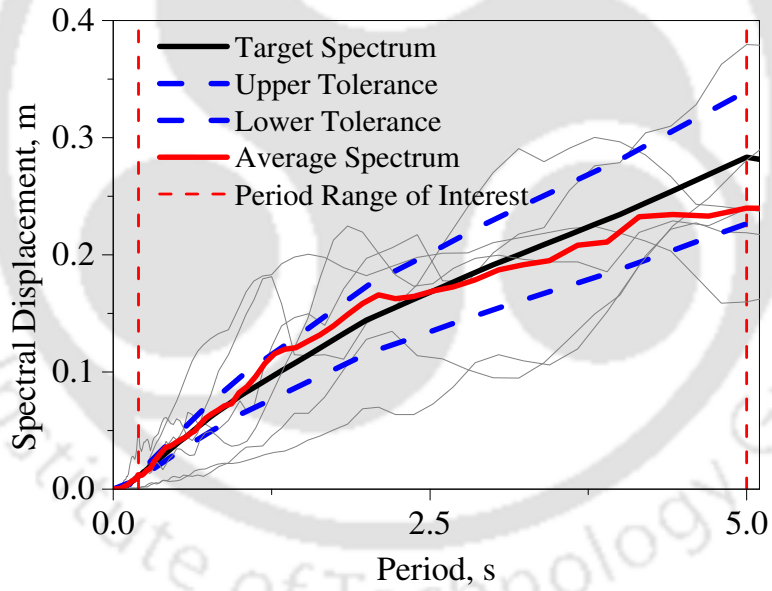

Fig. 4.4 Displacement spectra of all the ground motions used in present study

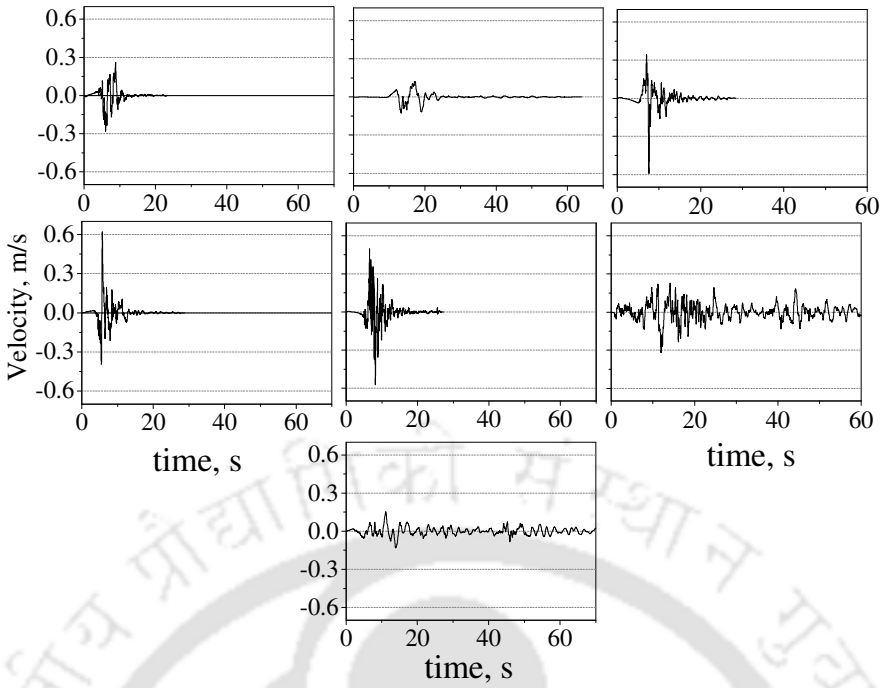

Fig. 4.5 Velocity time histories of all the seven ground motions used in the present study.

★★★

Chapter 5

Seismic Analysis of RC Integral Bridge

5.1 Introduction

In the present chapter, the influence of different modelling approaches is investigated on an RC integral bridge with pile foundation. The bridge geometry are considered similar to the Humboldt Bay Middle Channel (HBMC) bridge in California, the seismic response of which was already presented in the past (Zhang *et al.*, 2008; Elgamal *et al.*, 2008). The analysis of the different bridge-foundation-soil models are carried out using the program *OpenSees* with the parametric values and ground motion details discussed in Chapters 3 and 4, respectively.

5.2 Analysis

All the considered assumptions of different types of models have been given in Table 3.5. During the first part of analysis, three different types of models have been considered without abutment backfill, namely (a) *only B_FF* (Fig. 5.1), (b) *only B_SSI* (Fig. 5.1) and (c) *full SSI no BA* (Fig. 5.2)). In the second part, linear response of bridge with possible nonlinear behaviour of soil (*lin str+nl soil no BA* model) and nonlinear response of bridge with possible linear behaviour of soil (*nl str+lin soil no BA* model) are compared. In the third or final part, the response of *full SSI no BA* model is compared with the response of *full SSI with BA* model. Similarly, the response of *full SSI with/no BA* models are compared with the response of *FB_SD with/no BA* models. In *full SSI no BA* model, four different soil layers and vertical mesh bias are also shown in Fig. 5.2. The material properties of the different layers in the soil domain are shown in Figs. 3.2(b) and 3.2(c).

The fundamental natural frequencies of vibration for the different models are compared in Table 5.1. Natural frequencies of only soil domain and *full SSI no BA* model

have been obtained by applying Ricker pulse of PGA as 0.001m/s^2 at the base of the soil domain and monitoring the seismic motion at the soil surface. From the amplification ratio of soil surface motion and input motion, the frequencies at which first three amplified spikes are obtained, have been considered as natural frequencies of the first three modes. From the comparison, *only B_FF* model's fundamental frequency is 2.619 Hz and reflects the maximum lateral stiffness amongst all the models. Whereas, only soil domain and *full SSI no BA* model have similar natural frequencies in the first mode because in those two models, the mass of the soil tends to dominate the behaviour of the overall model under natural vibration. But in the 2nd and the 3rd modes, stiffness of bridge structure also participates in the natural modes of vibration.

Table 5.1 Natural mode of frequencies of different models

Models	f_1 , Hz*	f_2 , Hz*	f_3 , Hz*
only B_FF	2.62	5.01	8.73
Only soil domain	0.79	0.87	0.95
full SSI no BA	0.79	1.21	1.4
FB_SD no BA	2.05	4.46	4.76

$^*f_1$, f_2, f_3 represent natural frequencies of 1st, 2nd and 3rd modes of vibration

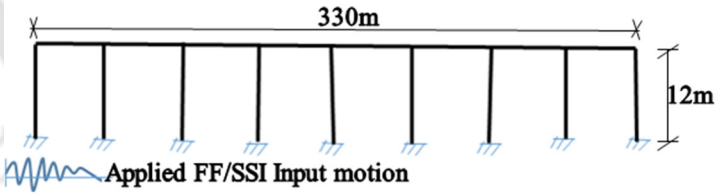

Fig. 5.1 Schematic diagram of *only B_FF/SSI* model in *OpenSees*

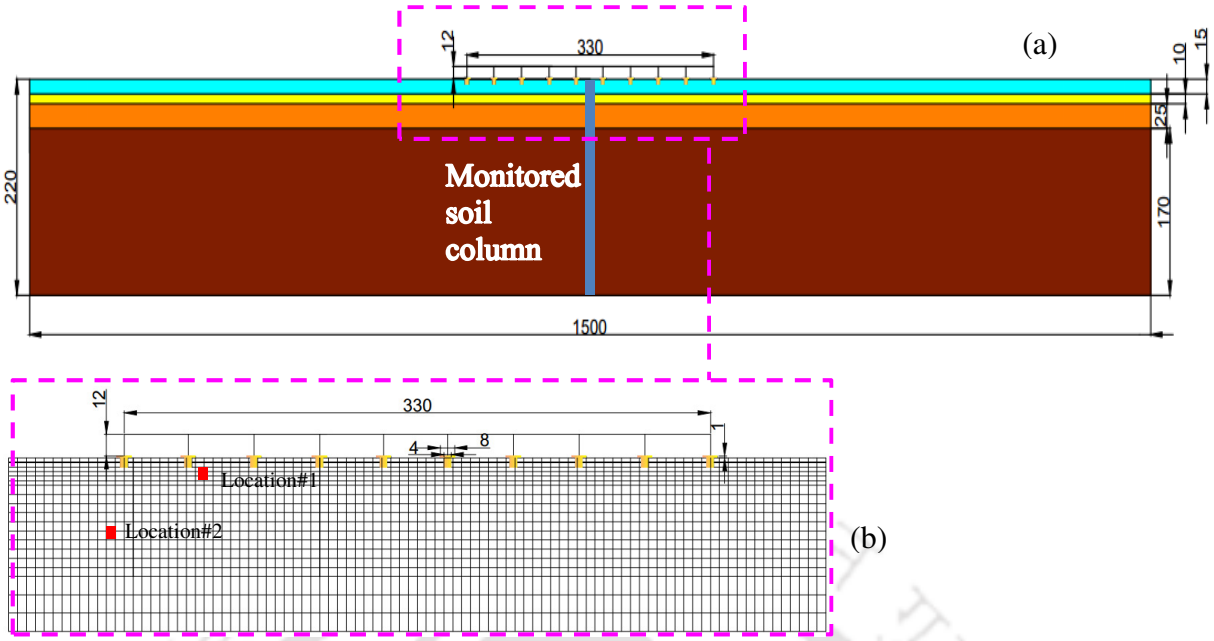

Fig. 5.2 Details of *full SSI no BA* model in *OpenSees*: (a) overall schematic diagram and (b) locations in soil domain for monitoring response (all dimensions are in m).

5.3 Time History Analyses of *only B_FF/SSI* and *full SSI no BA* models

Among the seven selected ground motions from REXEL-DISP (Smerzini *et al*., 2014), two chosen ground motions (denoted as GM#1 and GM#2 further in the text), are used to discuss the results at different stages of analysis in the present study with the PGAs of 3.06 m/s^2 (Fig. 5.3(a)) and 0.725 m/s^2 (Fig. 5.3(b)). The fundamental natural frequencies of the different models are marked on the Fourier transform plots of GM#1 and GM#2 in Figs. 5.3(c) and 5.3(d) respectively, to investigate the influence of the ground motions on the structural response with correlated natural frequencies of the studied models. Fourier content of GM#1 is significantly higher than GM#2. In GM#2, similar amount of energy is distributed over the entire frequency range. In linear time history analysis (LTHA), o*nly B_FF* model is the stiffest and *full SSI no BA* model is the most flexible one among the other models considered for the comparison in Table 5.1. From Figs. 5.3(c) and 5.3(d), the dominant frequency range of the ground motions can't be specified. Almost similar seismic energy content can be found in low and high frequency ranges for both the GMs.

So, natural frequencies of the models can't be correlated with dominant period range of the GMs directly.

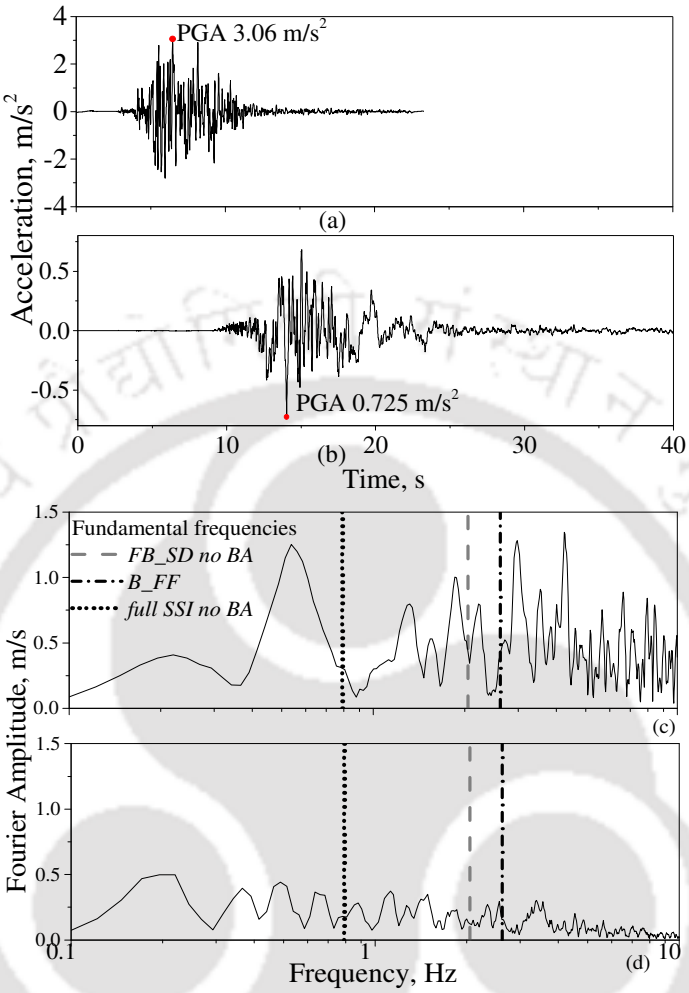

Fig. 5.3 Rock outcrop earthquake (scaled) ground motions (a) GM#1 and (b) GM#2; Fourier amplitudes of (c) GM#1 and (d) GM#2 with fundamental frequencies (marked) for the different models.

5.3.1. Structural response

From the LTHA, the pier response is found to be the maximum at the locations of the first and the eighth piers. This is due to the location of those piers adjacent to the abutments and higher forces are transmitted to the piers during the linear elastic behavior of the abutments. Figures 5.4(a) and 5.4(b) show the bridge response at the top of eighth pier for the three different models in Linear Time History Analysis (LTHA) under GM#1 and GM#2, respectively. From the Shear Force Time History (SFTH), expectedly the *only B_FF* model shows maximum response for the bridge piers due to high accelerations

introduced at the completely restrained ends of the piers and the abutments. As *only B_SSI* and *full SSI no BA* models have the same inputs at the bottom of each pier, similar response is obtained for those two models. This indicates given for the same input motions at the end of piers and abutments, the response of the bridge-foundation system is governed by the inertial response of the bridge itself, rather than the kinematic interaction between the foundation and the surrounding soil. The peak response from different cases almost occur at the same time in *only B_SSI* and *full SSI no BA* models. In *only B_FF* model, the peak shear force (SF) is 5,427 kN at 7.47 s and for the other two cases the peaks are at 6.265 s and 6.44 s time instants with the SF values of 4,038 kN and 3,661 kN, respectively. Under GM#2 in Fig. 5.4 (b), the peaks of SFTHs are in similar order as in Fig. 5.4 (a). Figs. 5.4(c) and 5.4(d) show normalized Fourier transforms (FTs) of SFTHs plotted in Figs. 5.4(a) and 5.4(b), respectively. The FTs of the SFTHs are normalized with respect to the peak amplitude value from all the six Fourier transforms, which corresponds to the unit value after normalization in *only B_FF* model's peak Fourier amplitude (Fig. 5.4(c)). Normalized FT of *only B_FF* model carries the highest seismic force, forming a quite sharp peak as compared to the other two models under both ground motions in frequency domain. In Fig. 5.4(a), peaks of *only B_FF, only B_SSI* and *full SSI no BA* models are at 2.65 Hz, 2.23 Hz and 2.24 Hz, respectively. *Full SSI no BA* model's peak is at lower frequency with lesser Fourier amplitude. The frequency shift of peak amplitudes from 2.65 Hz to 2.24 Hz means that in presence of foundation soil, *full SSI no BA* model is the most flexible one and its SFTH contains a reduced content in frequency distribution.

Velocity Time Histories (VTHs) at eighth pier top have been monitored to investigate the overall response at deck level in Figs. 5.5(a) and 5.5(b) under GM#1 and GM#2, respectively. The deck is axially very stiff which causes the superstructure to

respond like an SDOF system. The response at the same location for LTHA follows similar pattern under both the GMs. From the velocity histories, under GM#1, it's very difficult to comment on the peak response of three different cases as they are mostly incomparable under GM#2. But numerically, *only B_FF* model shows highest velocity and *full SSI no BA* model has lowest peak from the time history plots. Fourier transform of VTHs under GM#1 and GM#2 are plotted in Figs. 5.5(c) and 5.5(d), respectively. The velocity content of *only B_FF* model velocity content in frequency domain is higher than the other two models under both the GMs, because founded on fixed base, *only B_FF* model carries significantly higher seismic energy at deck level.

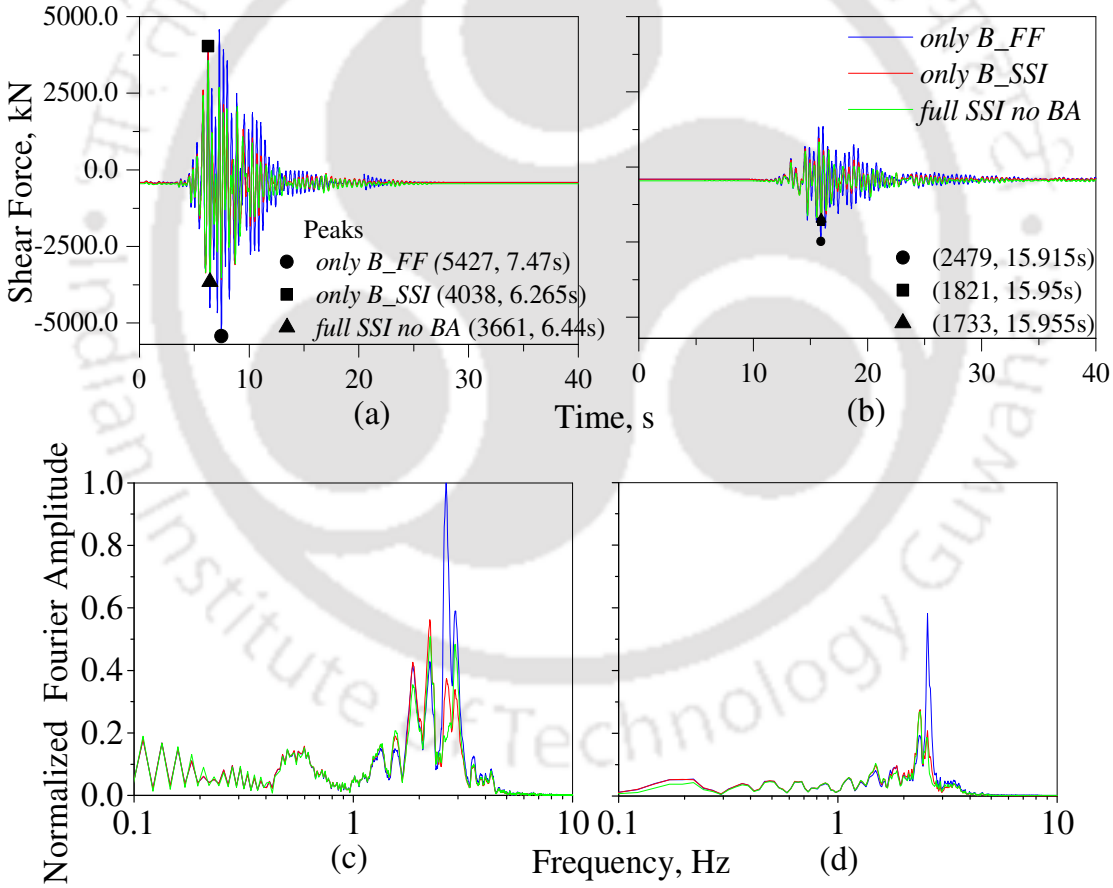

Fig. 5.4 SFTHs in LTHA (a) under GM#1, (b) under GM#2 and normalized Fourier transform of SFTHs for (c) GM#1 and (d) GM#2.

Figures 5.6(a) and 5.6(b) show the bridge SF response at the top of 8th pier for the three different models with NTHA under GM#1 and GM#2, respectively. For that

analysis, nonlinearity gets developed in bridge piers and foundation soil for the appropriate models. Due to material nonlinearity in pier and foundation soil, seismic energy dissipation due to hysteretic damping occurs and overall system tends to get more flexible. Significant energy dissipation occurs in the inelastic piers that leads to the reduction in the overall response of the bridge. For all the three models, the peak response in NTHA gets reduced by 65–70% as compared to the response during LTHA under GM#1 for all the three models. In NTHA, the *only B_FF* model shows the maximum values of the peak shear force under both GMs. The same is reflected in the variation of Fourier amplitude of the shear force response for the three models (Figs. 5.6(c) and 5.6(d)) under GM#1 and GM#2, respectively. For the *full SSI no BA* model, the peak Fourier amplitude gets shifted from 2.24 Hz (for LTHA) to 0.54 Hz (for NTHA) under GM#1 (Fig. 5.6(c)) which implies increased deformability of the nonlinear model during dynamic analysis.

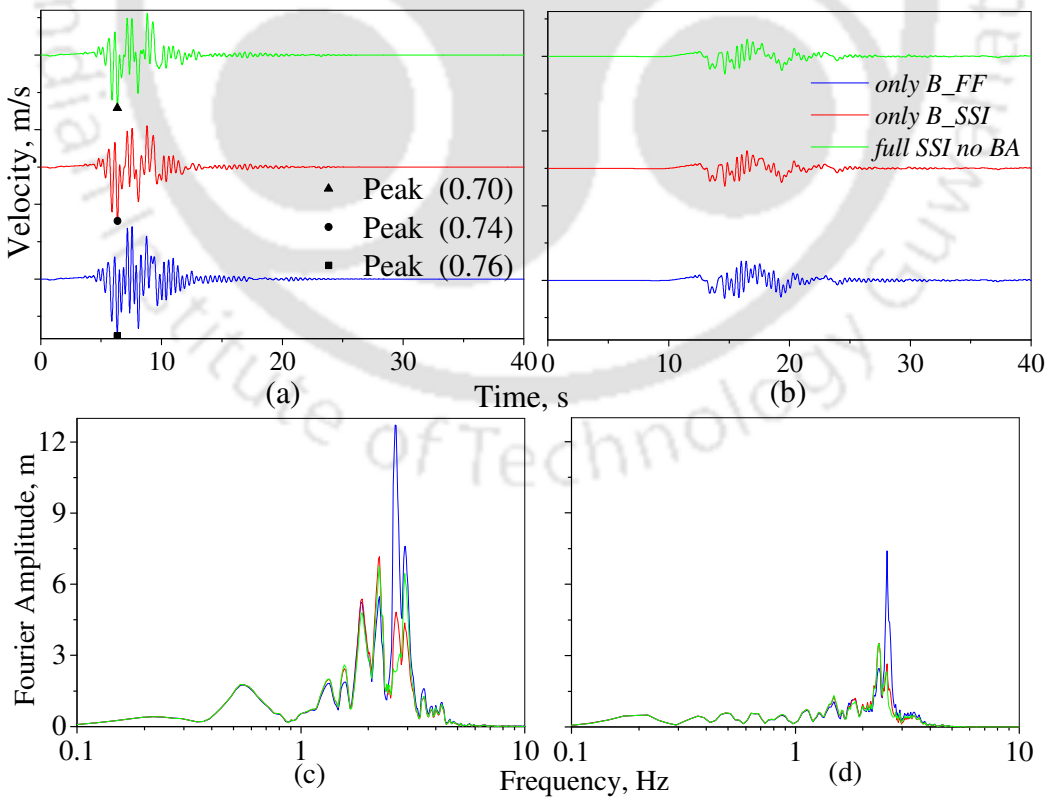

Fig. 5.5 Velocity time histories (VTHs) in LTHA at the top of 8th pier from LTHA (a) under GM#1 and (b) under GM#2; Fourier amplitude of VTHs (c) under GM#1 and (d) under GM#2.

As the intensity of input motion increases, the nonlinearity in *full SSI no BA* model increases, so the overall response under dynamic motion gets reduced due to high material nonlinearity. At the end of each ground motion, there is some residual response from structure and soil in NTHA. For the *only B_FF* and *only B_SSI* models, the developed nonlinearity in the structural behavior is less as compared to the developed nonlinearity in the *full SSI no BA* model which has nonlinearity developed from both soil and bridge components. Thus, the residual response for *full SSI no BA* model, in terms of shear force, bending moment and displacement are higher as compared to the *only B_FF/SSI* models.

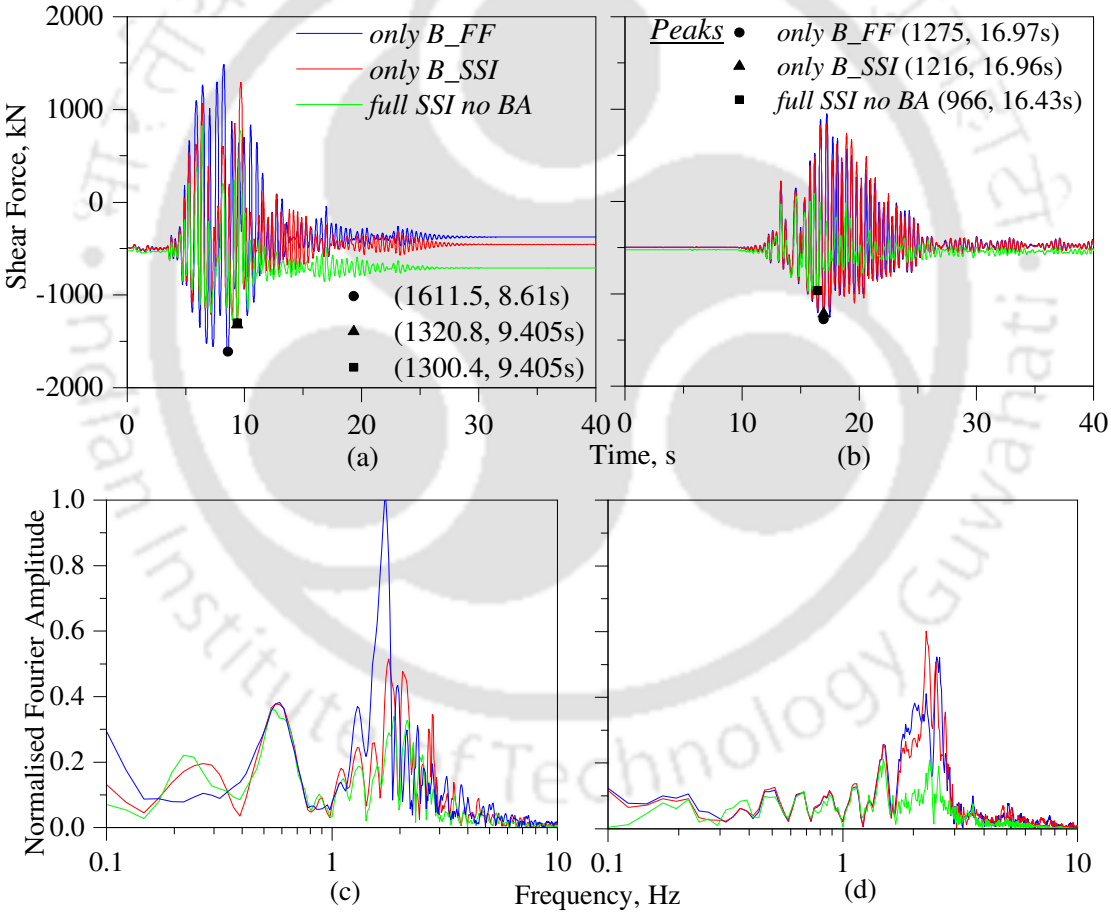

Fig. 5.6 SFTHs under from NTHA under (a) GM#1 (b) GM#2, normalized FTs of SFTH for (c) GM#1 and (d) GM#2.

At the top junction of the deck and the 8th pier, velocity time histories are monitored under GM#1 and GM#2 for NTHA (Figs. 5.7(a) and 5.7(b)), respectively. Under GM#1, *only B_FF* model response is coming out to be higher than the other two

models. Under GM#2, *full SSI no BA* model has lower peak velocity from the other two cases because of induced nonlinearity of underlying soil. In Fig. 5.7(c), within the frequency range of 1.1-2.0 Hz in the Fourier Transform plot, the velocity content of *only B_FF* model is higher as compared to the other two models. Soil nonlinearity is influencing the behavior of bridge beyond 1 Hz of frequency in *only B_SSI* and *full SSI no BA* models under GM#1. Thus, in *only B_FF* model FT (in Fig. 5.7(c)) is significantly higher between 1–3 Hz of frequency range where there is no influence of soil domain. In Fig. 5.7(d), velocity content of *only B_SSI* model is comparatively higher in the frequency range of 1.8–2.5 Hz. Under low intensity of ground motion, the amplification of velocity response in *only B_FF* model is lower than *only B_SSI* model due to the effect of soil nonlinear behavior.

To study the imposed seismic energy at the base of *only B_FF* and *only B_SSI* models, spectral accelerations of input motions are compared in Fig. 5.8. In the time period range (T_p) of 0.3 sec. (i.e., 3.33 Hz) to 1.4 sec. (i.e., 0.71 Hz), the spectral accelerations for the two cases vary. Specifically, within that frequency range, the Fourier amplitude of the SFTHs also varies in those two models; this leads to higher response in *only B_FF* model (Fig. 5.6(a)). Natural periods of the *only B_FF* and *FB_SD no BA* models are 0.48 s and 0.38 s, respectively, which also remain near the peak of the spectral acceleration curve.

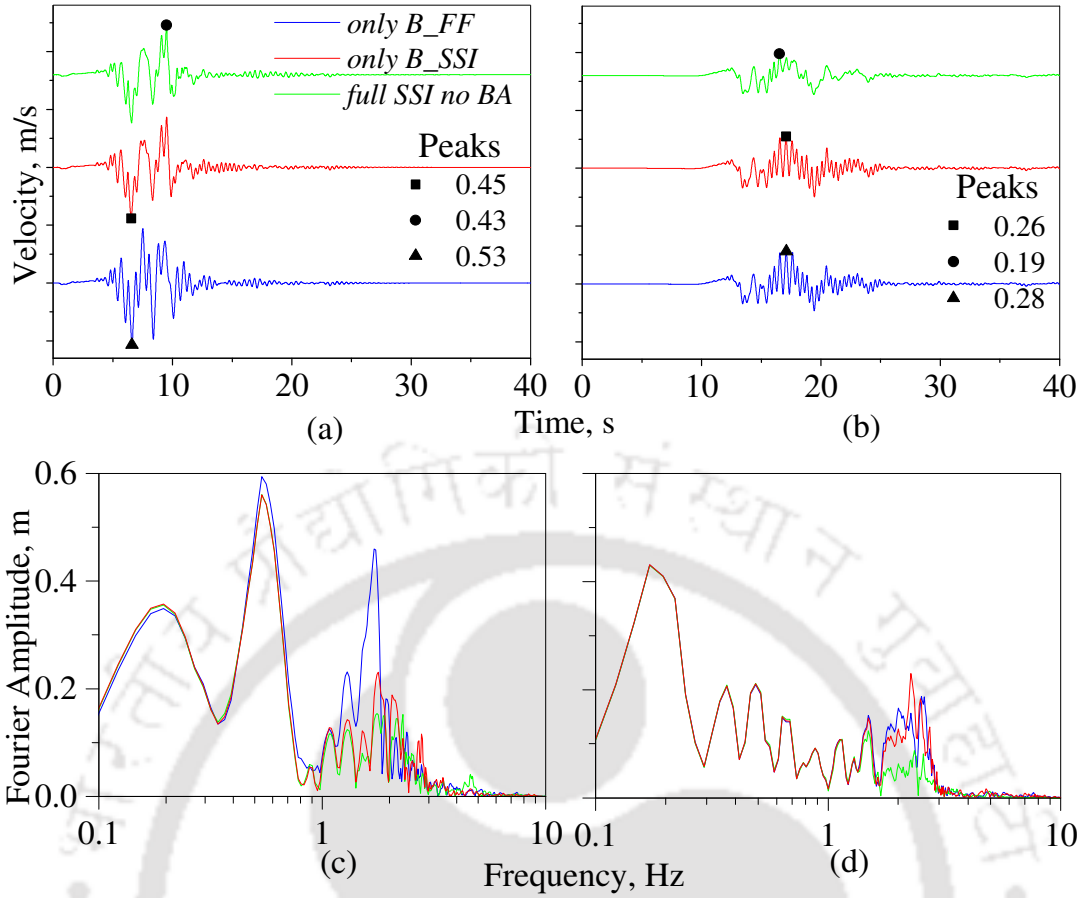

Fig. 5.7 Velocity time histories (VTHs) in NTHA at the top of 8th pier from NTHA under (a) GM#1 and (b) GM#2; Fourier amplitude of VTHs under (c) GM#1 and (d) GM#2.

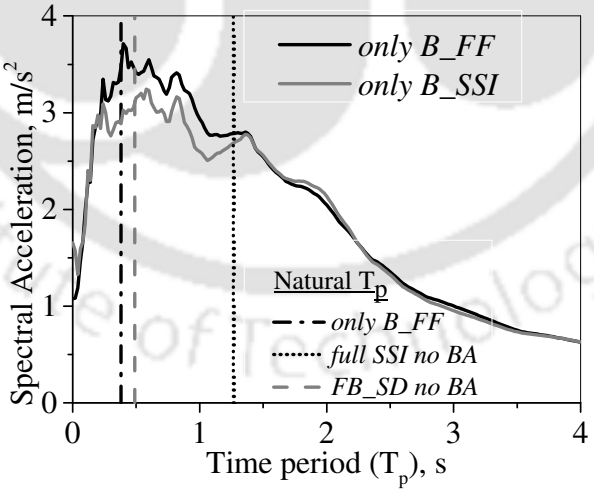

Fig. 5.8 Average spectral acceleration at the base of only bridge models under GM#1.

5.3.1.1 Response of pier sections

In *full SSI no BA* model under GM#1, the response of steel fibers, core concrete fibers and cover concrete fibers are monitored at the top of 8th pier cross section (shown in Fig.

3.1) and shown in Fig. 5.9. Stress–strain response in Steel fiber 1 (in Fig. 5.9(a)) is nonlinear in tension and has yielded (with yield strength f_y = 276 MPa), and forming nonlinear excursions during dynamic analysis. In Fig. 5.9(b), the behaviour of Steel fiber 2 remains in linear elastic range under axial compression. Core concrete (Figs. 5.9(c) and 5.9(d)) fibers are linear elastic and have not reached the maximum compressive strength of 34.5 MPa. Although the cover concrete fibers undergo cracking (Figs. 5.9(e) and 5.9(f)), the crushing of cover concrete is not observed. However, the cover concrete at Cover Concrete fiber 1 undergoes nonlinear behaviour under GM#1 although the level of nonlinearity is very small. Fibers have some residual response after the nonlinear dynamic analysis. Residual response in each fiber depends on individual fiber's nonlinearity that has developed during the earthquake motion and on nonlinear deformation of under lying foundation soil. The permanent deformation of soil domain can influence the residual response of the bridge structure.

In Fig. 5.10, the moment-curvature response is shown at the top of the 8th pier and base of the 1st pier during NTHA under GM#1 and GM#2. Under GM#1, the negative moment-curvature are higher at the top (Fig. 5.10(a)) and positive moment-curvature are higher at base (Fig. 5.10(c)) of pier cross-section, respectively. In Figs. 5.10(b) and 5.10(d) under GM#2, there is insignificant nonlinearity in structural members with very less nonlinear excursions. At end of dynamic analysis, the residual responses under GM#2 is mainly due to gravity load analysis.

5.3.2 Response of soil

Figures 5.11(a) and 5.11(b) show the shear stress-shear strain response of soil elements at location#1, at the depth of 7 m from soil surface in (Fig. 5.2) under GM#1 and GM#2, respectively. In Fig. 5.11(a) extensive soil nonlinearity in observed with wider loops. In Fig. 5.11(b,) one small loop has formed and the stress-strain variation range is quite low

due to lower intensity of input motion. While at location#2 (in Fig. 5.11(c)), at the depth of 34 m from soil surface, the loops are comparatively narrower than those formed at location#1 because the soil element at higher depth gets more confined than the soil element at shallow depth. Under GM#2, in Fig. 5.11(d), soil is linear elastic.

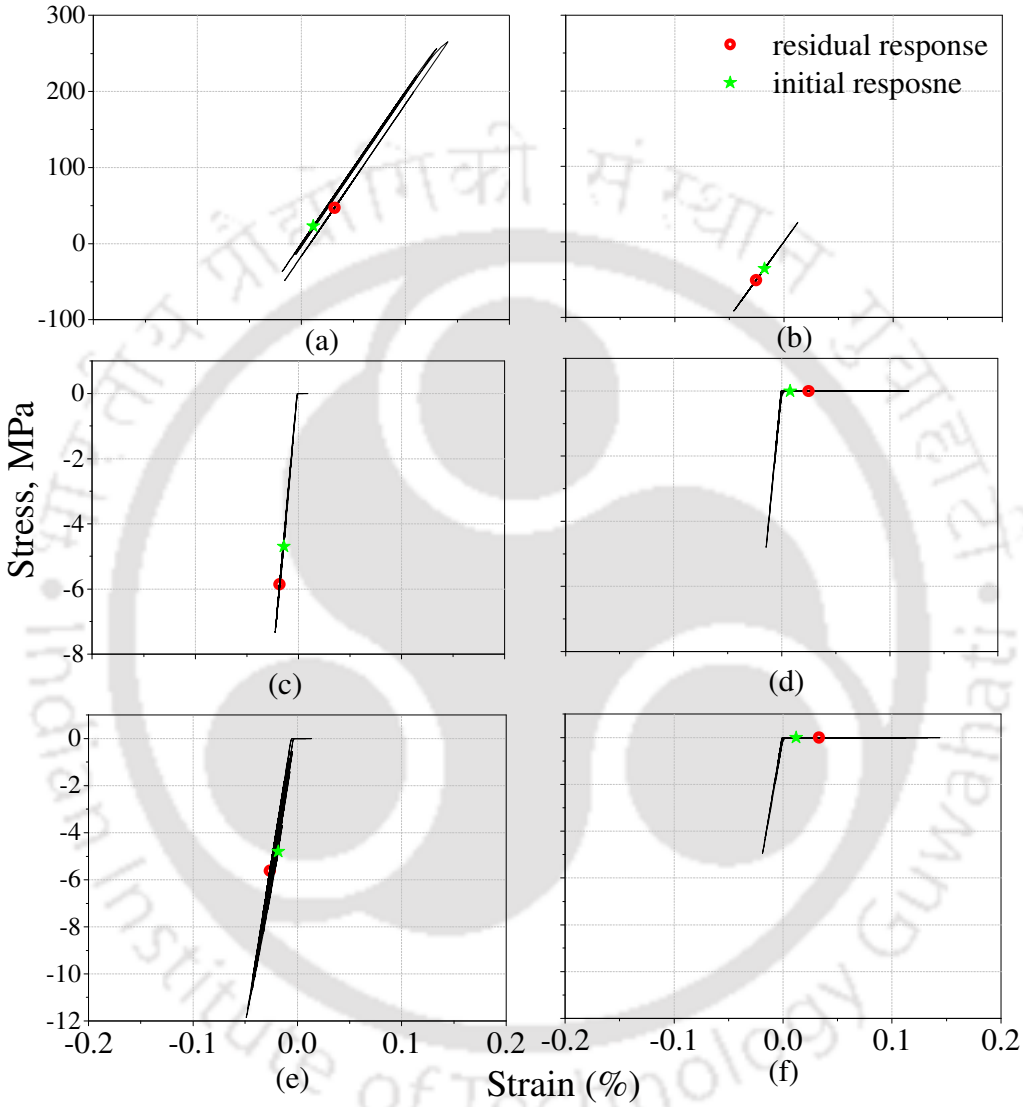

Fig. 5.9 Stress-strain response of fibers under GM#1 at top cross section of 8th pier: for (a) Steel fiber 1, (b) Steel fiber 2, (c) Core Concrete fiber 1, (d) Core Concrete fiber 2 (e) Cover concrete fiber 1 and (f) Cover concrete fiber 2 for *full SSI no BA* model

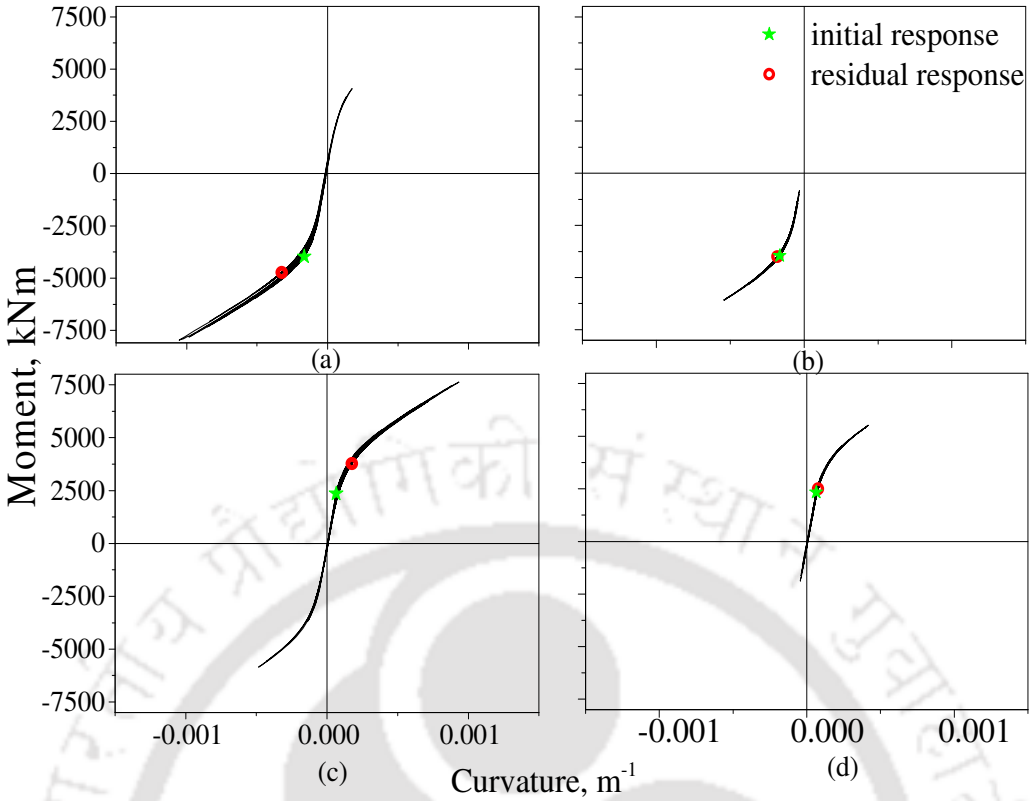

Fig. 5.10 Moment-curvature response at top cross section of 8th pier (a) under GM#1, (b) under GM#2, at base cross section of 1st pier (c) under GM#1 and (d) under GM#2 for *full SSI no BA* model

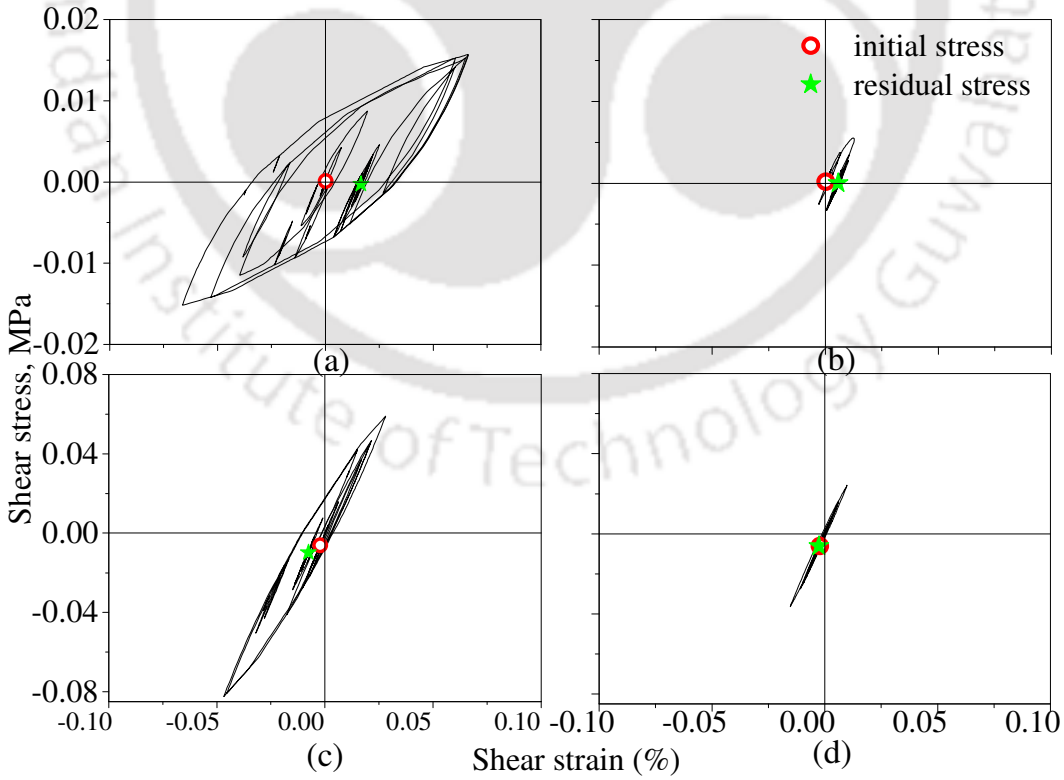

Fig. 5.11 Variation of shear stress with shear strain in *full SSI no BA* model at Location#1, due to (a) GM#1, (b) GM#2, at Location#2 due to (c) GM#1 and (d) GM#2.

Figures 5.12(a) and 5.12(b) show the undeformed and deformed shapes of *full SSI no BA* model under GM#1. Pile groups are very stiff as compared to the surrounding soil, so the soft soil between the pile groups tends to bulge out in the vertically upward direction after dynamic analysis. From the deformed shape it is visible that the abutments move towards two different directions after the dynamic analysis. So, both the abutmets with foundation and surrounding soil tend to deform away from the center of the bridge. This typical deformation of bridge abutments occurs due to the absence of abutment backfill soil behind the abutment. Once the abutment backfill is modelled, the overall deformed shape of bridge-foundation system is expected to get changed, which is discussed in the following sections.

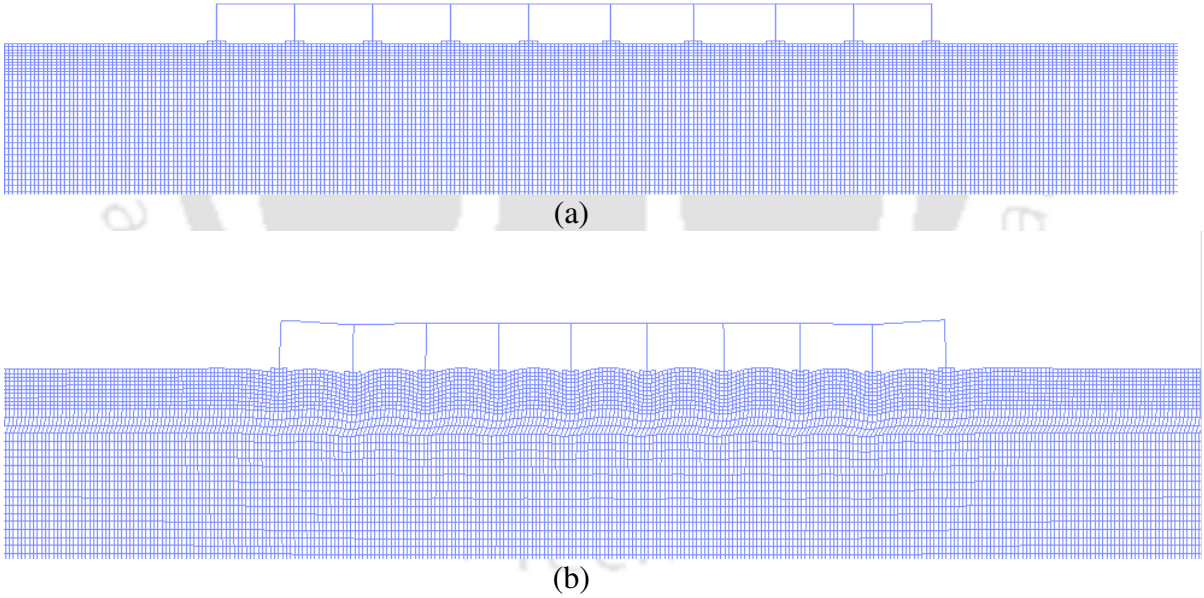

Fig. 5.12 (a) Undeformed shape of *full SSI no BA* model and (b) deformed shape of *full SSI no BA* model after dynamic analysis under GM#1 [image amplification factor is 100].

The nonlinear dynamic response of soil is monitored at different locations in the domain under GM#1 and shown in Fig. 5.13. In Fig. 5.13(a), at different locations below 1 m depth of pile groups, DTHs are compared. The residual displacements at different

locations are observed to vary because of different extents of soil nonlinearity at different locations of the soil domain. At a depth of 1 m below the bottom of abutment piles, soil gets displaced in two different directions (Fig. 5.12(b)). The minimum residual response is observed below 1 m depth of left pile group due to development of lesser nonlinearty in the soil elements as compared to the other two monitored locations. In Fig. 5.13(b), DTHs at the boundary (far field zone) of soil domain are quite similar between the *full SSI no BA* and the free field soil domain models due to similarity of energy dissipation mechanisms. The soil boundary of *full SSI no BA* model is far enough from near field excited zone of bridge which is unable to radiate any spurious waves back into the excited zone of soil domian, so the boundary behaves like a free field soil column.

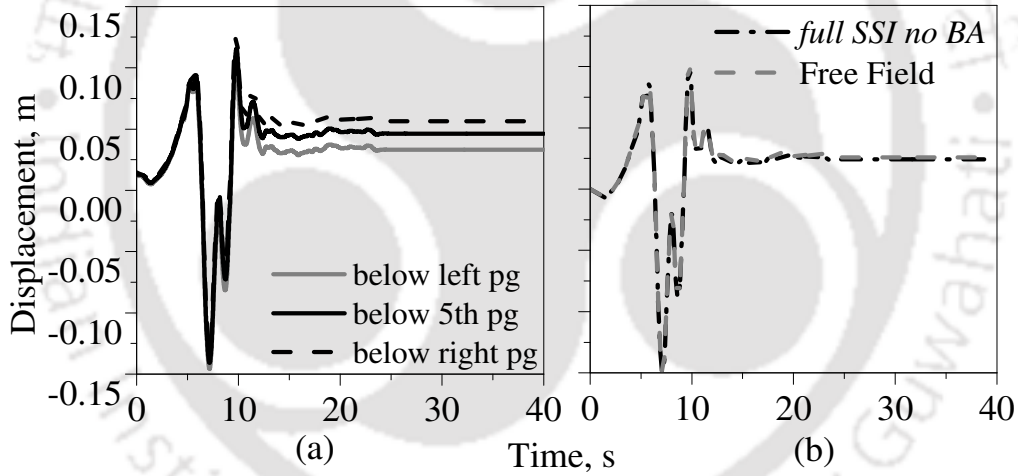

Fig. 5.13 Comparison of horizontal DTHs in soil domain at (a) different locations below the bridge and (b) near the boundaries in free field soil domain and *full SSI no BA* models under GM#1 ('pg' stands for pile group).

In Figs. 5.14(a) and 5.14(b), the maximum acceleration profiles are shown for nonlinear free field soil domain model along with the response of *full SSI no BA* model under linear and nonlinear behaviours at the monitored soil column (Fig. 5.2) under GM#1 and GM#2, respectively. For the GM#1, linear *full SSI no BA* model shows higher response in terms of both acceleration and strain parameters. In peak acceleration profile obtained for nonlinear behaviour under GM#1 (Fig. 5.14(a)), the peak acceleration

increases upto a depth of 25 m then decreases upto 75 m and after that it slightly increases till the bottom of the column. But for linear behaviour of the same model, the peak acceleration decreases from the soil surface to the depth of 35 m then increases upto 50 m of depth followed by decreasing acceleration upto 120 m depth; finally, the profile becomes similar for both the behaviours. For nonlinear behaviour of the *full SSI no BA* model, the peak acceleration near the soil surface reduces as the pile groups are acting as binding elements at foundation soil layer. In linear soil domain, due to seismic wave's amplification, the peak acceleration increases near the soil surface. But for nonlinear cases, peak acceleration depends on the nonlinearity of soil; due to nonlinearity of soil elements acceleration gets reduced. Under GM#2, soil nonlinearity is effective upto 25 m depth from the soil surface. Below that depth, the peak response for the linear and the nonlinear behaviours of the *full SSI no BA* model and free field soil model are almost same due to insignificant nonlinearity developed in soil domain.

The observed peak shear strain profiles at the monitored soil column under GM#1 and GM#2 are shown in Figs. 5.14(c) and 5.14(d), respectively. The peak shear strains of the *full SSI no BA* models under linear and nonlinear behaviours increase upto 20 m depth then decreases till a depth of 70 m. Seismic waves amplified at the soil surface from bed rock level and the nonlinearity of soil is found to be maximum in the ground level. Thus, this results in higher shear strain upto a certain depth of 20 m from the soil surface in both linear and nonlinear soil domains. Beyond that depth, the peak strain profile remains almost constant for both the models. Peak strain of free field nonlinear soil model is less at the depth of 20 m then it starts to increase leading to similar profile trends. Under GM#2, strain profiles vary in terms of strain upto a depth of 30 m, then follow similar profile trends as obtained under GM#1. Peak shear strain increases in SP/SM soil layers as in this layer, the soil undrained shear strength of the soil is considerably low. For linear

behaviour of *full SSI no BA* model, higher peak acceleration causes reduction in peak shear strain. For nonlinear behaviour of the same model, the peak shear strain also increases with the peak acceleration. Peak acceleration and shear strain both are found to be significantly higher in silty sand (SP/SM) than other soil layers because of its considerably lower undrained shear strength than the top and bottom layers.

5.3.3 Response of full SSI no BA model across depth

During NTHA, the observed variation of horizontal acceleration at different points along the vertical line of right abutment pile-group of *full SSI no BA* model is shown in Figure 5.15. As the nonlinearity of soil is higher below the right abutment pile group as compared to the other locations in the soil domain (Fig. 5.13(a)), the ATHs are obtained at right abutment-deck joint, base of right abutment and below the right abutment pile group under GM#1 and GM#2 (Figs. 5.15(a) and 5.15(b)). Under GM#1, the ATH gets amplified from 1 m depth below the pile group to the bottom of the abutment and further up to the deck level. Under the GM#2, amplification of ATH at deck level is also observed. Under GM#2, the variation of horizontal acceleration also shows similar trend at all the monitored locations. From the normalized Fourier amplitude of ATHs under GM#1 in Fig. 5.15(c), significant deck amplification is visible in the range of 1–10 Hz of frequency. Whereas, at base of the abutment and below the pile group nodes contain similar Fourier amplitude upto 5 Hz. Beyond 5 Hz of frequency, the base of the abutment motion contains marginally higher acceleration. Under GM#2, motion at deck gets amplified beyond 1 Hz of frequency as compared to the other two locations. Below the pile group, acceleration response is minimum because linear elastic pile foundation has a restraining effect on the foundation soil. At deck level, maximum amplification of the response occurs due to the absence of abutment backfill soil which would have offered some restraint at both the ends of the bridge in the longitudinal direction.

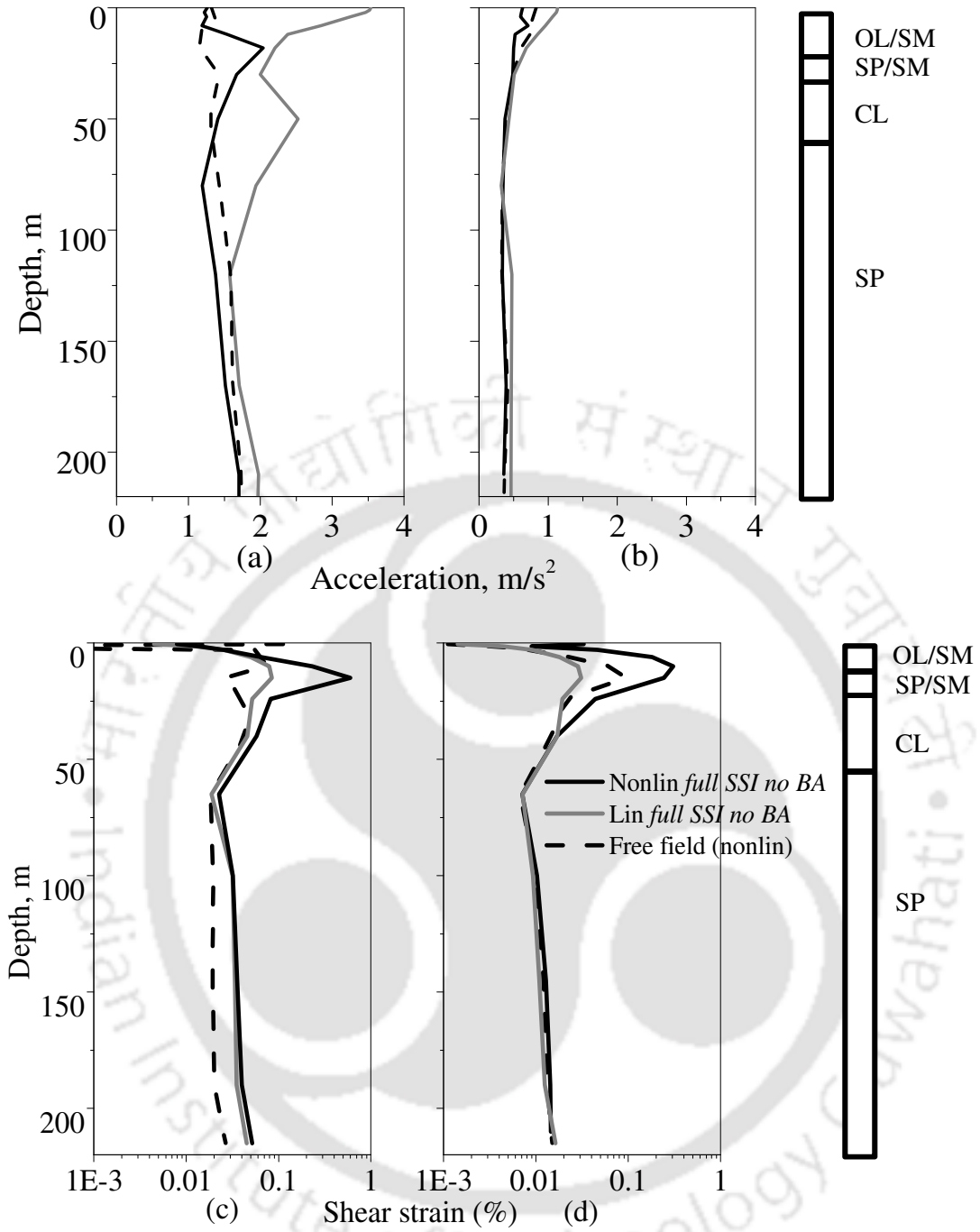

Fig. 5.14 Maximum horizontal acceleration profile along the depth of monitored soil column under (a) GM#1 and (b) GM#2; maximum shear strain profile along the depth of monitored soil column under (c) GM#1 and (d) GM#2.

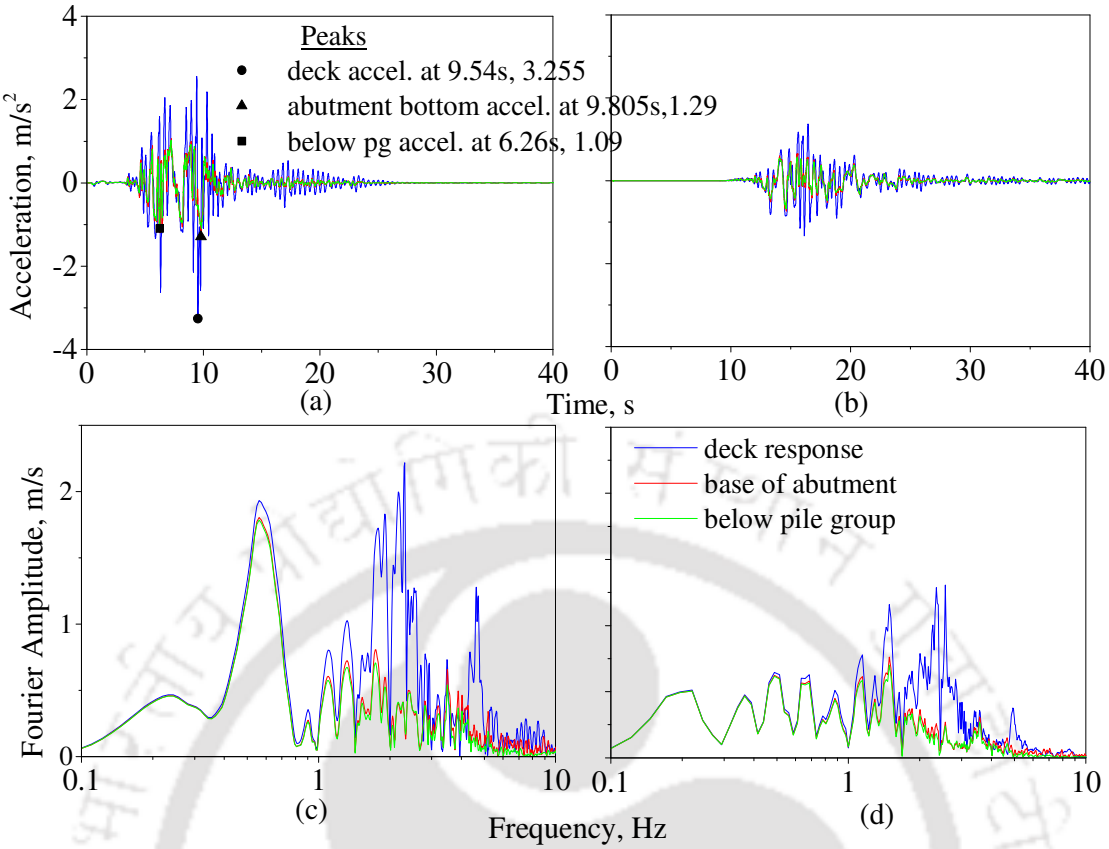

Fig. 5.15 Recorded ATHs along the vertical profile of right abutment-pile group-foundation (a) under GM#1, (b) under GM#2; FTs of ATHs (c) under GM#1 and (d) under GM#2 in *full SSI no BA* model.

5.4 Complementary Investigation of Material Properties in *Full SSI No BA* Model

The response of bridge-foundation-soil system with linear and nonlinear behaviours of different components are discussed in this section, i.e., linear behaviour of bridge with nonlinear behaviour of soil (*lin str+nl soil no BA*) model and nonlinear behaviour of bridge with linear behaviour of soil (*nl str+lin soil no BA*) model. The intention of the study is to investigate the individual effect of material nonlinearity on the overall response of the bridge. Under low level of shaking, *nl str+lin soil no BA* model remains linear like linear *full SSI no BA* model. *Lin str+nl soil no BA* model can be taken as an example of very stiff structure with very flexible soil profile e.g., nuclear structure. Although the vice versa is not realistic physically, still to investigate the influence of nonlinear structure on linear soil domain this case has been considered for the study.

5.4.1 Linear structural behaviour

For linear behaviour of the superstructure and the substructure, the influence of soil nonlinearity is visible by comparing the response of the linear behaviour of *full SSI no BA* model with the response of *lin str+nl soil no BA* model. From the observed SFTHs shown in Figs. 5.16(a) and 5.16(b), the nonlinearity of soil dominates the response in high intensity of shaking under GM#1for the *lin str+nl soil no BA* model. The peak shear force at the top of 8th pier gets reduced by a factor of 2.9 from the linear behaviour of *full SSI no BA* model to the response of *lin str+nl soil no BA* model. Normalized Fourier spectra of SFTHs are shown in Figs.5.16(c) and 5.16(d) under GM#1 and GM#2, respectively. From the Fig.5.16(c), it is observed that under GM#1, the shear force content is higher in frequency domain as compared to the content obtained under GM#2. Once the soil is nonlinear, the peaks of SFTHs occur at different frequencies in these two models. To study the shift in the frequency corresponding to the occurrence of peak Fourier amplitude, normalized FTs are studied. From the normalized response spectra plot in Fig. 5.16(c), it is visible that peaks of Fourier amplitudes are occurring at the frequency of 2.25Hz and 2.38Hz for the linear behaviour of *full SSI no BA* model and *lin str+nl soil no BA* model, respectively. Due to nonlinearity of soil domain, the latter model is more deformable and comparatively less seismic forces are imposed at the base of bridge substructure. Due to linear elastic material behaviour, the bridge structure is stiffer under this condition and leads to the mentioned shift in frequency. In Fig. 5.16(d), FTs of SFTHs of Fig. 5.16(b) are plotted and normalized by the peak amplitude value obtained from FT under GM#2 for the linear behaviour of *full SSI no BA* model to emphasize on the nonlinearity developed in *lin str+nl soil no BA* model under both the ground motions. The overall response for both the models gets reduced due to low intensity of shaking under GM#2, thus, the difference in the FT curves is not that significant.

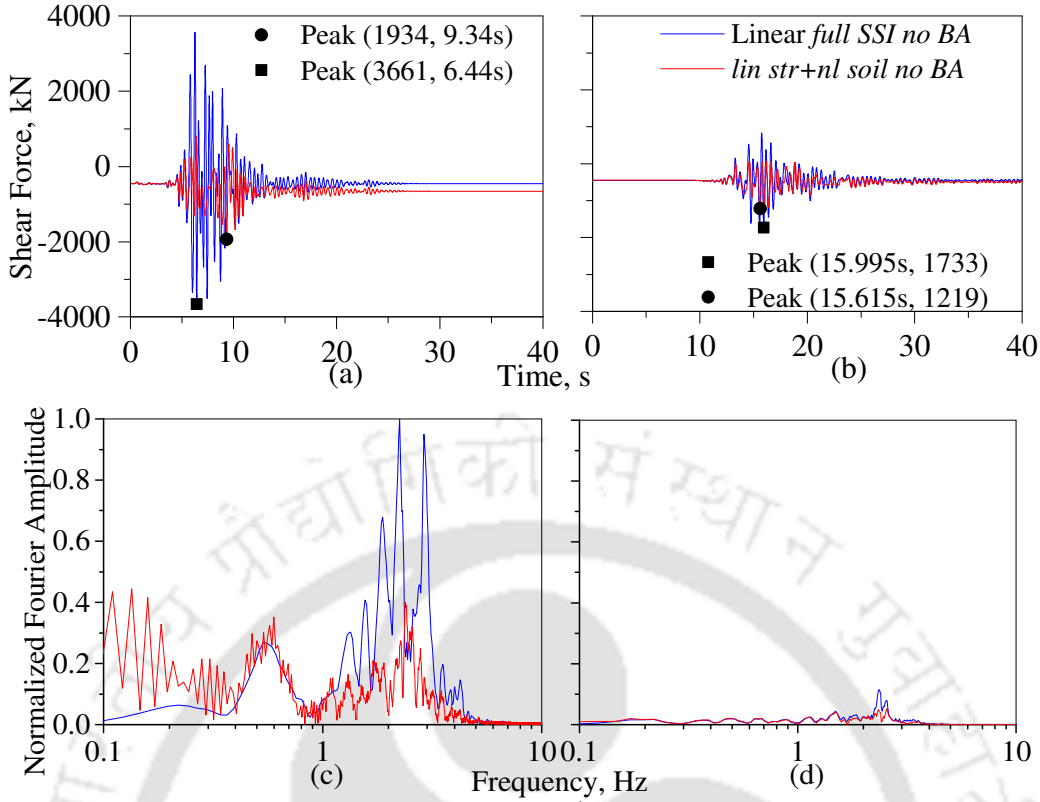

Fig.5.16 Comparison of SFTHs at the top of 8th pier of bridge for linear behaviour of *full SSI no BA* model and *lin str+nl soil no BA* model under (a) GM# 1, (b) GM#2 and normalized FTs of (c) SFTHs shown in (a) and (d) SFTHs shown in (b).

The same trend, as noted for the SFTHs, is observed in the velocity time history at the deck level for the two models under GM#1 and GM#2 (Figs. 5.17(a) and 5.17(b)). The observed peak velocities are 0.71 m/s and 0.40 m/s for the linear behaviour of *full SSI no BA* model and *lin str+nl soil no BA* model, respectively. Under GM#2, the overall response gets reduced which leads to very small difference in the VTHs of the two models. However, both the normalized FT plots show a significant frequency shift in the occurrence of peak Fourier amplitude of VTHs (Figs. 5.17(c) and 5.17(d)). Even for the VTH under GM#2, the difference in the distribution of deck velocity response in frequency domain is very obvious for the two models, unlike the FTs of SFTHs where the difference was very small.

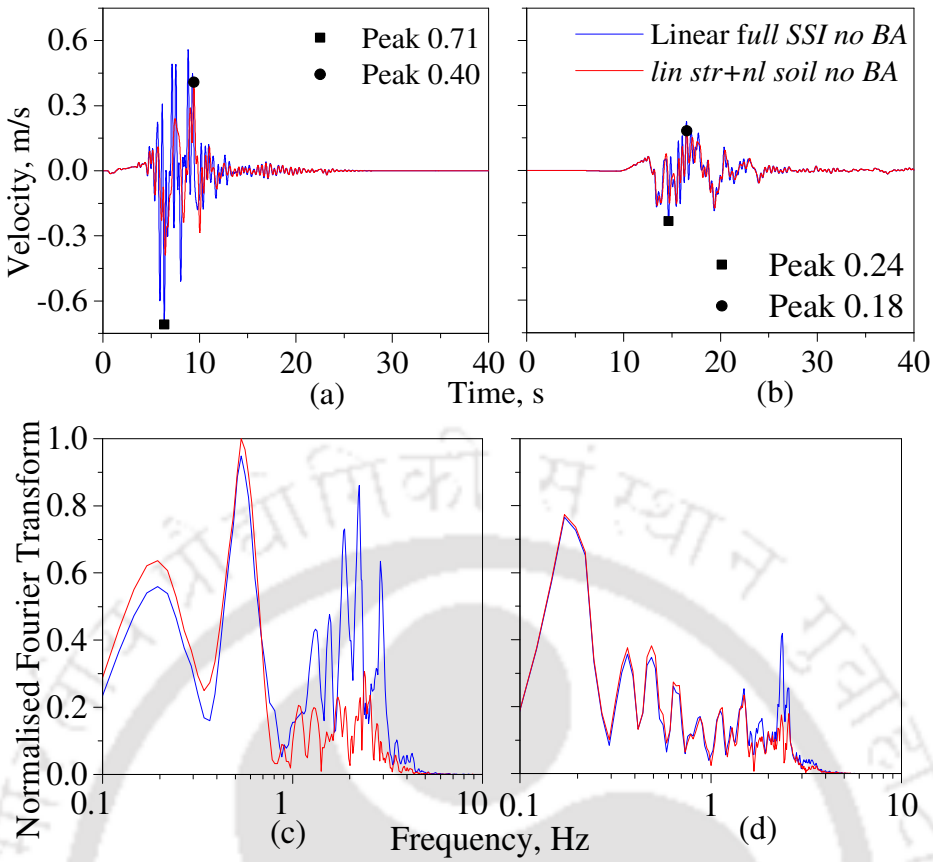

Fig. 5.17 Comparison of VTHs for linear behaviour of *full SSI no BA* model and *lin str+nl soil no BA* model at the 8th pier top under (a) GM#1and (b) GM#2; normalised FTs of VTHs under (c) GM#1 and (d) GM#2.

5.4.2 Nonlinear structural behaviour

The nonlinear behaviour of *full SSI no BA* model and the response of *nl str+lin soil no BA* model are compared to investigate the effect of soil nonlinearity (when the pier behaviour can be nonlinear) on the bridge response. From the SFTHs at the top of 8th pier for the two models under GM#1, the shear force for the nonlinear behaviour of *full SSI no BA* model is atleast 20% lesser than the shear force obtained for *nl str+lin soil no BA* model (Fig. 5.18(a)). However, under GM#2 also, the shear force response of *nl str+lin soil no BA* model exceeds that obtained for nonlinear behaviour of *full SSI no BA* model (Fig. 5.18(b)). This is due to the fact that for low intensity of earthquake shaking under GM#2, linear elastic behaviour is mobilized for the piers. Even the residual response after the dynamic analysis are similar in both the models which eventually depicts the response

under the initial static gravity analysis. So, in the modelling of this specific soil-foundation-bridge system, under higher PGA (≥ 0.48g of base excitation) nonlinearity of structure is likely to govern the response.

As observed in the results of the previous section, the normalized FT plots of SFTHs for the models show the same trend in the shift of frequency for the occurrence of peak Fourier amplitude under GM#1 (Fig. 5.18(c)). The peaks of normalized Fourier amplitude occur at 1.2 Hz and 0.6 Hz for *nl str+lin soil no BA* and nonlinear behaviour of *full SSI no BA* model, respectively. Under GM#2, the peaks of the Fourier amplitudes occur at 2.27 Hz and 2.34 Hz, respectively, for the two models (Fig. 5.18(d)). Due to high energy content in linear soil domain, *nl str+lin soil no BA* model's Fourier amplitude is significantly higher than the other one (Fig. 5.18(c)). For the nonlinear behaviour of *full SSI no BA* model, the input seismic energy gets reduced through soil damping around the bridge foundation; this further reduces the possibility of nonlinear behaviour in the bridge piers. Hence, for that model, the bridge behaviour is comparatively stiffer as compared to the behaviour obtained for *nl str+linsoil no BA* model. From the velocity time histories at right abutment-deck junction, the peak velocities occur at 8.885 s and 9.495s under GM#1 and at 17.065 s and 16.525 s under GM#2 for *nl str+lin soil no BA* model and for nonlinear behaviour of *full SSI no BA* model, respectively (Figs. 5.19(a) and 5.19(b)). Due to nonlinearity of soil, the peak velocity response of bridge reduces significantly under both the ground motions for the nonlinear behaviour of *full SSI no BA* model. Under both the ground motions, the frequency for the occurrence of peak Fourier amplitude is observed to be higher for the *nl str+lin soil no BA* model as compared to the other model (Figs. 5.19(c) and 5.19(d)). The difference in the magnitude of the peak Fourier amplitudes for the models also reflects the higher velocity response of the *nl str+lin soil no BA* model as compared to the other model. From these type of comparisons, it is easy

to conclude that under low intensity of ground motion, nonlinearity of soil highly influences the nonlinear behaviour of structure.

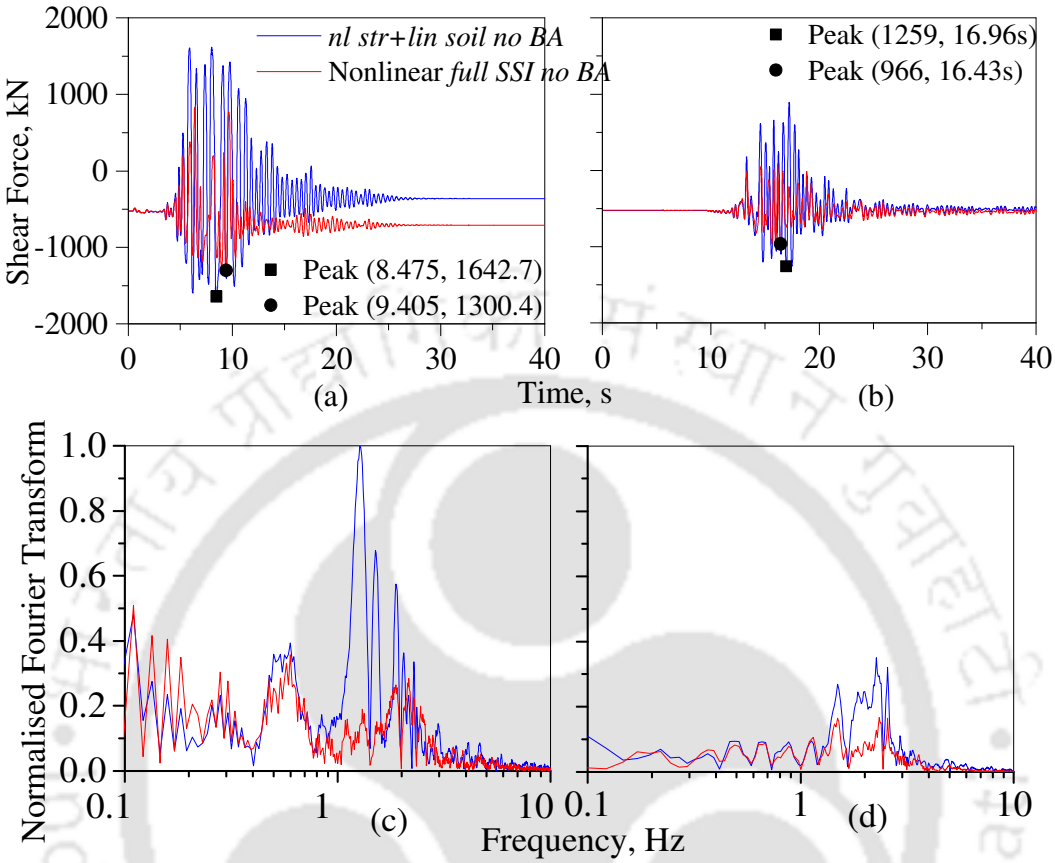

Fig. 5.18 Comparison of SFTHs for the nonlinear behaviour of *full SSI no BA* model and the *nl str+lin soil no BA* model at the top of 8th pier of bridge under (a) GM# 1 and (b) GM#2; normalized FTs of SFTHs under (c) GM#1and (d) GM#2.

5.5 Influence of Abutment Backfill Interaction

After studying different modelling cases without abutment backfill interaction, finally abutment backfill soil is modelled with four noded quadrilateral elements having pressure independent multi-yield material properties. Nonlinear material properties of the backfill soil are kept the same as that of the top surface soil layer. Abutment and backfill interface nodes are connected with equal degrees of freedom in horizontal and vertical directions in the 2D plain strain model. The soil-foundation-bridge system with abutment backfill soil is referred to as *full SSI with BA* model in the further study. The undeformed and deformed shapes of the *full SSI with BA* model in the near field zone are shown in Figs.

5.20(a) and 5.20(b), respectively. From the Fig. 5.20(b), it is observed that in presence of abutment backfill, the overall deformation and imposed forces in the different bridge components get reduced because the abutment backfill tends to restrain both the ends of the bridge in the longitudinal direction. The backfill soil helps bridge members to sustain less amount of seismic forces through reduction in displacement at bridge substructure. Also, the density and stiffness of the backfill soil are expected to play a major role in the response of the bridge structure. The backfill should neither be too stiff to be undeformable nor too loose such that it is unable to withstand seismic forces coming from bridge.

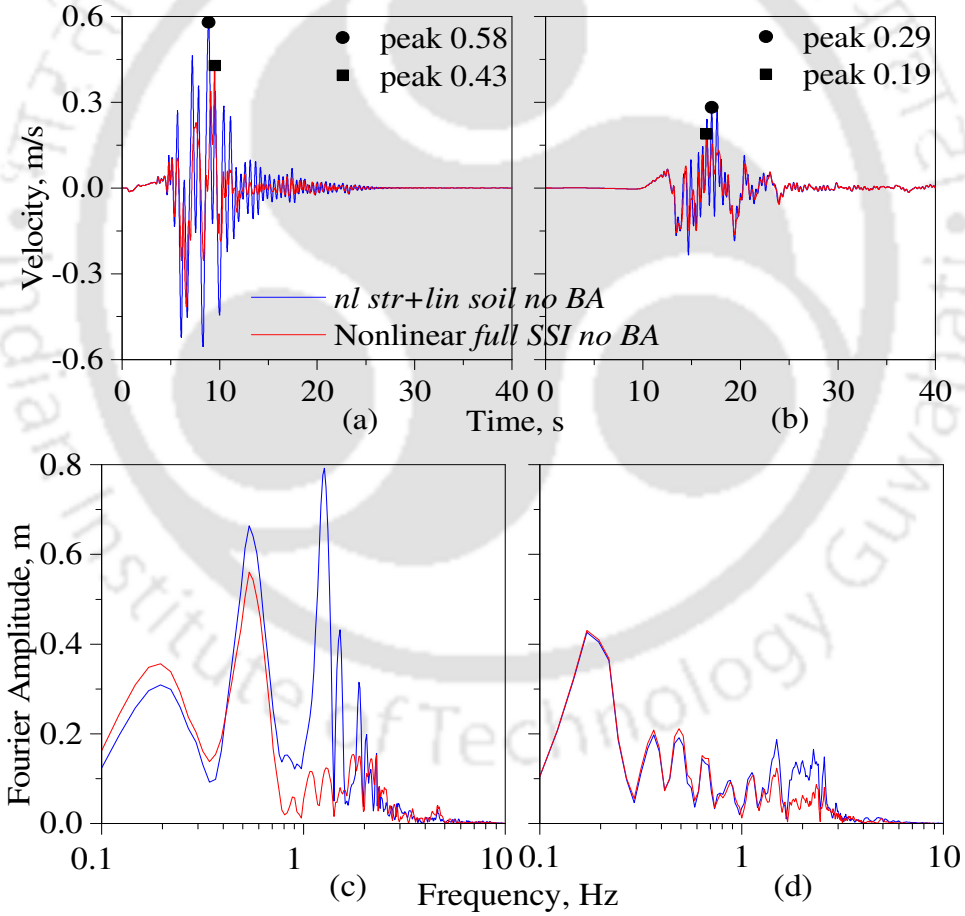

Fig.5.19 Comparison of VTHs at right abutment deck joint for the nonlinear behaviour of *full SSI no BA* model and the *nl str+lin soil no BA* model under (a) GM#1 and (b) GM#2; Fourier amplitudes of VTHs under (c) GM#1 and (d) GM#2.

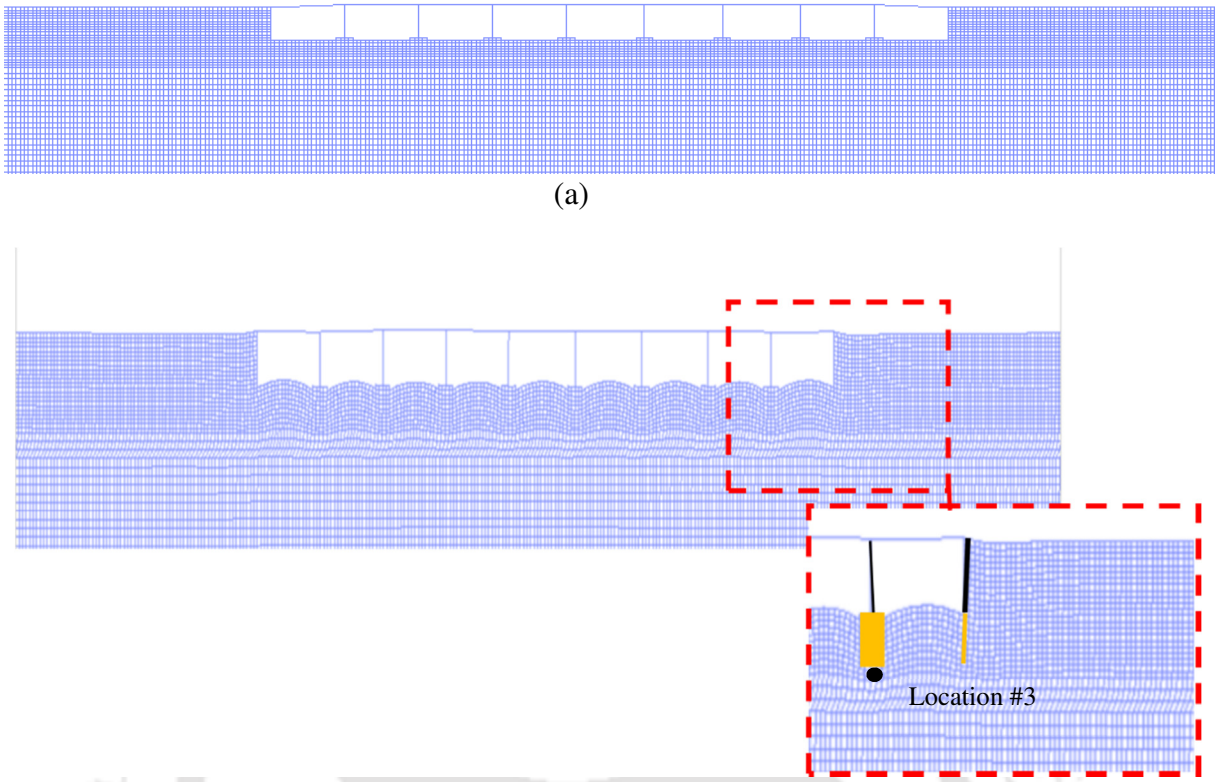

Fig.5.20 (a) Undeformed shape and (b) deformed shape of *full SSI with BA* model after dynamic analysis under GM#1.

SFTHs are plotted at the top of 8th pier in Fig. 5.21(a) for *full SSI no/with BA* models under GM#1. Peak SF at the top of 8th pier is atleast 31% lower in *full SSI with BA* model as compared to the other one. From the residual shear force at the end of GM#1, it can be stated that due to abutment backfill interaction the residual force at the top of the 8th pier is 133 kN; whereas, in *full SSI no BA* model, the residual SF is 709 kN. Thus, the sructure is going through significant nonlinearity at the end of dynamic motion for the *full SSI no BA* model. From the normalised fourier amplitude of SFTHs in Fig. 5.21(b), *full SSI no BA* model's peak Fourier amplitude is higher than *full SSI with BA* model as it carries more seismic forces. With backfill soil, the abutments and the superstructure (deck) undergo less amount of deformation because the seismic forces dissipate through backfill and it results in significant backfill deformation by the end of dynamic analysis (Fig.5.20(b)). At a depth of 1 m below the tip of pile foundation underneath the 8th pier,

displacement time histories (DTHs) are shown for both the models (Fig. 5.21(c)) and in *full SSI with BA* model, foundation soil is more deformable than the other one. The peak acceleration at the top of 8th pier reduces from 2.98 m/s^2 to 1.94 m/s^{2}in *full SSI with BA* model (Fig. 5.21(d)). Hence, seismic acceleration of the bridge stricture in *full SSI with BA* model is less than *full SSI no BA* model under GM#1, which reduces the overall deck response. At location#3, free field soil has a peak displacement of 0.15 m. The *full SSI with BA* model and the free field soil domain have a relative displacement of 0.02 m after the instant of peak response and relative residual displacement is also 0.027 m which is insufficient to mobilize the passive pressure under dynamic loading. According to AASHTO (2012), integral abutment should be allowed to get displaced upto maximum limit of 0.091 m under cyclic loading.

In Fig. 5.22, SFTHs are monitored at the top of 8th pier under GM#2. The abutment backfill soil influences the response of structure as well as soil in case of low intensity of input motion too. In presence of abutment backfill, the peak shear force at the top of 8th pier reduces from 966.4kN to 805.8kN. The normalised Fourier amplitudes have been obtained by normalising the FT values with respect to peak amplitude of *full SSI no BA* model. In normalised fourier amplitude of SFTHs (Fig. 5.22(b)), the differences in Fourier amplitude for the frequency range of 1–4 Hz occur because *full SSI no BA* model carries higher seismic forces in that frequency range. In Fig. 5.22(c), ATHs are shown at left deck-abutment joint and the peaks of ATHs are 1.26 m/s^2 and 1.35 m/s^2 for *full SSI with BA* and *full SSI no BA* model, respectively. Fig. 5.22(d) shows fourier amplitude of ATHs shown in Fig. 5.22(c). The peaks of fourier amplitudes occur in the frequency range of 2.5 Hz to 3.3 Hz for the models.

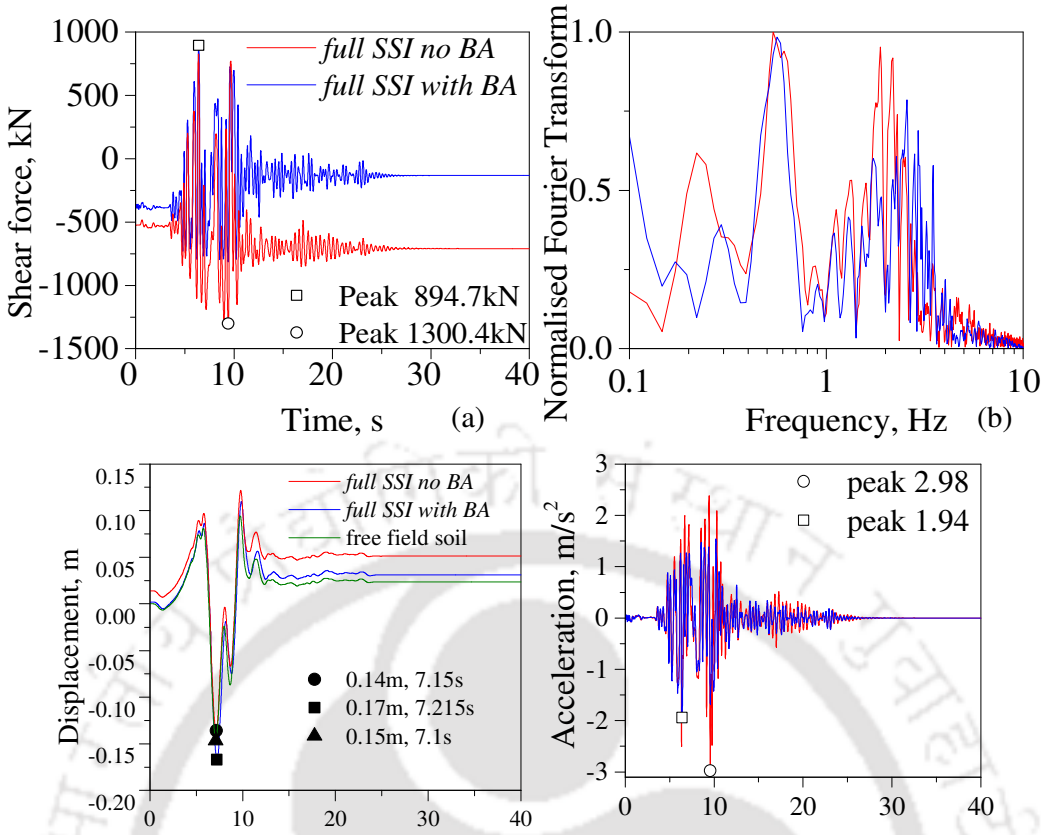

Fig. 5.21 Comparison of (a) SFTHs at the top of 8th pier, (b) normalized FTs of SFTHs shown in (a), (c) DTHs of soil node in pile-foundation below the 8th pier at location #3, and (d) ATHs at the top of 8th pier under GM#1 for *full SSI no BA* model and *full SSI with BA* model.

Moment-curvature response at the top and bottom cross-sections of the 8th pier under GM#1 are shown in Figs. 5.23(a) and 5.23(b), respectively. Although in both the models, very narrow nonlinear moment-curvature loops are forming, the extent of nonlinearity in *full SSI with BA* model is less as compared to the level of nonlinearity in *full SSI no BA* model. Hence, abutment backfill is expected to play a major role in the seismic analysis of integral bridges.

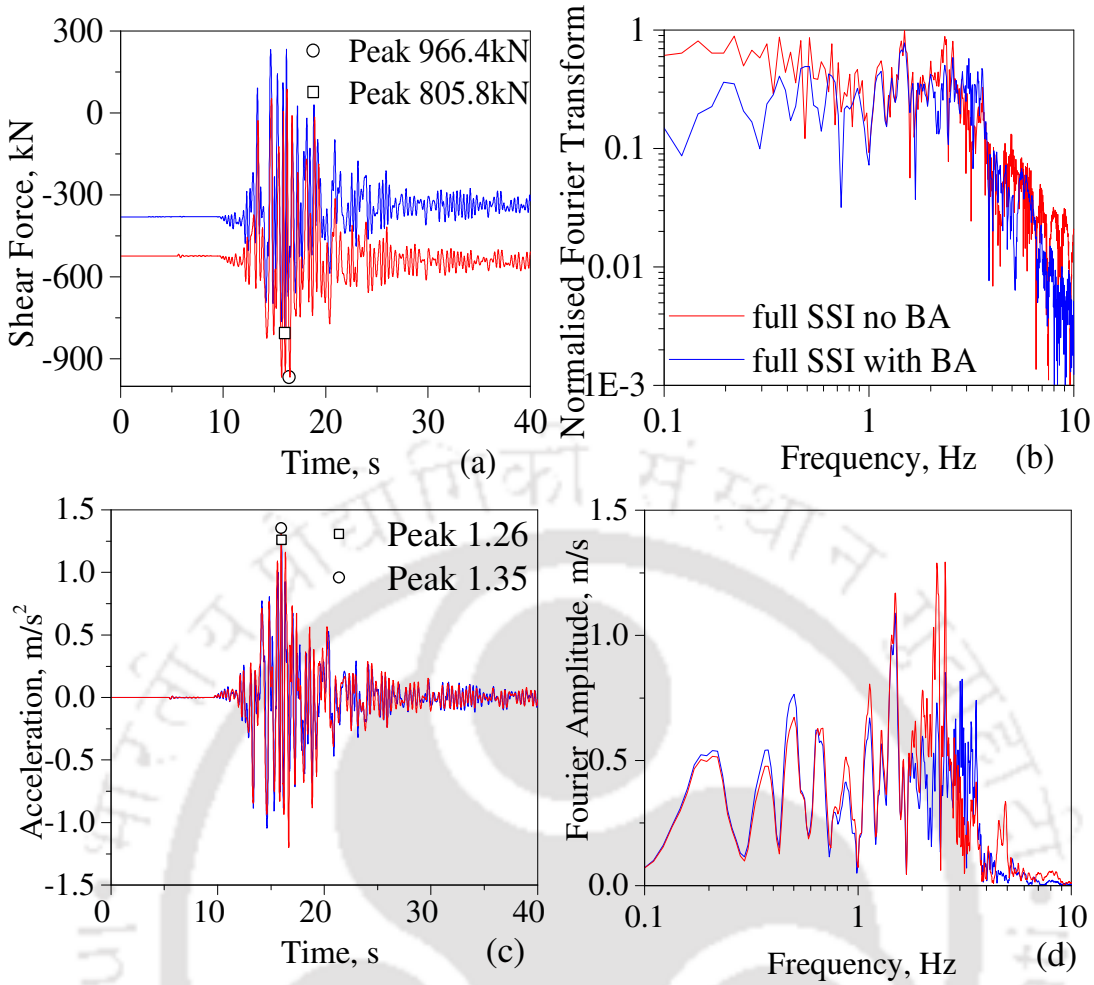

Fig. 5.22 Comparison of (a) SFTHs at the top of 8th pier, (b) normalized FTs of SFTHs shown in (a) in log-log scale, (c) ATHs at 1st pier top, (d) FTs of ATHs shown in (c) under GM#2 for *full SSI no BA* model and *full SSI with BA* model.

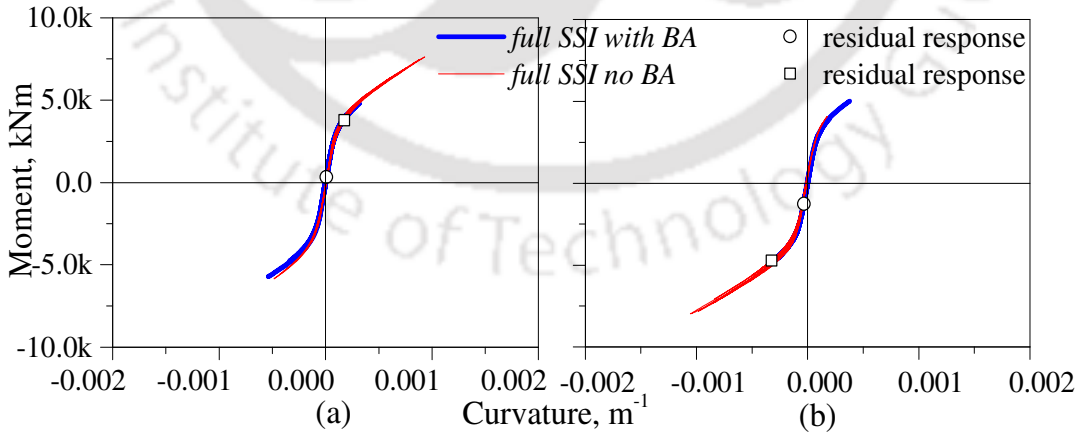

Fig. 5.23 Comparison of moment curvature response at the (a) bottom and (b) top cross-sections of the 8th pier under GM#1 for *full SSI no BA* model and *full SSI with BA* model.

To obtain the material level response, the behaviour of the steel, core concrete and cover concrete fibers (locations denoted in Fig. 3.1(c)) at the top level of 8th pier are monitored under GM#1. In *full SSI no BA* model, concrete fibers have not yielded. With the effect of backfill soil, further the strain demand reduces in the uniaxial response of the fibers. For Steel fiber 1 (Fig. 5.24 (a)), the response of *full SSI no BA* model larger strain deformation and yielding of steel; however the Steel fiber 2 (Fig. 5.24 (b)) shows linear elastic behaviour for both the models under GM#1. In *full SSI with BA* model, Core concrete fiber 3 and Cover concrete fiber 3 (in Figs. 5.24(c) and 5.24(d)) undergo lesser tensile deformation as compared to the behaviour of *full SSI no BA* model under GM#1. Based on the comparisons of bridge response between the *full SSI with BA* model and *full SSI no BA* model, it can be stated that the presence of abutment backfill soil can dominate the overall response of the integral bridge.

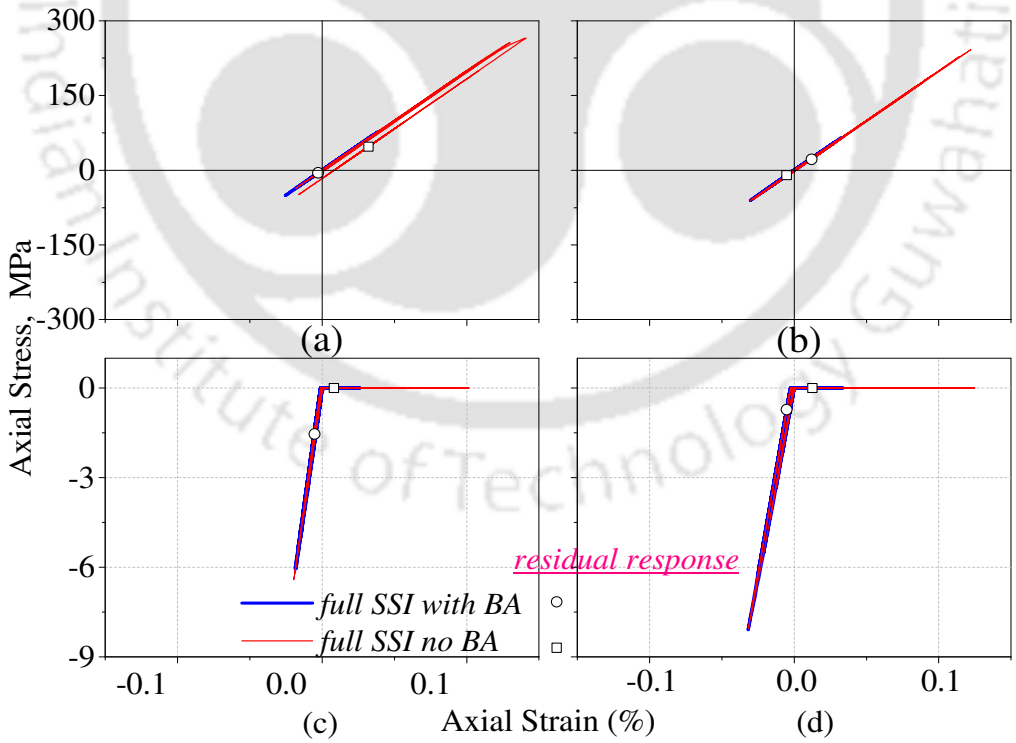

Fig. 5.24 Stress-strain response at top of 8th pier cross-section for (a) Steel fiber 1, (b) Steel fiber 2, (c) Core concrete fiber 3 and (d) Cover concrete fiber 3 shown in Fig.3.1(a), under GM#1 for *full SSI no BA* and *full SSI with BA* models.

5.6 Introduction of Nonlinear Spring-Dashpot Model

Analysis of SSI problems with detailed modelling of soil domain involves significant computational efforts. In order to reduce that effort, simplified modelling using spring-dashpot elements is adopted as an alternative method. Hence, nonlinear springs and dashpots are introduced to represent soil stiffness, replicating Soil-Pile Interaction (SPI) and Abutment Backfill Interaction (ABI) in bridge with spring dashpot model without abutment backfill soil (referred to as *FB_SD no BA* model) and in bridge with spring dashpot model with abutment backfill soil (referred as *FB_SD with BA* model). In this section, structural response are determined using nonlinear time history analysis, to investigate the overall seismic response of the integral bridge using both detailed domain modelling approach and spring-dashpot modelling approach of the soil.

5.6.1 Comparison between full SSI no BA and FB_SD no BA models

Under GM#1, the ATHs at the top and the bottom of the 8th pier are shown in Figs. 5.25(a) and 5.25(b). The respective Fourier Transforms (FT) are shown in the Figs. 5.25(c) and 5.25(d). The ATHs at the bottom of the pier match closely with each other (Figs. 5.25(a) and 5.25(c)), but at the deck level (Figs. 5.25(b) and 5.25(d)), *FB_SD no BA* model shows more amplified response as compared to the *full SSI no BA* model. However, the peaks of Fourier amplitude occur at 1.78 Hz and 2.29 Hz for *FB_SD no BA* and *full SSI no BA* models, respectively. Foundation of *FB_SD no BA* model is observed to be stiffer as the API curves overestimate the lateral soil stiffness at different depths of the piles. Thus, nonlinearity is unable to develop in the underlying soil. Moreover, an amplifying effect is also noted at 1.78 Hz as the natural frequency of the model is 2.05 Hz, which is not present in the *full SSI no BA* model.

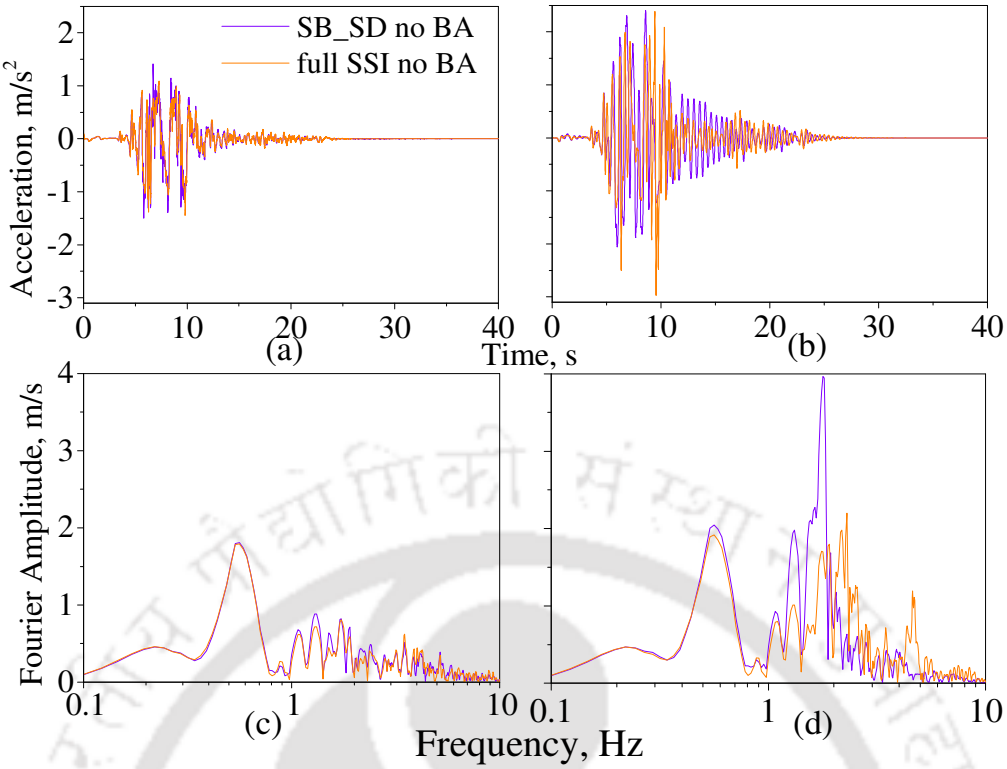

Fig. 5.25 Comparison of ATHs for *full SSI no BA* model and *FB_SD no BA* model under GM#1 at (a) the bottom and (b) the top of the 8th pier; (c) FT of the ATHs shown in (a) and (d) FT of the ATHs in (b).

Similar response is observed for SFTHs shown in Fig. 5.26(a). Due to amplification of seismic waves at the deck level, the peak shear force is higher in *FB_SD no BA* model as compared to the *full SSI no BA* model. From the SFTH, it can be stated that *FB_SD no BA* model carries significantly more seismic forces as compared to the *full SSI no BA* model. Normalized FTs of the SFTHs are shown in Fig. 5.26(b) and the magnitude of Fourier amplitude is significantly higher in *FB_SD no BA* model than *full SSI no BA* model. The same behavior is also reflected from the moment-curvature response at the top and bottom cross-sections of the 8th pier (Figs. 5.26(c) and 5.26(d)). Moment-curvature response at the top of 8th pier is found to be lesser in *FB_SD no BA* model and mainly forms negative moment-curvature loops in the third quadrant. At the base of the 8th pier, moment curvature response (Fig. 5.26(d)) shows similar pattern on the opposite quadrants. Thus, it can be stated that the response of the *FB_SD no BA* model gets more amplified from the foundation to the deck level as compared to the *full SSI no*

BA model. In conventional bridges, piers at the bottom sections are more prone to form hinges. But in an integral bridge, in absence of any bearing and energy dissipating device, top section of the pier can also attract high forces and moments, thus, making it prone to formation of plastic hinges and subsequent failure.

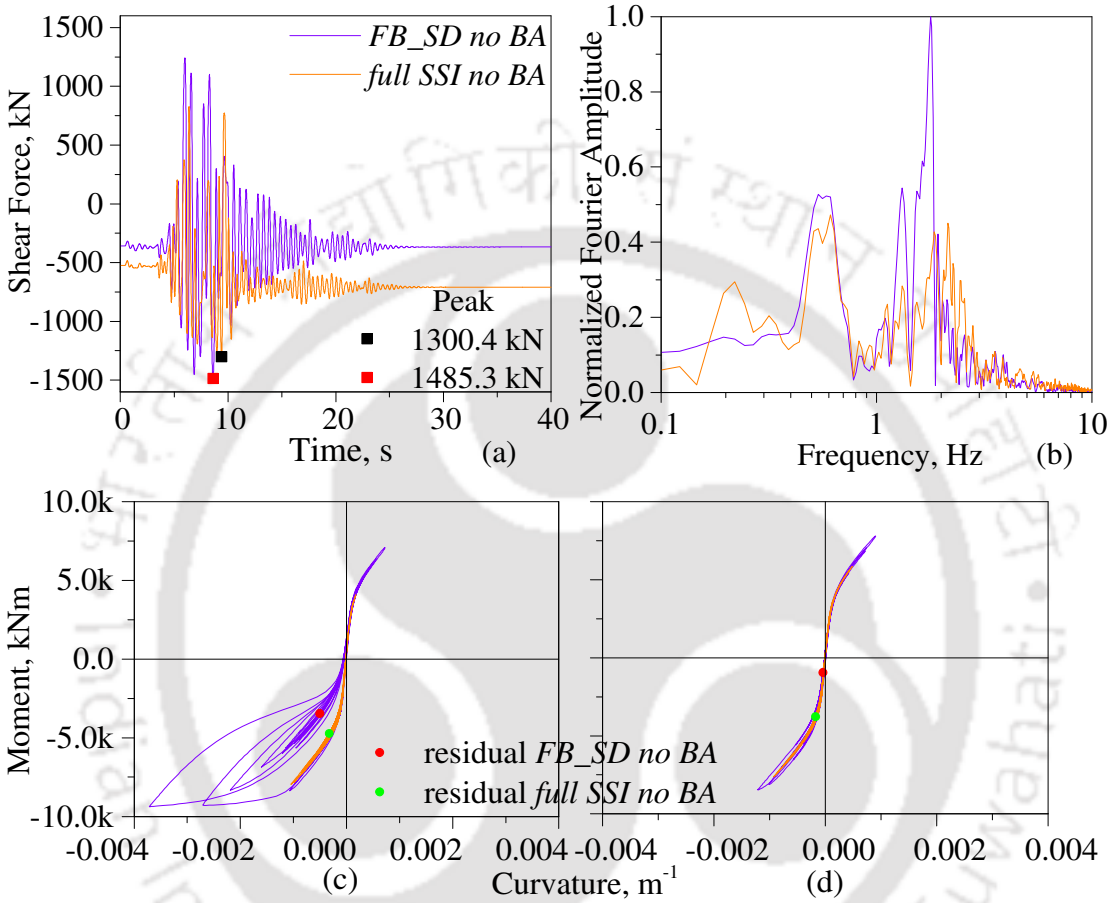

Fig. 5.26 Comparison of (a) Shear Force time history at the top of 8th pier and (b) normalised FTs of the SFTHs for the *full SSI no BA* model and *FB_SD no BA* model; moment-curvature response at the (c) top and (d) bottom cross-sections of the of 8th pier under GM#1.

Under GM#2, SFTHs at the top of 8th pier (deck level) are shown for the two models in Fig. 5.27(a). The difference in energy content of the response is observed through the normalized FT of SFTHs in Fig. 5.27(b). Similar response is also obtained under GM#2.

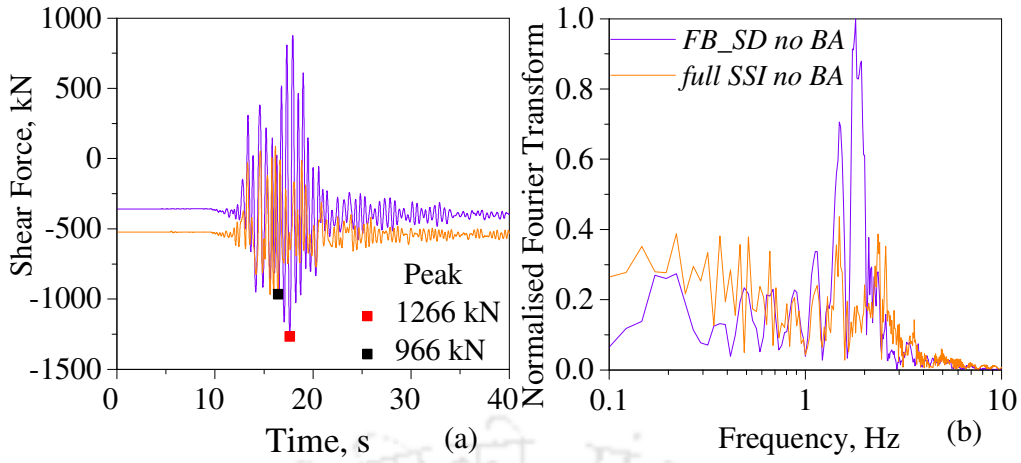

Fig. 5.27 (a) SFTH at the top of 8th pier and (b) normalised FTs of the SFTHs in (a) under GM#2.

5.6.2 Comparison between full SSI with BA and FB_SD with BA models

For comparison, the ATHs under GM#1 are shown at the bottom and the top of the eighth pier in Figs. 5.28(a) and 5.28(b), and the corresponding Fourier amplitudes of ATHs are shown in Figs. 5.28(c) and 5.28(d). Peak acceleration at the base of the pier in *FB_SD with BA* model is marginally higher than that obtained for *full SSI with BA* model. Thus, in Fig. 5.28(c), the Fourier amplitude is almost incomparable in frequency domain. However, at the top of 8th pier (Fig. 5.28(b)), ATHs are quite comparable for both the models. In Fig. 5.28(d), the peak Fourier amplitudes for *FB_SD with BA* and *full SSI with BA* models are at 2.83Hz and 2.12Hz, respectively, which indicates that *FB_SD with BA* model contains marginally higher seismic acceleration as compared to the *full SSI with BA* model. Hence, the possibility of nonlinear behaviour is likely to be higher for *FB_SD with BA* model.

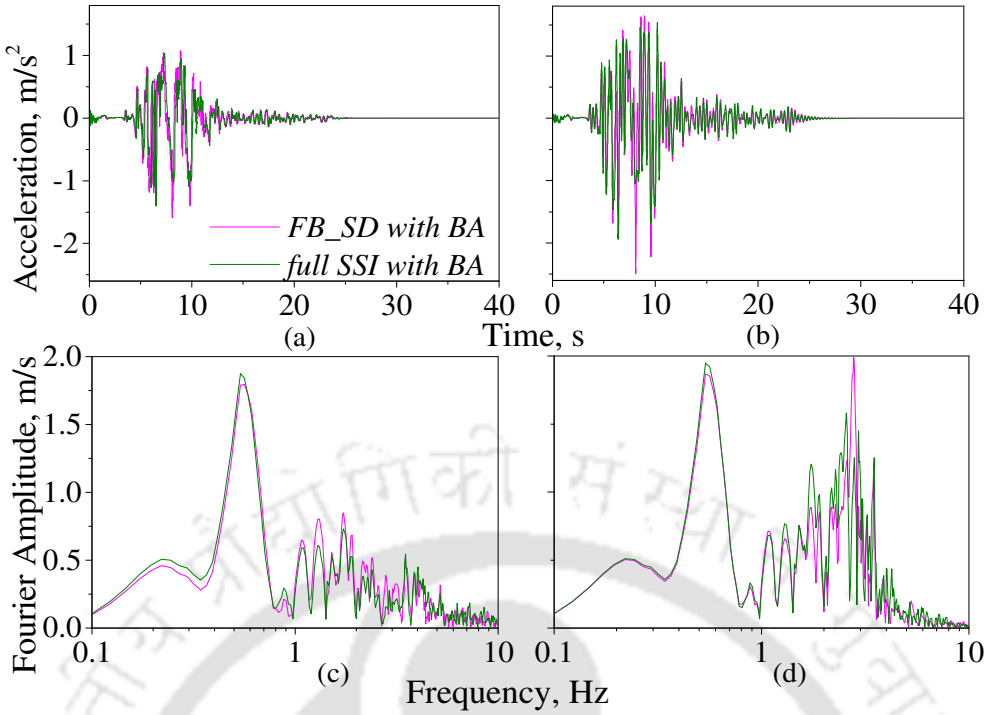

Fig. 5.28 Comparison of ATHs for *full SSI with BA* model and *FB_SD with BA* model at the (a) top and the (b) bottom of 8th pier; (c) Fourier transform of the ATHs shown at the (a) bottom and (d) the top of 8th pier under GM#1.

Under GM#2, similar responses are observed for the ATHs at the bottom and top of first pier (Figs. 5.29(a) and 5.29(b)); their corresponding FTs are shown in Figs. 5.29(c) and 5.29(d), respectively. Due to low intensity input motion, the ATHs at the base of the pier are quite similar for both the models along with their FTs. In Fig. 5.29(d), peak amplitudes occur at the frequencies of 1.48 Hz and 3.07 Hz for *FB_SD with BA* and *full SSI with BA* model, respectively. At low intensity of PGA input, foundation soil is expected to remain linear elastic. The influence of nonlinearity of the foundation soil links on the behaviour of the superstructure is insignificant, thus the bridge response is observed to get amplified at deck-level with higher nonlinearity mobilized in *FB_SD with BA* model as compared to the *full SSI with BA* model. Thus, the peak of FT in Fig. 5.29(d) for *FB_SD with BA* model is at a lower frequency than the frequency for peak FT of the *full SSI with BA* model. Moreover, amplitudes are quite the same both temporally and spectrally.

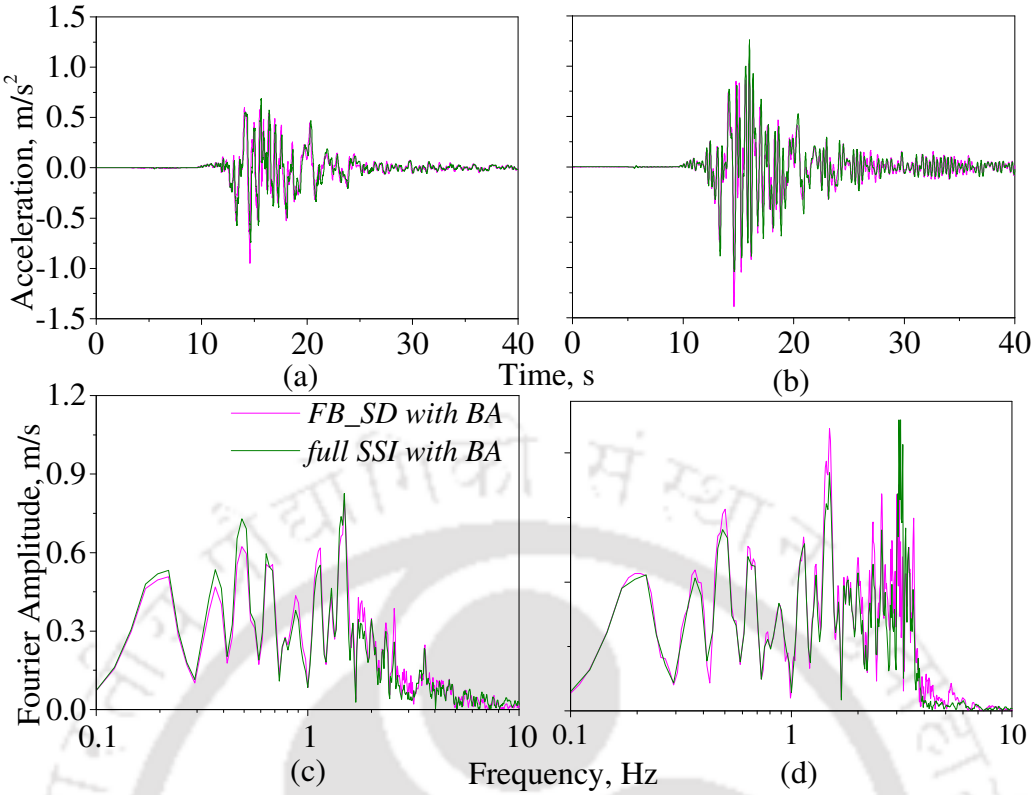

Fig. 5.29 Comparison of ATHs for *full SSI with BA* model and *FB_SD with BA* model at the (a) top and the (b) bottom of the 8th pier; Fourier transform of the ATHs shown at the (c) bottom and the (d) top of the pier under GM#2

Under GM#1, the SFTHs at the top of the 8th pier in *FB_SD with BA* model are shown in Fig. 5.30(a). Both the peak and the residual shear forces are higher as compared to the *full SSI with BA* model due to large nonlinearity developing in the *FB_SD with BA* model. The Fourier amplitude plot of SFTHs in Fig. 5.30(b) also shows that in *FB_SD with BA* model, the seismic forces are higher as compared to the *full SSI with BA* model below the frequency of 0.8 Hz, beyond which the SSI model shows higher seismic force. The peaks of Fourier amplitudes occur at 0.42 Hz and 1.06 Hz for *FB_SD with BA* and *full SSI with BA* models, respectively. Thus, it signifies that in the former model, seismic response is being more amplified at deck level and more nonlinearity develops at pier sections as compared to the *full SSI with BA* model. Under GM#2, the variation of SFTHs at the top of ninth pier shows that the peak shear force in *FB_SD with BA* model is higher as compared to the *full SSI with BA* model (Fig. 5.30(c)); also the *FB_SD with BA* model

shows higher residual response. Thus, in *FB_SD with BA* model, piers have developed significant nonlinearity as compared to the *full SSI with BA* model. From the comparison of Fourier amplitudes of SFTHs in Fig. 5.30(d), the shear force content is observed to be higher in *FB_SD with BA* model upto a frequency of 1Hz, beyond which the *full SSI with BA* model carries higher forces in the high frequency range. This further proves that the *FB_SD with BA* model shows higher extent of nonlinear behaviour and as compared to the *full SSI with BA* model. At low frequencies, the discrepancies in the FT plots (Figs. 5.30(b) and 5.30(d)) are due to the residual response in SFTHs (Figs. 5.30(a) and 5.30(c)), respectively.

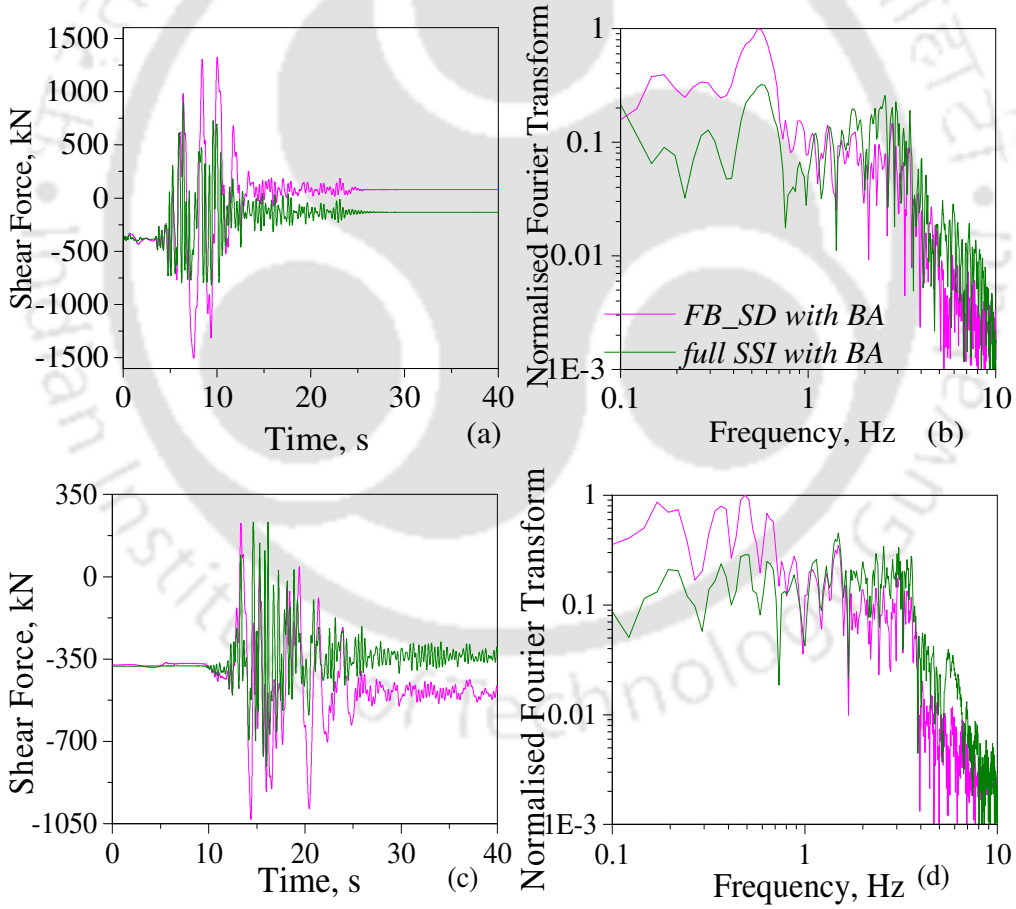

Fig. 5.30 Comparison of SFTHs for *full SSI with BA* model and *FB_SD with BA* model (a) at the top of the 8th pier and (b) normalised FTs of the SFTHs in (a) under GM#1; (c) SFTHs at the top of 8th pier and (d) normalised FTs of the SFTHs in (c) under GM#2 [FT plots in log-log scale]

5.7 Mean Maximum Response

Based on the analyses of the different models, the average of the maximum response is evaluated from all the seven ground motions (Table. 5.2). For the linear and nonlinear time history analyses, it is observed that for the *B_FF*, *B_SSI* and *full SSI no BA* models, the mean peak response corresponding to the bending moment and shear force in piers follow similar trends. *Only B_FF* model shows higher response as compared to the *only B_SSI* and *full SSI no BA* models. In LTHA and NTHA, the mean peak lateral drifts at deck level do not follow the trend as that observed for shear force and bending moment. The observed mean peak drifts are higher in *full SSI no BA* model than the drift levels of *only B_FF* and *only B_SSI* models. This occurs due to the underlying soil continuum elements that tend to impart increase deformability of the bridge structure. Maximum deck acceleration follows the usual trend but mean peak acceleration in nonlinear THA is highest for nonlinear *full SSI no BA* model as nonlinearities in substructure and soil influence the response of bridge superstructure in this case.

In linear THA, the residual response becomes the same as the static response from staged gravity analysis. But to investigate the influence of nonlinearities in soil and structure separately, two contemporary cases are considered, namely the (a) *lin str+nl soil no BA* model and the (b) *nl str+lin soil no BA* model. The bending moment and shear force response in piers of the *lin str+nl soil no BA* model are approximately 0.26 times less and 1.67 times more than the response from the linear and nonlinear behaviours of *full SSI no BA* model, respectively. On the other hand, the bending moment and shear force response in piers of the *nl str+lin soil no BA* model are 0.19 times less and 1.18 times more than the response from the linear and nonlinear behaviours of the *full SSI no BA* model, respectively. So, nonlinearity of structure is observed to govern the response under the considered set of site specific ground motions for which the average PGA is

0.48g. On the contrary, it is observed in Section 5.4.2, nonlinearity of soil tends to dominate the response under low PGA of ground motions. Once the abutment backfill soil is introduced in the *full SSI no BA* model, the bending moment and shear force get further reduced by approximately 20% during its nonlinear behaviour. Residual shear force is also the lowest for the nonlinear behaviour of the *full SSI with BA* model, but the residual displacement in *full SSI with BA* model is more than nonlinear *full SSI no BA* model. Deck acceleration and displacement are lower in *lin str+nl soil no BA* model as compared to the nonlinear behaviours of *full SSI no BA* model and *nl str+lin soil no BA* model. Because of soil nonlinearity, high frequency seismic waves get filtered and lesser forces are imposed on the bridge structure. Residual displacement is lowest in *nl str+lin soil no BA* model as compared to the values obtained in the nonlinear behaviour of all other models. This is due to the occurrence of static drift as residual response at the end of dynamic analysis.

Thus, after comparing the two contemporary cases, it is observed that the residual response depends primarily on the deformation of the foundation soil. Under NTHA, the shear force and bending moment response in piers for *FB_SD no BA* model are observed to be higher than those obtained for *full SSI no BA* model. Residual shear force is higher for the nonlinear behaviour of the *full SSI no BA* as compared to that in *FB_SD no BA* model because of nonlinearity in the continuum soil domain. Similarly, response for *FB_SD with BA* model is observed to be significantly higher than the nonlinear response of *full SSI with BA* model with respect to the monitored bridge parameters, like bending moment, shear force, moment-curvature and horizontal acceleration at deck level. Overall, Table. 5.2 gives insight into the response of the structure under different input motions (free field or SSI), material properties (linear or nonlinear) and boundary conditions (presence or absence of abutment backfill soil).

Table 5.2 Mean maximum response from time history analyses

Parameters	Linear Analyses		Nonlinear Analyses	
Pier Bending Moment, kNm	*Only B_FF*	61,649	*Only B_FF*	7,475
	Only B_SSI	49,039	*Only B_SSI*	7,291
	full SSI no BA	46,021	*full SSI no BA*	6,984
			FB_SD no BA	7,003
			Lin Str+nl Soil no BA	12,361
			nl Str+Lin soil no BA	82,45
			full SSI with BA	5,687
			FB_SD with BA	6,407
Pier Shear Force, kN	*Only B_FF*	9,984	*Only B_FF*	1,419
	Only B_SSI	7,889	*Only B_SSI*	1,382
	full SSI no BA	7,467	*full SSI no BA*	1,332
			FB_SD no BA	1,473
			Lin Str+nl Soil no BA	2,031
			nl Str+Lin soil no BA	1,562
			full SSI with BA	1,078
			FB_SD with BA	1,417
Residual shear Force, kN	*Only B_FF*	Static shear forces	*Only B_FF*	409
	Only B_SSI		*Only B_SSI*	408
	full SSI no BA		*full SSI no BA*	650
			FB_SD no BA	416
			Lin Str+nl Soil no BA	639
			nl Str+Lin soil no BA	395
			full SSI with BA	169
			FB_SD with BA	553
	Only B_FF	18.8	*Only B_FF*	2.6

Deck Acceleration, m/s^2	*Only B_SSI*	14.6	*Only B_SSI*	2.5
	full SSI no BA	13.9	*full SSI no BA*	2.9
			FB_SD no BA	2.1
			Lin Str+nl Soil no BA	2.8
			nl Str+Lin soil no BA	3.2
			full SSI with BA	2.4
			FB_SD with BA	2.5
Total deck displacement, m	*Only B_FF*	0.166	*Only B_FF*	0.165
	Only B_SSI	0.156	*Only B_SSI*	0.162
	full SSI no BA	0.16	*full SSI no BA*	0.164
			FB_SD no BA	0.165
			Lin Str+nl Soil no BA	0.162
			nl Str+Lin soil no BA	0.18
			full SSI with BA	0.178
			FB_SD with BA	0.166
Total residual displacement, m	*Only B_FF*	0.002	*Only B_FF*	0.041
	Only B_SSI	0.002	*Only B_SSI*	0.036
	full SSI no BA	0.015	*full SSI no BA*	0.045
			FB_SD no BA	0.06
			Lin Str+nl Soil no BA	0.04
			nl Str+Lin soil no BA	0.02
			full SSI with BA	0.054
			FB_SD with BA	0.071

5.8 Discussion

Different modelling aspects to incorporate SSI have been studied in this chapter to understand the behaviour or importance of soil on structural response of the bridge.

Although the effect of SSI is not considered in the structural design guidelines of the integral bridge extensively, still the seismic behaviour of an integral bridge can significantly differ for various types of input motion and material properties. Similarly, difference in seismic response will be obtained by considering different modelling approaches. The present study is intended to provide an overview of the variation in response that can be obtained by adopting different modelling approaches. The easiest way to consider SSI in modelling is to replace the soil continuum with suitable springs and dashpots, representing the surrounding soil medium's stiffness and damping respectively. The influence of site-specific ground motions, as obtained from REXEL-DISP software in the present study, on the seismic response of bridge-foundation-soil system is also investigated. The ground motions have been selected in such a way that the mean displacement spectrum from all the ground motions matches closely with the site-specific target displacement spectrum. Limitations of analysis *full SSI* models are they need computational as well as numerical efficiency, so to build the models high performing computer systems are required which are also uneconomical. The execution of analysis are time consuming due to the presence of soil domain. Limitations of analysis *FB_SD* models are they are numerically efficient to model in different programs. But, only spring-dashpots cannot depict the actual behaviour of realistic soil domain under dynamic shaking. For say, past studies have been carried out to replicate actual soil strength by assigning spring-dashpots at corresponding locations of soil domain. But, still the response from these studies cannot matches the response of physical domain. Soil liquefaction or excess pore water pressure dissipation cannot be incorporated through spring-dashpots of soils.

The brief conclusions from the present study are stated below:

1. For application of free field input (from site response analysis) at the fixed base of bridge (*only B_FF* model), the structural response of substructure gets overestimated for linear or nonlinear cases because the true behaviour of foundation embedded inside continuous soil domain cannot be predicted from the response of a free-field soil column at the desired depth.
2. When ground motion obtained from SSI effect is given as an input to the bottom of the fixed base piers (*only B_SSI* model), the response is the quite similar as that obtained from *full SSI no BA* model resulting in minimal kinematic interaction (i.e. surficial, rigid foundations).
3. True incorporation of soil structure interaction results in reduced response as compared to the uncoupled approach (as mentioned in 1). That observation is valid for both linear (linear soil + linear structure) and nonlinear (linear soil + nonlinear structure, nonlinear soil + nonlinear structure) behaviours of appropriate models.
4. Presence of backfill tends to reduce the force demand on the bridge structure, thus reducing the nonlinear response considerably.
5. Under strong ground motions (PGA $\geq$0.48g for this study), the structural nonlinearity governs the overall response of the bridge-foundation-soil system, whereas for low intensity of shaking (PGA $\leq$0.1g for this study), soil nonlinearity tend to governs the overall response. For the intermediate range of shaking, both influence the overall behaviour.
6. The *full SSI with BA* model has the lowest response on bridge structure in NTHA. As the backfill soil provides longitudinal restraints to the bridge, seismic force from superstructure dissipates through backfill soil leading to reduced displacement level in the bridge superstructure.

7. Modelling of soil behaviour using Winkler spring-dashpot (API and BA) approach tends to overestimate the seismic demand, thus, that approach can be possibly used in case of seismic design of bridge-foundation-soil system.
8. As compared to the nonlinear behaviour of the *full SSI no BA* model and the *full SSI with BA* model, the shear forces and bending moments in the piers are higher for *FB_SD no BA* model and *FB_SD with BA* model because the foundation soil stiffness is higher with the API force-displacement curves.
9. The response of the *FB_SD no BA* model is higher as compared to the *full SSI no BA* model as API overestimates soil stiffness for foundation soil. Structural response is amplified significantly at deck level for *FB_SD no BA* model and results in higher forces and moments at pier-deck junctions.
10. For *FB_SD with BA* and *full SSI with BA* models, the former model is stiffer at super-structural level and deforms in higher curvature after dynamic analysis, thus, the observed nonlinearity is higher for this modelling approach and residual response after dynamic analysis is also higher. Due to insufficient soil nonlinearity at foundation and backfill region, *FB_SD with/no BA* models overestimate the overall stiffness.
11. In *full SSI with/no BA* models, due to significant nonlinearity soil domain, bridge response does not amplify at deck level; thus in this type of modelling bridge response is lower as compared to the response obtained using simplistic SSI modelling approach.

After the present study, it can be concluded that modelling of continuous soil domain to assess SSI may not be always required in conventional seismic design, but from the research point of view its gives detailed insight on the seismic behaviour of the bridge-foundation-soil system. Spring-dashpot model can predict bridge response to some extent

but as the intricacy in modelling increases, the response may start to deviate from the real one. To study bridge design, modelling of abutment backfill is also a key parameter to examine the response of the bridge. The spatial variability in the geometry of bridge members has not been studied in this paper, but it is expected that it can surely show some important design guidelines on SSI modelling approaches.

Nonlinear interface element has not been modelled in the present study. In presence of interface elements in *OpenSees* models it is well known that the slip and gap (debonding) due to soil-pile interaction and abutment backfill interaction can be explicitly captured. Though, it is expected that it won't be resulting in too much changes in structural response because foundation soil is medium stiff clay and is nowhere near to plastic failure under the site specific ground motions. Interface element can reflect the nonlinear inelastic behaviour of soil which one could expect in reality.

★★★

Chapter 6

Study on Overall Length of Integral Bridge

6.1 Introduction

The influence of length of an integral bridge (IB) on the seismic behavior of the bridge in investigated in this chapter. Though, parametric studies have been carried out in the past on IBs (Erhan and Dicleli, 2017; Kong *et al.*, 2016; Huang *et al.*, 2008; Civjan *et al.*, 2007), but the influence of overall length has not been investigated on multispan IB with RC pile foundation. In order to achieve the objective, finite element modelling of a 3D IB, "inspired" by Humboldt Bay Middle Channel (HBMC) Bridge in California, USA, is carried out using SAP2000 *v*.19.2.1 software (CSI, 2017). The *FB_SD with BA* model overestimates the seismic response of bridge as compared to the *full SSI with BA* model in Chapter 5 under dynamic loading. Thus, further analysis is carried out with spring-dashpot model in 3D bridge to incorporate seismic SSI with one of the most accepted structural analysis programs, SAP2000. Soil flexibility is modelled by two noded nonlinear link elements. Four types of foundation soil are considered, namely (i) medium stiff clayey soil, (b) soft clay, (c) loose sand and (d) dense sand, to incorporate nonlinear dynamic Soil-Structure Interaction (SSI) at the soil-pile and abutment-backfill interfaces. Among these four types of soil, nonlinear time history analysis is performed in medium stiff clayey soil and loose sand. In loose foundation soil, the foundation becomes more flexible and results in forming hinges at different depth of piles. In medium stiff clay, the possibility of inelastic behaviour of the piers and the piles gets increased in an integral bridge.

6.2 Modelling

6.2.1 Structure and Foundation Properties

The geometry of the bridge is taken from the study by Elgamal *et al*. (2008). The original bridge consists of nine spans with the total length of the bridge as 330 m (Fig. 6.1). Piers, piles, deck girders and cap beams are modelled as beam-column elements. Abutment walls, pile caps and deck slab are modelled as thin shell elements. The deck slab is supported on four I-shaped prestressed concrete girders. The girders are rigidly connected to the piers by cap beams. The dimensions of the abutments are 10 m, 1.2 m and 5 m in breadth, width and height, respectively and are connected with foundation through 12m×3m sized and 0.7 m thick pile cap. Piers are supported on 7m×7m×1m sized pile caps. Abutments and piers are supported on pile group foundation. Abutment foundation consists of 0.6 m diameter reinforced concrete piles in double rows (9 nos. in each row) and each pier foundation consists of a pile group of five precast driven RC piles of 1.372 m diameter. Abutment and pier piles are designed for axial compressions of 500 kN and 400 kN, respectively.

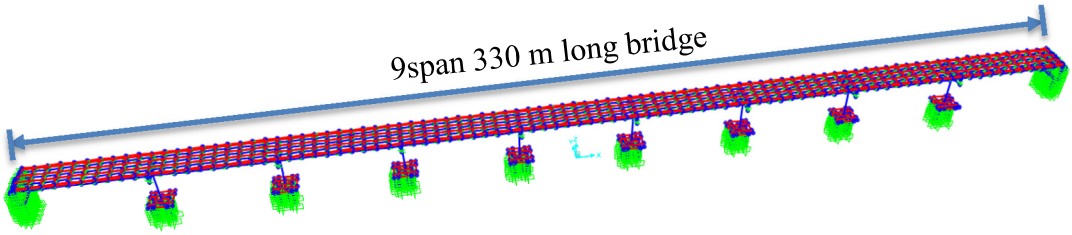

Fig. 6.1 3D bridge model in SAP2000 founded on medium stiff clay

Equivalent piers are modelled after Elgamal *et al*. (2008) keeping the amount of longitudinal reinforcement as 1% of gross cross-sectional area. The nonlinear behaviour of piers and piles is modelled using fiber hinges based on the concept of distributed plasticity. Pier and pile members are discretized into 3×3 fibers at cross section and

divided into 5 and 2 integration points along the length of the respective members. The reinforcement details of the cross-sections, with HYSD 415 bars, are shown in Figs. 6.2(a), 6.2(b) and 6.2(c). Cover and core concrete material properties are considered from Mander's model (1984) with characteristics compressive strength of 30 MPa. The lengths of the pier piles and abutment piles are changed in medium stiff clay and loose sand depending on soil properties (Prakash and Sharma, 1990). In medium stiff clay and dense sand, piles are 5.2 m in length and in loose sand, abutment and internal piles are 10 m and 15 m in length, respectively. In soft clay, abutment and intermediate piles are of 15 m and 10 m of length, respectively (Appendix D).

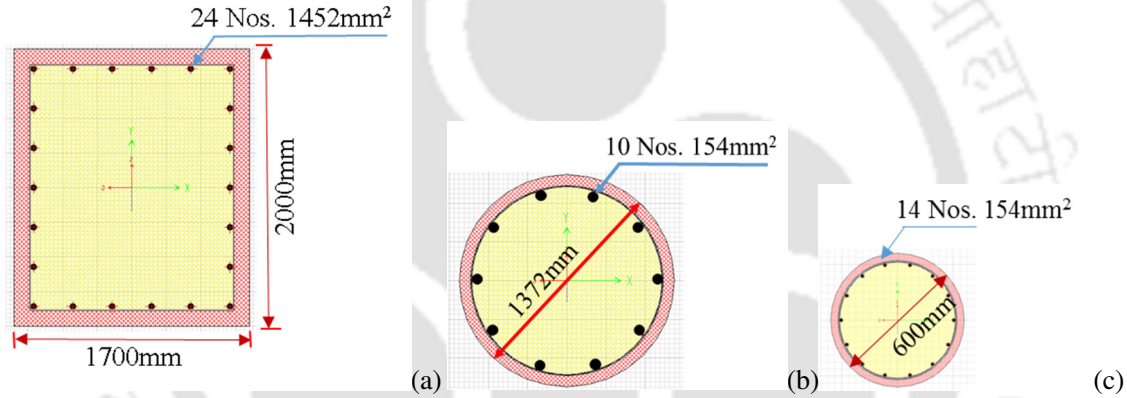

Fig. 6.2 Reinforcement detailing of cross-sections for (a) pier, (b) pier piles and (c) abutment piles.

6.2.2 Properties of Soil links

The considered properties of all four types of soil are given in Table 6.1. Two noded link elements are assigned at different depths of the pile foundation and abutment backwall (Figs. 6.3(a) and 6.3(b)). The assigned link properties account for lateral bearing capacity of soil at soil-pile interface (*p-y*), pile shaft skin friction (*f-y*) and pile tip load bearing capacity (*t-z*). Nonlinear links are modelled using 2-noded multilinear plastic force-deformation curves. To model the soil-pile interaction (SPI) for different types of soil, *p-y*, *f-y*, *t-z* curves are calculated from API (2000) guidelines. For lateral Abutment-Backfill

Interaction (ABI) (*p*-*y*), nonlinear curves to represent backfill soil are obtained from BA 42/96 (2003) provisions. At the end of link's restrained end, input motions are applied as displacement time histories (DTHs). Those motions are extracted from the corresponding depth of the free field soil column under dynamic site response analysis performed earlier. Abutment backwall links are modelled to take care of active and passive pressures of backfill soil. In Figs. 6.4 and 6.5, backbone curves of four types of soil are compared at the depths of 2m and 4m for pier piles and abutment piles, respectively (Appendix E and Appendix F).

Table 6.1 Soil properties used in the present study

Soil Type	Maximum shear modulus (MPa)	Poisson's ratio	Total unit weight (t/m^3)	Cohesion (MPa)	Internal friction angle
Medium stiff clay[1]	76	0.45	1.9	0.027	-
Loose sand[2]	55	0.45	1.6	-	29°
Soft clay	9	0.45	1.75	0.018	
Dense sand[2]	224	0.45	2.0		38°

[1]after Zhang *et al.* (2008)
[2]after Erhan and Dicleli (2017)

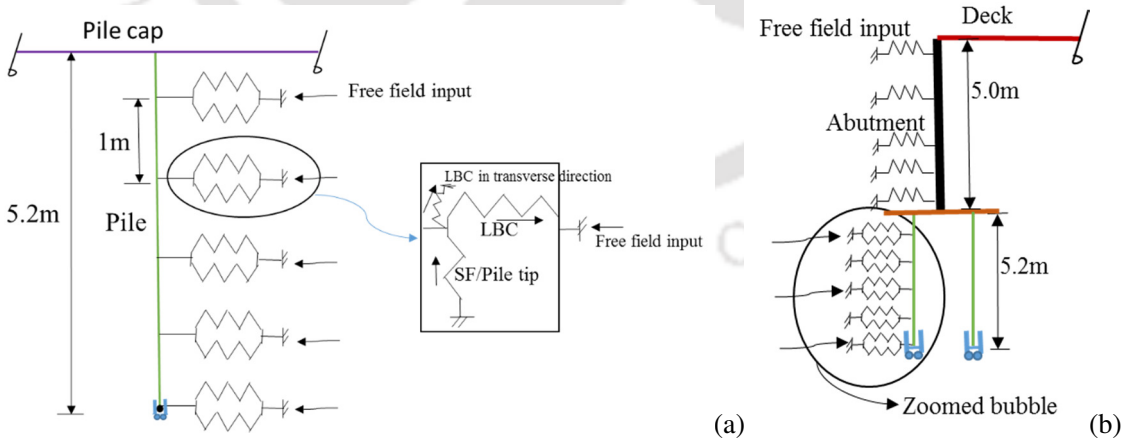

Fig. 6.3 (a) Soil-pile interaction and (b) abutment-backfill interaction in medium stiff clay

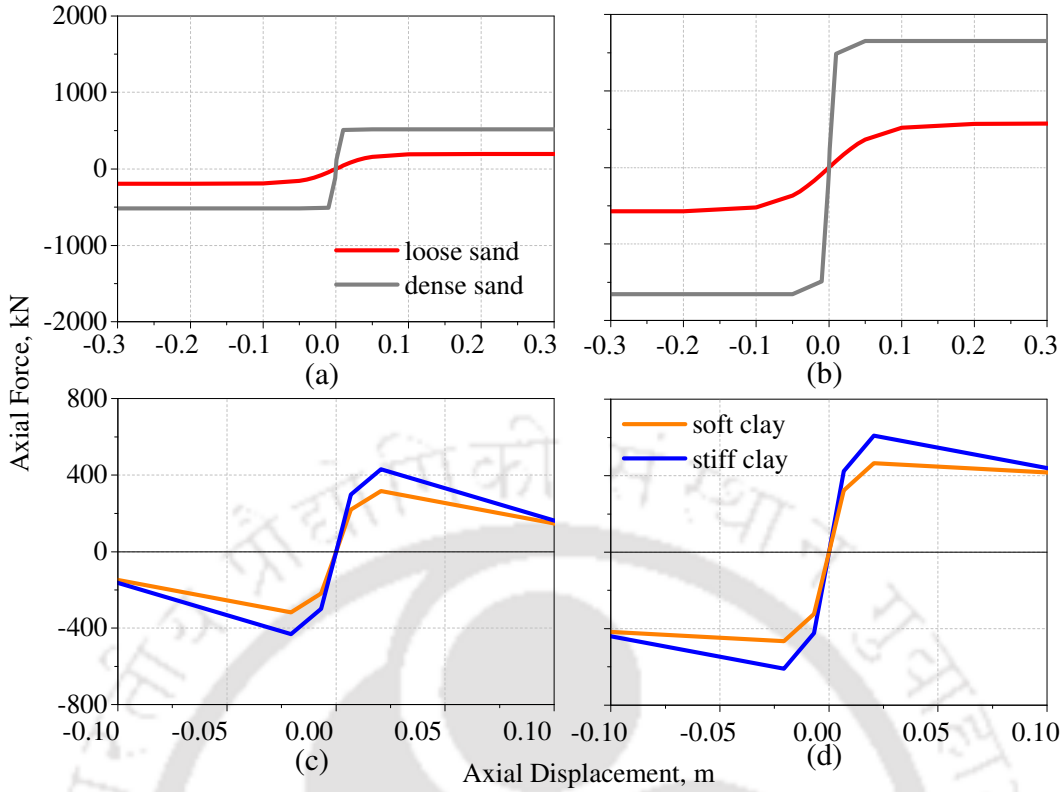

Fig. 6.4 Comparison of backbone curves for loose sand and dense sand at the depths of (a) 2 m and (b) 4 m, for soft clay and stiff clay at the depths of (c) 2 m and (d) 4 m in case of intermediate pier piles.

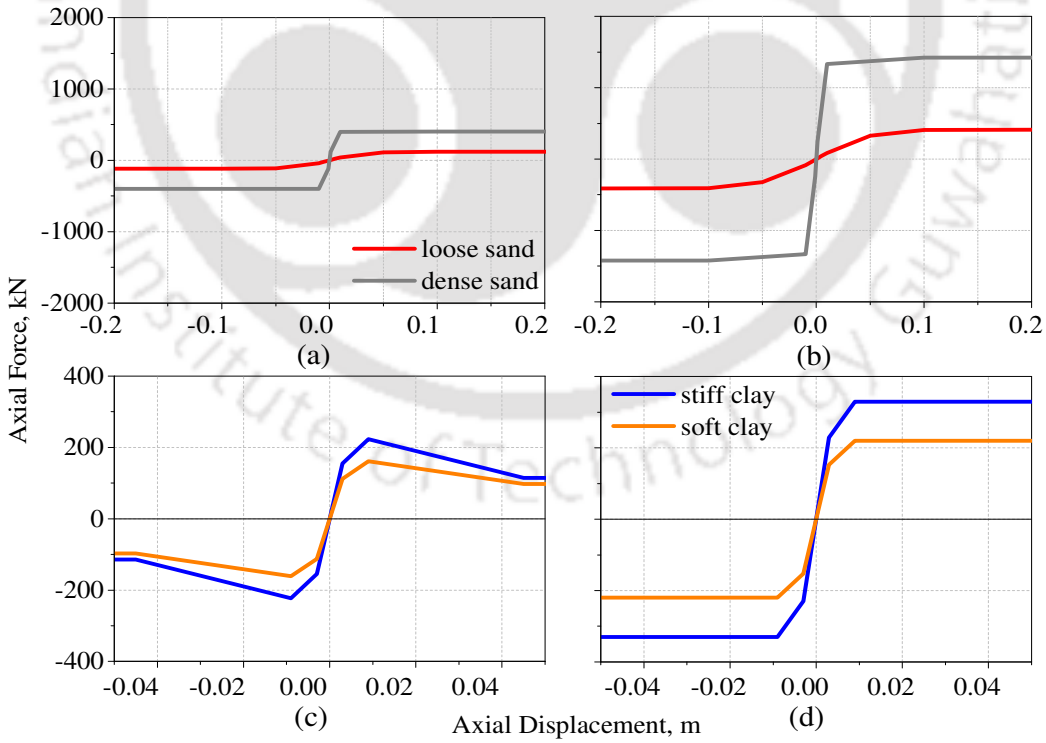

Fig. 6.5 Comparison of backbone curves for loose sand and dense sand at the depths of (a) 2 m and (b) 4 m, and for soft clay and stiff clay at the depths of (c) 2 m and (d) 4 m for abutment piles.

6.3 Analysis

In the first part of the analysis, to investigate the effect of length, the two end spans of the 9 span 330 m long integral bridge (IB) are removed so that the bridge becomes a 7 span bridge of 257 m. Further successive removals of two end spans, the bridge transform into a 5 span bridge of 184 m length and a 3span bridge of 112 m length (in Fig. 6.6). End spans of the bridge are removed to reduce the overall length of bridge. From the seven real record scaled ground motions, the GM#1 is replaced by Irpinia earthquake at ALT station on 23 Nov. 1980 having scaled PGA of 3.46 m/s^2. GM#2 is retain the same which has been chosen for previous study in Chapter 5. The chosen ground motions displacement spectra are specified in Fig. 6.7(a). Figs. 6.7(b) and 6.7(c) represent the Acceleration Time Histories (ATH) of the chosen GMs. In Figs. 6.7(d) and 6.7(e), Fourier transforms of GM#1 and GM#2 are plotted and natural frequencies of different bridge models considered are marked for both the foundation soil type. The natural frequencies of different bridge models are spreaded over below 1Hz of frequency. Seismic energy is higher beyond 1Hz of frequency for GM#1 and distributed over large frequency range for GM#2. Under different GMs, input DTHs at the end of fixed pile links are different. In Table 6.2, the natural periods of the bridges with different spans are shown for the four types of foundation soil. The bridge becomes stiffer with decreasing number of spans. To study the effect of length on seismic behaviour of bridge, nonlinear time history analysis (NTHA) is carried out in medium stiff clay and loose sand foundation soil under GM#1 and GM#2. In the 2nd part of the study, the damaged 9span bridge is retrofitted by encasement method in all four types of foundation soils and the comparison of response under GM#1 only is discussed in the next chapter.

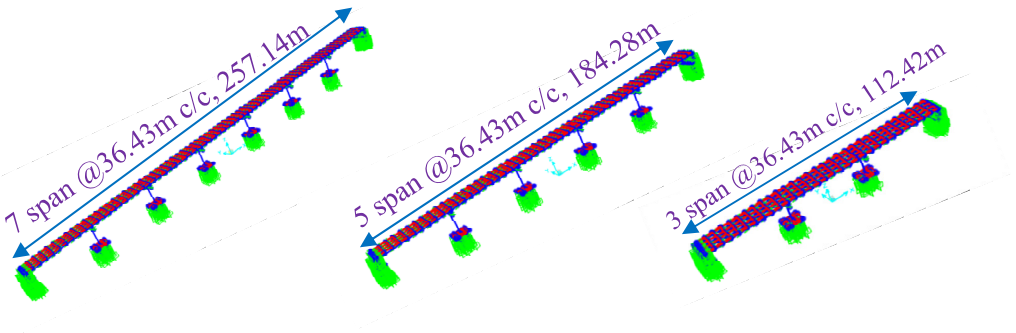

(a) (b) (c)

Fig. 6.6 Models of bridges with (a) 7 spans, (b) 5 spans and (c) 3 spans.

Table 6.2 Natural periods (in sec) of bridges with different spans considered in the study

Soil type	9Span	7span	5span	3span
Medium stiff clay	3.15	2.70	1.97	1.30
Loose sand	3.22	2.76	1.98	1.23

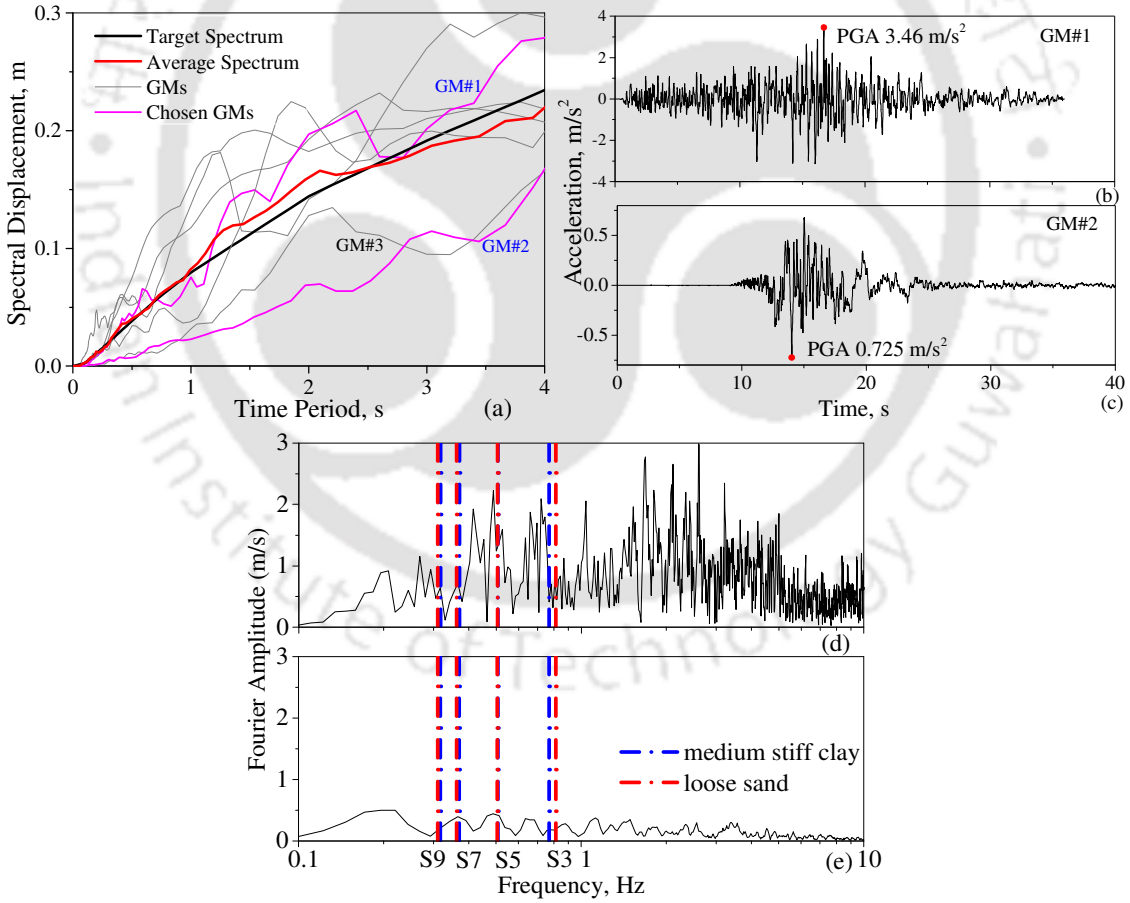

Fig. 6.7 (a) Displacement spectra for all the GMs, (b) acceleration time history of GM#1, (c) acceleration time history of GM#2 chosen for parametric study, (d) Fourier amplitude of GM#1 and (e) Fourier amplitude of GM#2 [notations S9, S7, S5, S3 stand for 9span, 7span, 5span and 3span bridges natural frequencies].

6.4 Results

6.4.1 Response for medium stiff clay soil

In medium stiff clay foundation soil, inelastic response is observed at the top of 3rd (Fig. 6.8(a)) and 6th piers and at their respective pile groups for 9span bridge under GM#1. Under GM#1, due to higher intensity of PGA (= 3.46 m/s^2), shear force has significant variation among 9span, 7span and 5span bridges after PGD at t = 12.06 s. The increase of nonlinearity leads to maximum residual shear force (SF) for the 9span and 7span bridges. From Figs. 6.8(a) and 6.8(c), 5span bridge pier is showing linear behavior which also results in insignificant residual SF in NTHA under GM#1. Response of 5span and 3span bridges are similar from the aspect of structural members. Thus it shows, as in the case of jointless bridge, forces coming from foundation to structure increase with increasing length of the bridge. Under GM#2, linear elastic behavior is observed in piers for all the bridges (Fig. 6.8(b)). Thus, only the results of 9span bridge are shown for the pier response in the following study under GM#2. In Fig. 6.8(c), the moment-rotation response at 1.25 m from the top of 3rd pier are shown. Inelastic behavior of the piers is observed in the 9span and 7span bridges after the dynamic analyses. For the 5span bridge, very narrow loops, signifying low level of inelasticity, are formed under GM#1. Under GM#2, i.e., at low intensity of PGA (i.e. 0.725 m/s^2), SFTH at the top of 3rd pier in 9span bridge shows insignificant residual response (Fig. 6.8(b)) and linear moment-rotation response is obtained at the end of dynamic analysis (Fig. 6.8(d)).

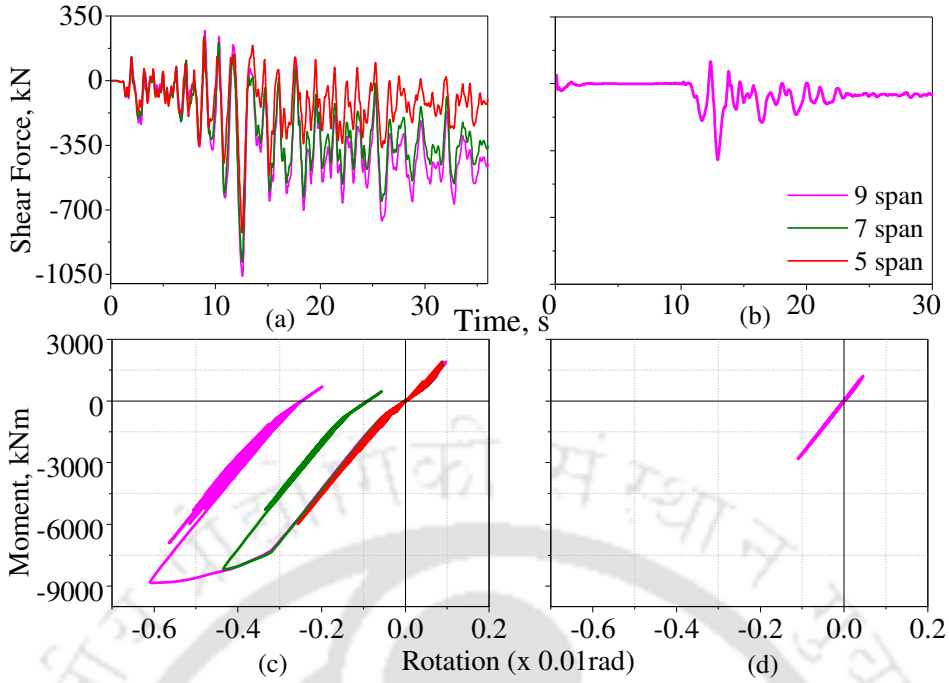

Fig. 6.8 Shear force response at the top of 3rd pier under (a) GM#1 and (b) GM#2; moment-rotation response at the top of 3rd pier under (c) GM#1 and (d) GM#2 in medium stiff clay soil.

Displacement time histories (DTHs) at the top and bottom of the abutments are monitored under GM#1 in Figs. 6.9(a) and 6.9(b), respectively. At the top of the abutment, the residual displacements of the 9span, 7span and 5span bridges are observed as 0.166 m, 0.123 m and 0.044 m, respectively. Those also signify that the 9span bridge has undergone the highest extent of nonlinearity. Significant deformation is accumulated at the integral deck-abutment-backfill joint. Similar response is observed at the bottom of abutment as shown in Fig. 6.9(b). Under GM#2 for 9span bridge in Fig. 6.9(c), the top and bottom DTHs of abutment are quite similar and the bridge model has no significant residual response after dynamic analysis; this also confirms linear elastic behavior of the bridge.

At the depth of 1.25 m of abutment piles, moment rotation curves are shown in Figs. 6.10(a) and 6.10(b) under GM#1 and GM#2, respectively. Under GM#1and GM#2, abutment piles are showing linear elastic response for all considered bridge spans. In contrary to that, extensive nonlinearity of pier piles at the depth range of 1–2 m are

observed in Figs. 6.10(c) under GM#1. Under GM#1, the piles of the 3rd pier foundation in 9span, 7span and 5span bridge models undergo severe nonlinearity, along with inelastic behavior of the pier piles in 3span bridge too. Under GM#2, pier piles exhibit insignificant nonlinear response for all the bridges in medium stiff clay foundation soil.

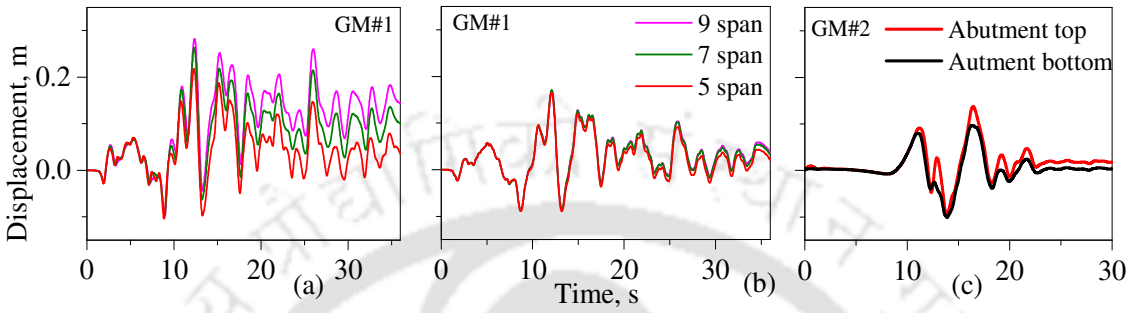

Fig. 6.9 Displacement time histories (DTHs) for bridges of 9span, 7span and 5span at (a) top of abutment and (b) bottom of abutment under GM#1, (c) DTHs of 9span bridge under GM#2 in medium stiff clay foundation soil.

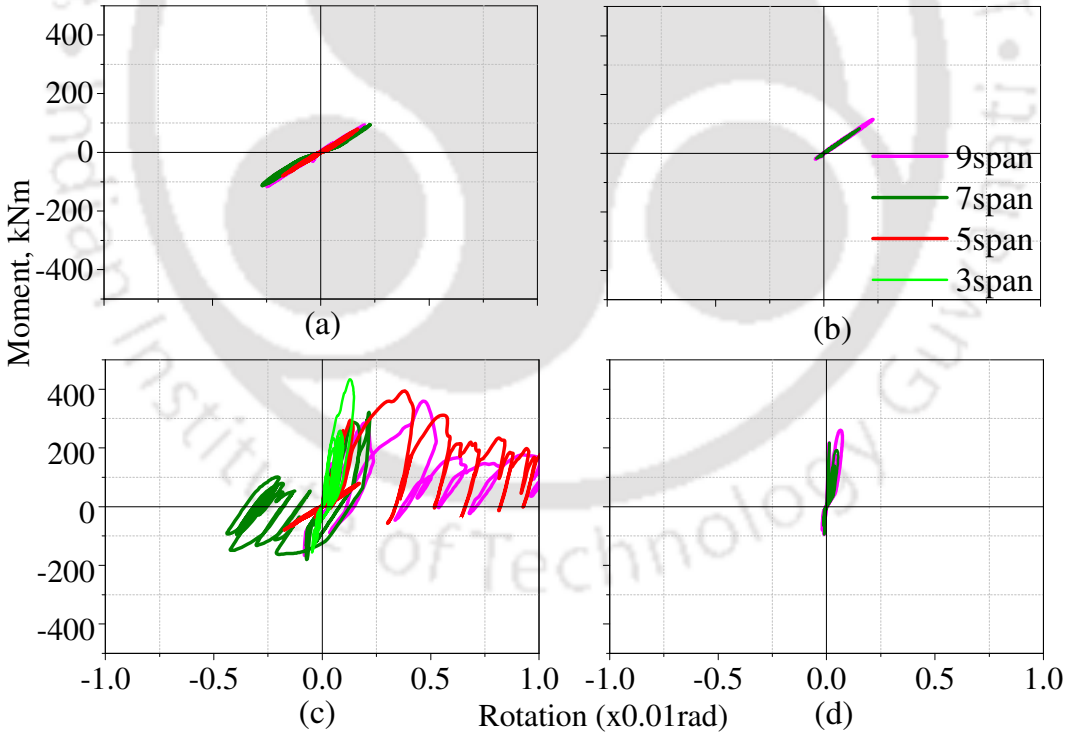

Fig. 6.10 Moment-rotation response of abutment pile under (a) GM#1 and (b) GM#2, and for pier pile under (c) GM#1 and (d) GM#2 in medium stiff clay foundation soil at the depth of 1.25 m from ground level.

6.4.2 Response for loose sand

Under GM#1, the 9span bridge shows more residual displacement at the top of left abutment as compared to the 7span bridge (Fig. 6.11(a)). However, the residual displacement at the bottom of the abutment for the 7span bridge is almost the same as 9span bridge because the deformation decreases from deck to foundation level (Fig. 6.11(b)). The overall deck displacement of a bridge model in loose sand is less as compared to the deck displacement of the same model in medium stiff clayey soil. 7span bridge superstructure also results in insignificant residual deformation and remains linear elastic after DTHA. DTHs at the top and the bottom locations of left abutment are plotted in Fig. 6.11(c) for 9span bridge under GM#2 which shows similar response in DTHA.

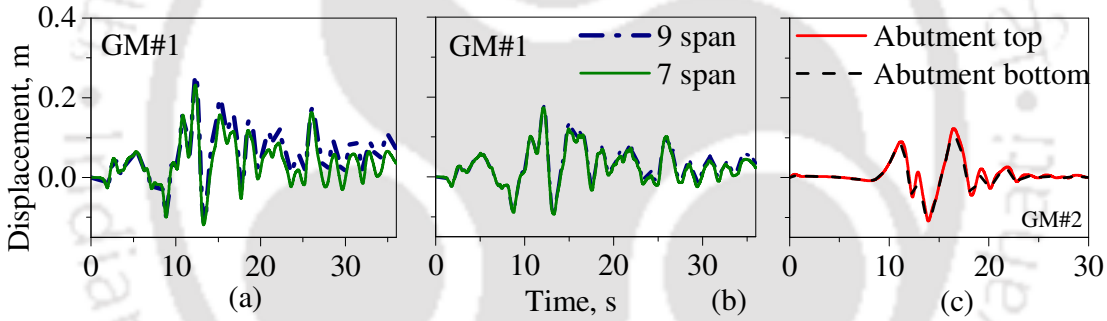

Fig. 6.11 Displacement time histories (DTHs) for 9span and 7span bridges at (a) top of abutment and (b) bottom of abutment under GM#1, (c) DTHs for 9span bridge under GM#2 in loose sand.

Unlike the previous case, pile foundation in loose sand helps the foundation to respond in a more flexible manner. Under GM#1, it is observed that the residual SF at the top of 3rd pier of the 9span bridge is insignificant like that for the 7span bridge (Fig. 6.12(a)). However, the obtained moment-rotation response at 1.2 m from the top of the 3rd pier shows marginally nonlinear response and linear elastic response for 9span and 7span bridges (Fig. 6.12(c)), respectively. Thus, the bridge substructure behaves in a linear elastic manner in loose foundation soil under GM#1 for the 7span, 5span and 3span bridges. Where, under GM#2, at the top of 3rd pier, SFTH is shown in Fig. 6.12 (b) and

the pier is linear elastic from moment rotation response at the location of 1.2 m from the top of the pier (Fig. 6.12 (d)).

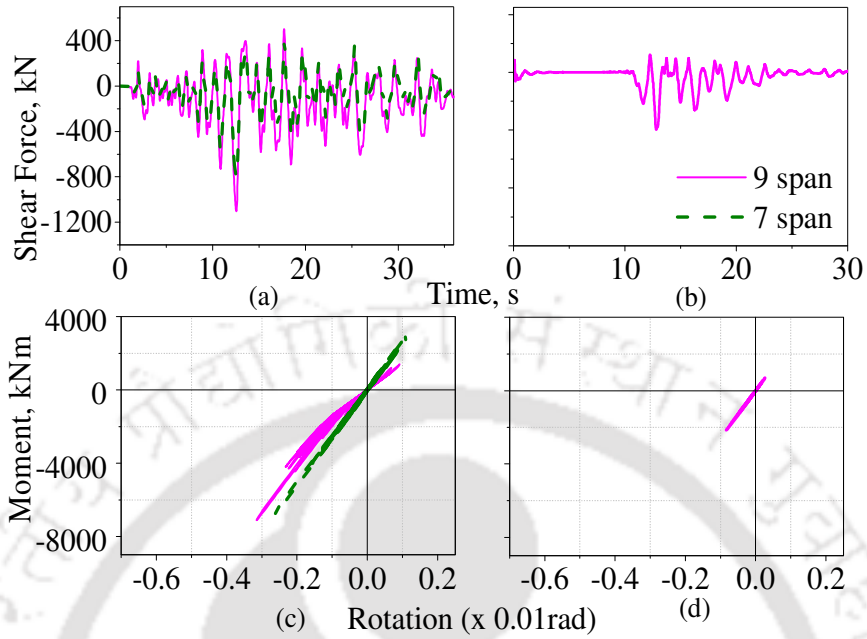

Fig. 6.12 Under GM#1 (a) shear force time history, (b) moment rotation response, under GM#2 (c) shear force time history, (b) moment rotation response at the top of 3rd pier, in loose sand

Although the bridge substructure does not show significant nonlinearity for the 9span bridge, the abutment piles and the pier piles show inelastic behavior under GM#1 (Figs. 6.13(a) and 6.13(c)). The moment-rotation response of the pile section at the depth of 1.25 m below ground level shows more nonlinearity for the pier piles in 9span bridge. However, for bridges with lesser spans, nonlinearity has reduced in foundation level. In Figs. 6.13(b) and 6.13(d), the moment-rotation curves of the abutment pile and pier pile are shown under GM#2, respectively and for all the locations of foundation part, piles have formed narrow inelastic loops. So, unlike in medium stiff clayey foundation soil, only the 9span bridge shows nonlinear response of piers in loose sand under GM#1. Though, the rest of the considered span of bridge models have nonlinear response limited to the foundation part only. Plastic hinge formation is limited to a depth of 8 m along the

pile, so special attention is needed to design the pile foundation in soft soil for larger jointless bridges.

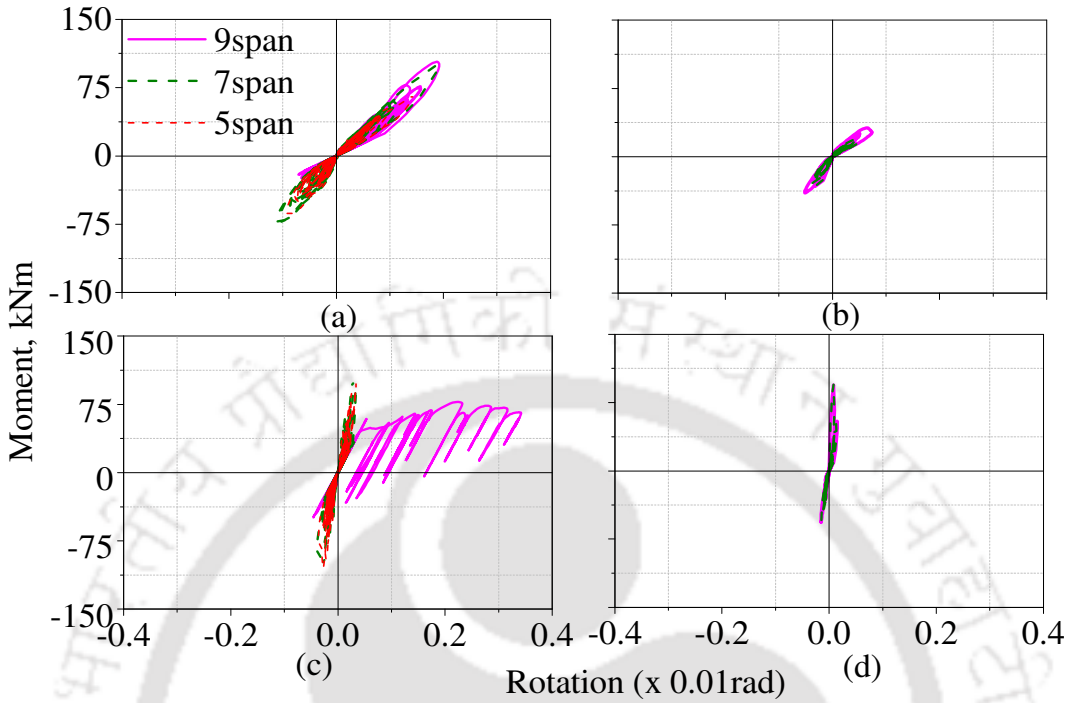

Fig. 6.13 Moment-rotation response of abutment piles under (a) GM#1 and (b) GM#2, and of pier piles under (c) GM#1 and (d) GM#2 in loose sand at the depth of 1.25 m from ground level.

6.4.3 Comparison of response in loose sand and medium clay soil

In Fig. 6.14, at the depth of 2 m and 4 m, the *p-y* response of the soil link elements is monitored for left abutment piles in both types of foundation soil. In case of medium stiff clay and loose sand, the soil links show linear elastic behaviour. Soil links in stiff clay are deforming less than 0.001 m at both the monitored depths of 2 m and 4 m of abutment pile. Thus, it can be concluded that in stiff clayey soil, soil links undergo less relative deformations and impose higher seismic forces on the piles; this leads to formation of plastic hinges at different locations in the piles.

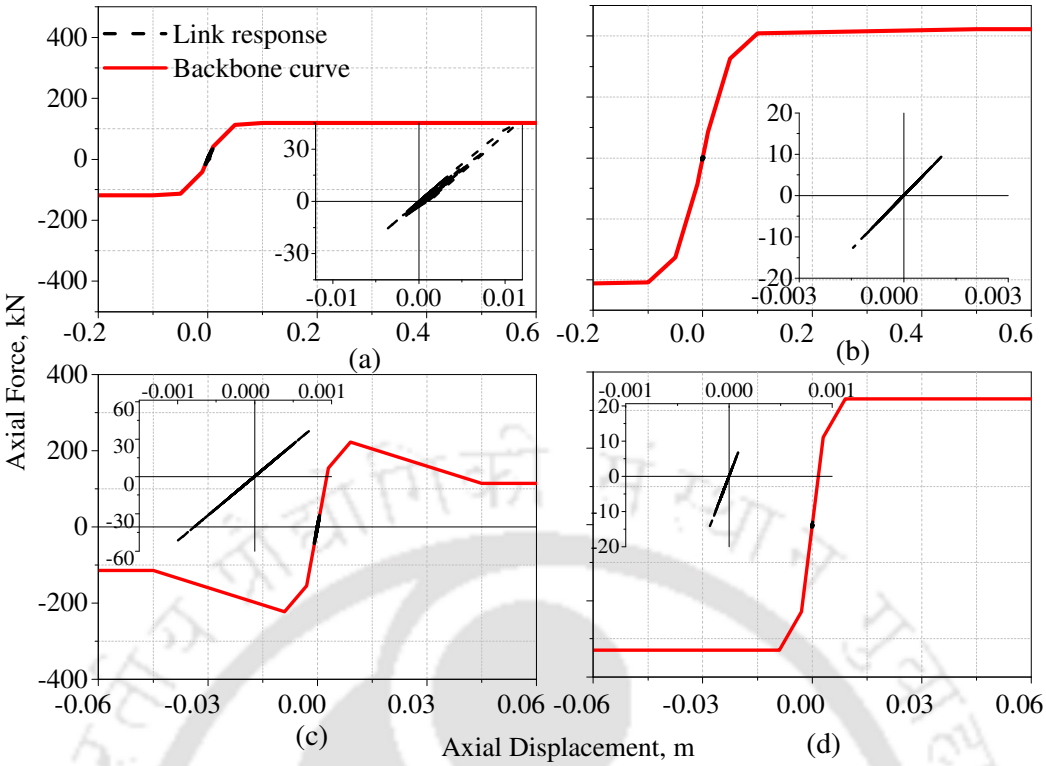

Fig. 6.14 Variation of axial force with axial displacement for soil link elements at the depths of (a) 2 m and (b) 4 m in loose sand and at the depths of (c) 2 m and (d) 4 m in medium stiff clay for abutment piles.

Under GM#1, at the top of 3rd pier, normalized Fourier transform of SFTHs for 9span bridge, are plotted in Figs. 6.15(a) and 6.15(b), under GM#1 and GM#2, respectively. Under GM#1, SFTH in loose sand contains higher forces than medium stiff clayey soil. As in loose soil the bridge pier is linear elastic in DTHA, so, the structure carries higher seismic energy during THA. But the Fourier amplitudes are similar in both the foundation soil under GM#2, where the nonlinearity in the structure and the foundation soil are not present. In the medium stiff clayey soil, foundation piles induce more forces and moments on the overall structure and the superstructure carries more forces. Thus, nonlinearity in substructure is also higher. So, due to higher nonlinearity seismic energy gets more dissipated and Fourier amplitude get reduced as compared to the bridge in loose sand foundation soil under GM#1. Among the 7 site specific rock outcrop GMs, under GM#2 and GM#3 (in Fig. 6.7(a)), the superstructures of the 7span,

5span and 3span bridges remain linear elastic, with observation of marginal inelasticity for piles in both the types of soil. Under GM#1 and rest of them, 9span bridge has failed either at different locations of piles or at both piles and piers, which is followed by the failure of piles in 7span, 5span and 3span bridges. In Fig. 6.15(c), comparison of average Fourier amplitude of seven rock outcrop GMs and output average Fourier transform of ATHs monitored at the top of 3rd pier in SAP2000 are plotted. Output Fourier amplitude is considerably higher throughout 0.1–10 Hz frequency range. This is because of the presence of structural and soil nonlinearities as seismic waves get amplified during vertical propagation from bedrock to superstructure level. In Table 6.3, overall behaviour of bridge piles and piers are summed up for all the considered bridge spans in DTHA.

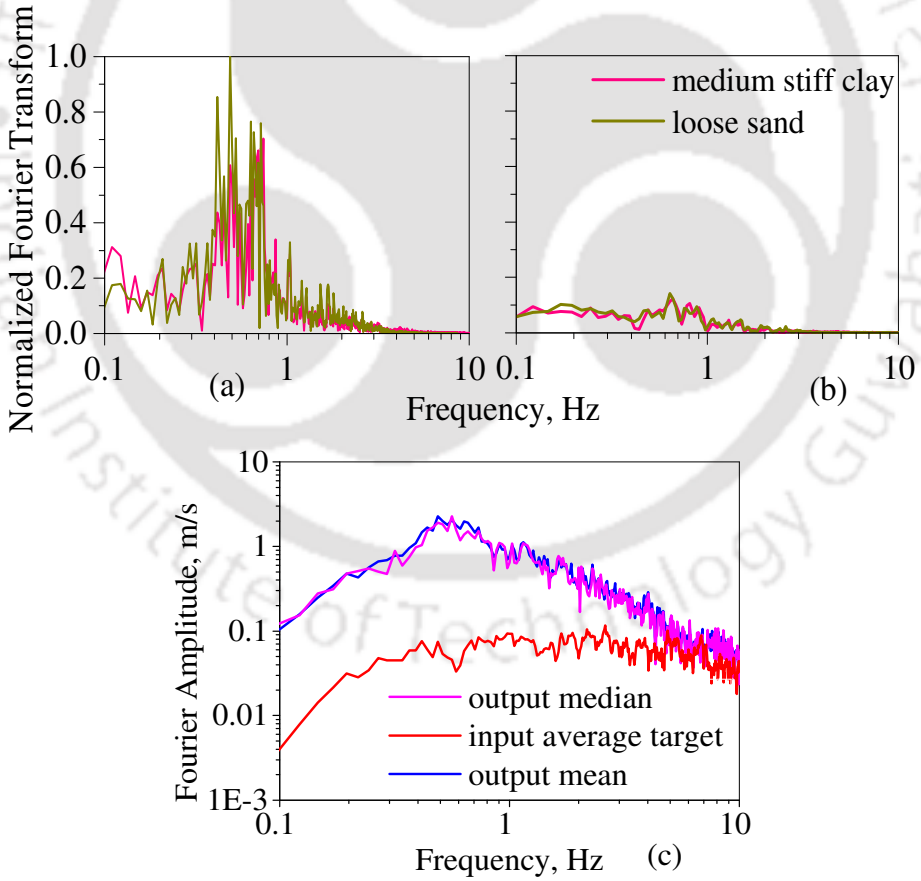

Fig. 6.15 (a) Normalized Fourier transform of SFTH under GM#1, (b) normalized Fourier transform of SFTH under GM#2 at the top of 3rd pier for 9span bridge and (c) comparison of Fourier amplitude at input and output stages of analysis for 9span bridge in medium stiff clayey soil.

Table 6.3 Behavior of bridge members after DTHA in medium stiff clay and loose sand

Members	GM	Soil type	9span	7span	5span	3span
Piers	GM#1	Medium stiff clay	*inelastic*	*inelastic*	elastic	elastic
		Loose sand	*inelastic*	elastic	elastic	elastic
	GM#2	Medium stiff clay	elastic	elastic	elastic	elastic
		Loose sand	elastic	elastic	elastic	elastic
Pier piles	GM#1	Medium stiff clay	*inelastic*	*inelastic*	*inelastic*	*inelastic*
		Loose sand	*inelastic*	*inelastic*	*inelastic*	*inelastic*
	GM#2	Medium stiff clay	*inelastic*	*inelastic*	*inelastic*	elastic
		Loose sand	*inelastic*	*inelastic*	*inelastic*	elastic
Abutment piles	GM#1	Medium stiff clay	elastic	elastic	elastic	elastic
		Loose sand	*inelastic*	*inelastic*	*inelastic*	*inelastic*
	GM#2	Medium stiff clay	elastic	elastic	elastic	elastic
		Loose sand	*inelastic*	*inelastic*	*inelastic*	elastic

6.4.4 Response of bridge in dense sand and soft clay

Response of the bridge in dense sand and soft clay foundation can be studied from backbone curves (Figs. 6.4 and 6.5) of respective soils. In dense sand, backbone curves are steeper, which means links will be carrying higher forces as compared to the loose sand and higher response would be imposed on the bridge foundation. Thus, extensive nonlinearity is expected to govern the response of the bridge substructure. So, even bridges with lesser number of spans can be expected to show nonlinear response in dense sand. In soft clay, backbone curves of the links are less steep than those for stiff clay. Thus, the imposed forces on the piles will reduce. So, response of substructure will also reduce and nonlinearity is expected to be lesser than in medium stiff clayey soil.

6.5 Summary

To provide a closure to this study, dynamic analysis is carried out with all seven scaled GMs from REXEL-DISP. Only under GM#2 and GM#3, the piers are linear elastic in DTHA. From the present study, it can be concluded that the bridge with maximum number of spans attracts more forces and moments than the shorter ones as there is no intermediate joint or bearing to dissipate seismic energy at superstructure level. Pile foundation in loose foundation soil can become very flexible and deform easily, thus nonlinearity gets reduced in the foundation members. Hence, failure of structural members can be limited to the foundation part only. On the other hand, it can also result in seismically vulnerable foundation which will not be suitable for performance in severe seismic zone. For this specific bridge model, the 3rd and the 6th piers and the corresponding pile groups are more susceptible to dynamic shaking. Large span bridges (with overall length more than 300 m) in medium stiff clayey soil are likely to sustain higher seismic damage during strong earthquake shaking due to imposition of more forces from soil to piles. It is observed that the 9span and 7span bridges undergoes extensive inelastic behavior as compared to the 5span and 3span bridges after DTHA under GM#1 in medium stiff clayey soil. Major nonlinearity is seen at pier pile sections for all bridge spans in medium stiff clayey soil. Hence, it won't be advisable to construct 9span and 7span bridge in these specific geological conditions. In loose sand, 9 span bridge shows insignificant nonlinearity in piers and foundation piles whereas, substructure is completely linear elastic for 7span, 5span and 3span bridges in loose sand under GM#1. Thus, if proper measures are taken in further pile and pier designing, 9span bridge in loose sand and upto 5span bridge in medium stiff clay soil can be constructed.

Site response analysis must be carried out prior to design of integral abutment bridge in stiff clayey soil. Specially, the influence of SSI on seismic behaviour of

foundation tends to be significant during earthquake shaking. Moreover, piles in stiffer soil attract more seismic forces under earthquake motion which results in increased nonlinear behaviour of the foundation. Seismic design of piles also becomes a critical aspect due to their role in the soil-pile-bridge interaction during transfer of seismic forces. Apart from the pile group, proper backfill soil is required to withstand transfer of dynamic forces generated during shaking of bridge. Backfill soil should not be too stiff to impose extra load on bridge neither too loose to permit large lateral deformations of the bridge. Thus, detailed guidelines are required for proper seismic design of the piers and foundation piles in order to obtain desirable seismic behaviour of the integrated soil-pile-bridge system.

Depending on proper geological investigation and site specific characteristics, the integral bridges should be constructed so that due to larger length, yielding of foundation piles can be prevented. In that case, foundation needs to be designed more carefully with higher endurance capacity and proper retrofitting of foundation should be a scope to make the bridge more sustainable under high intensity GMs.

★★★

Chapter 7

Retrofitting of Pile Foundation

7.1 Introduction

In the previous chapter, nonlinear behaviors of the abutment piles and the pier piles are observed along with large displacement at deck level for the bridge with the longest span under GM#1. As the mentioned response can lead to seismic failure of the overall bridge structure, one of the possible retrofitting measures for the pile foundation is discussed in this chapter. In this retrofitting method, RC piles are added along the periphery of the abutment pile cap and the pier pile cap, and jet grouting is carried out in the surrounding region of each new pile. In the first stage of analysis, the new piles encased in jet grouting are considered only below the abutments and the response are compared with the response of the original bridge model without the new piles. Then, new piles encased in jet grouting are added below two piers of the bridge. So, in the second stage of analysis, the response of the bridge model with retrofitted abutment and pier pile foundations is compared with the response of the bridge model with only retrofitted abutment pile foundation. For both the stages, the nonlinear response of individual pile gets reduced below the abutments and the piers. This further leads to the reduction of nonlinearity in piers as well as deformation at the deck level and reflects the effectiveness of the retrofitting method. Although the response of the retrofitted bridge will change with the height of the abutment, the scope of the present study is limited to the investigation of the bridge response for the two stages of retrofitting mentioned earlier. To the best of the author's knowledge, numerical study of the mentioned retrofitting method has not been carried out previously. Detailed parametric studies involving multiple ground motions and other bridge parameters can be carried out separately in future.

7.2 Retrofitting of RC Pile Foundation

In the past, different methods of retrofitting of RC pile foundation have been attempted and some of those studies have been discussed in Chapter 2. The selection of any particular method depends on the cost as well as the difficulty level in the installation procedure. Among the different methods, extension of existing pile cap and addition of new piles in the foundation is very difficult and cost ineffective. Similarly, thickening of pile cap involves challenges in construction and also required significant vertical clearance. Although micropiles can be added surrounding the pile cap, proper seismic strengthening of the overall pile group may not be achieved in absence of grouting of the micropiles. If grouting is implemented in an existing pile foundation, the increase in the lateral bearing capacity of the pile group is expected to be less than the increase in the lateral bearing capacity achieved through jet grouting around installed new piles. So, the present study focuses on the numerical modeling of additional RC piles surrounding the pile cap and embedded in jet grouting which can enhance lateral bearing capacity and bear the additional passive pressure generated during earthquake shaking. The properties of the jet grouting used in the present studies (He *et al*., 2016) are: injection pressure of grout = 27MPa; water cement ratio of grout = 1:1; life rate = 0.025 m/min; rotation speed = 18 rad/min; replacement ratio of cement = 33%; modulus of elasticity = 120 MPa; tensile strength = 0.18 MPa.

7.2.1 Modelling of encasement method

In the first stage of the present study, encasement method is incorporated by encasing RC piles in jet grouting around the periphery of the pile cap below each abutment. From the NTHA of the 9-span integral bridge model under GM#1, it is observed that the bending moment diagram in the abutment piles shows significant moment upto a depth of 4 m from the ground level for soft clay (Fig. 7.1(a) and loose sand (Fig. (7.1(b)), respectively.

Below the depth of 4m from soil surface, mostly linear elastic behavior of piles is observed. So, the length of the new encased piles is considered as 4 m for the abutment pile foundation. The new encased piles are modelled with a minimal diameter of 0.4 m considered as cast in place driven RC piles. Henceforth, the original bridge model before retrofitting (in Fig. 6.1) and the retrofitted bridge model only at abutment foundation, will be referred to as M1 and M2 models, respectively.

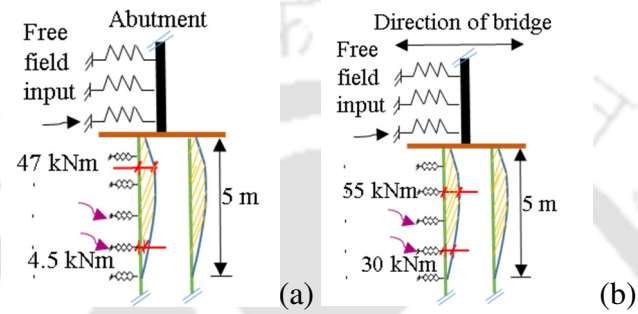

Fig. 7.1 Maximum bending moment diagram (not to scale) in piles below left abutment for the original bridge model in (a) soft clay at t =12.52 s and (b) loose sand at t = 12.56 s under GM#1.

The schematic diagrams of the retrofitted abutment foundation for M2 model are shown in Figs. 7.2(a) to 7.2(c). In the numerical model of the encased new piles, the spring-dashpot elements representing the lateral strength, lateral stiffness and the damping characteristics of the grout are modelled in series configuration with the soil spring-dashpot elements. The force-displacement characteristic corresponding to the lateral bearing capacity of jet grouting, is taken from He *et al*. (2016). For the original piles, the same spring-dashpot elements used in the study in Chapter 6, are modelled.

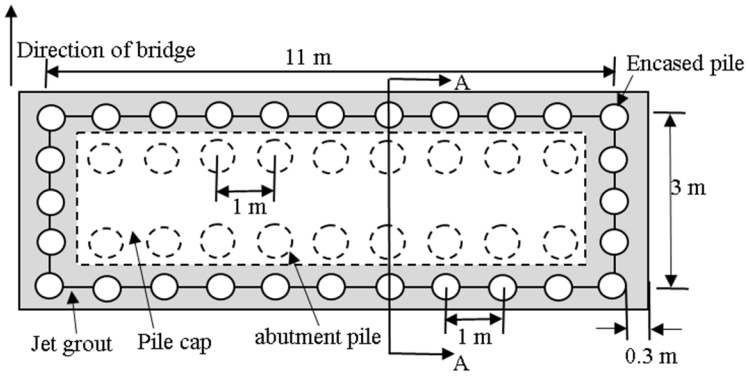

(a)

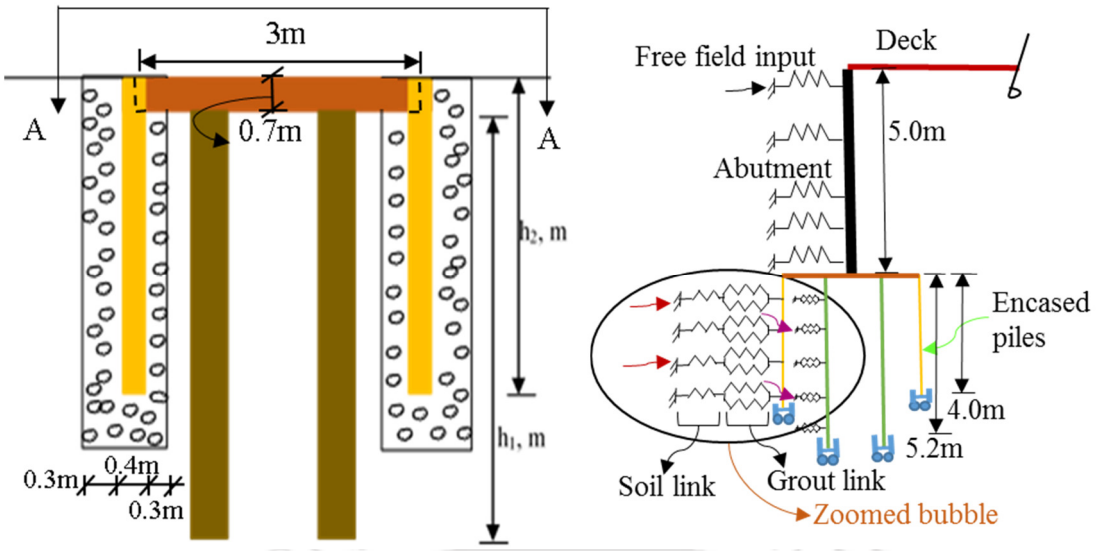

(b) (c)

Fig. 7.2 (a) Schematic diagram of retrofitted abutment foundation in plan,(b) vertical section A-A (h_1 = height of abutment pile; h_2 = height of encasement pile) and (c) spring-dashpot model of the abutment and its retrofitted foundation in medium stiff clay.

7.2.2 Encasement method at pier pile foundation

For M2 model, the maximum bending moments are observed in the piles below the 3rd and the 6th piers (Fig. 7.3). Like the extent of the significant bending moment diagram observed in the original abutment piles, the pier piles are also subjected to significant bending moment till a depth of 4 m during NTHA under GM#1. So, the length of new encased piles is kept as 4 m. However, the diameter of the new encased piles is considered as 0.8 m. To integrate the new encased piles with the original pile cap, the original pile cap is extended (Wang, 2015) equally along both the directions from the size of 7m×7m to 8m×8m in plan. The schematic diagram of the retrofitted pier pile foundation is shown in Fig. 7.4. Henceforth, the bridge model with retrofitted abutment and pier pile foundations will be referred to as M3 model.

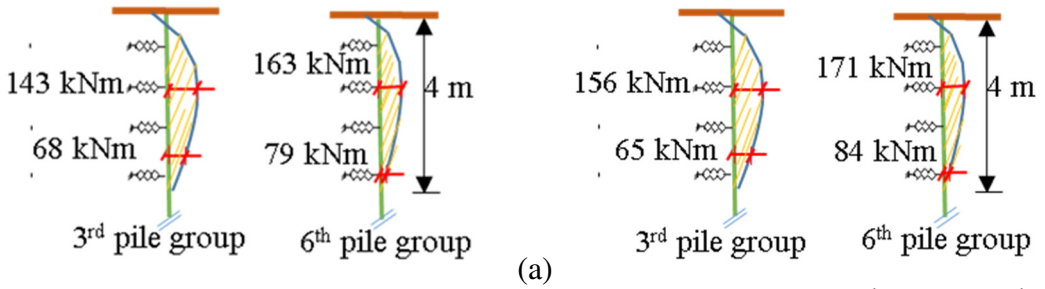

Fig. 7.3 Maximum bending moment diagram of pier piles below 3rd pier and 6th pier from M2 models in (a) soft clay and (b) loose sand foundation soil, as obtained under GM#1

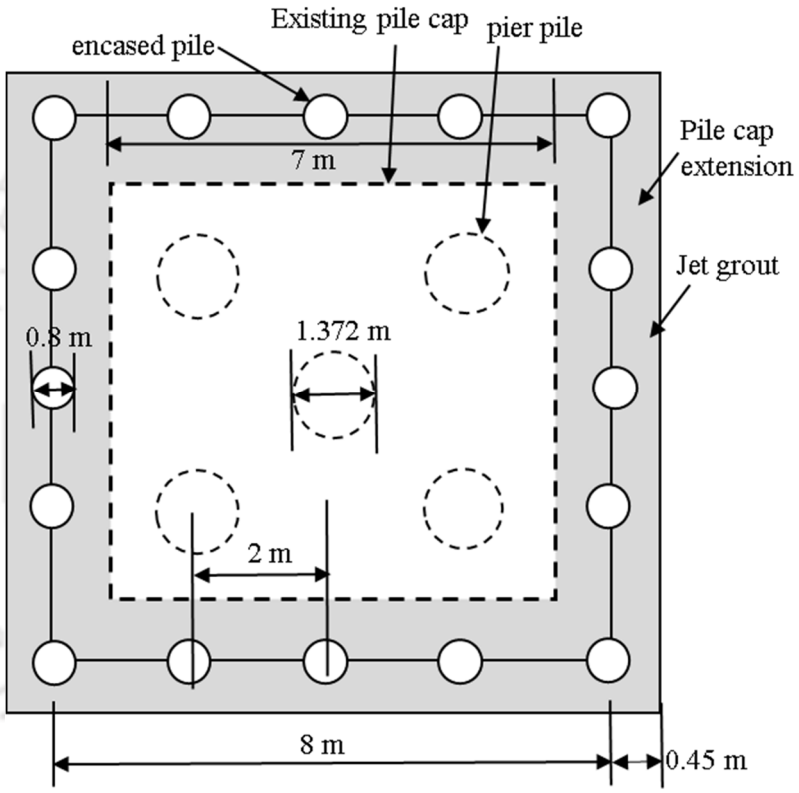

Fig. 7.4 Plan view of pier pile foundation with encased piles in jet grout

7.3 Analysis

To investigate the effect of encasement method on the bridge response, NTHA is carried out for the 9-span integral bridge with the models M1, M2 and M3 only under the ground motion GM#1 (shown in Fig. 6.7(b)). The dynamic analysis is carried out for the four types of foundation soil (properties given in Table 6.2), namely (a) medium stiff clay, (b) soft clay, (c) dense sand and (d) loose sand for the mentioned models. In the first stage of

analysis, the dynamic response of M1 and M2 models are compared and in the second stage of the analysis, the response of M2 and M3 models are compared. In Table 7.1, the natural periods of the M1 and M2 models in four different types of foundation soil for are compared. The comparison reflects the higher stiffness of M2 model as compared to the M1 model for all the types of soil.

Table 7.1 Natural period of 9 span integral bridge model in different foundation soils

Model	Medium stiff clay	Loose sand	Soft clay	Dense sand
M2	2.49	2.60	2.65	2.38
M1	3.15	3.22	3.25	3.15

7.4 Results

7.4.1 Comparison between M1 and M2 models

In Fig. 7.5, the moment-rotation response of the original abutment piles and the pier piles at a depth of 1.25 m from soil surface are compared for M1 and M2 models. Although the moment-rotation response gets reduced for M2 model in all the types of soils except dense sand for abutment piles (Figs. 7.5(a) and 7.5(c)). For M1 and M2 models, in medium stiff clay and dense sand, pier piles are going through extensive nonlinearity (Figs. 7.5(b) and 7.5(d)). In soft clay foundation soil, the response in the pier piles and the abutment piles get reduced in M2 model as compared to the M1 model. Though in loose sand, the pier piles are forming nonlinear loops, the moment-rotation response are similar in magnitude for both M1 and M2 models. The reduced response in the retrofitted foundation imposes lesser seismic deformation demand on the bridge substructure and superstructure.

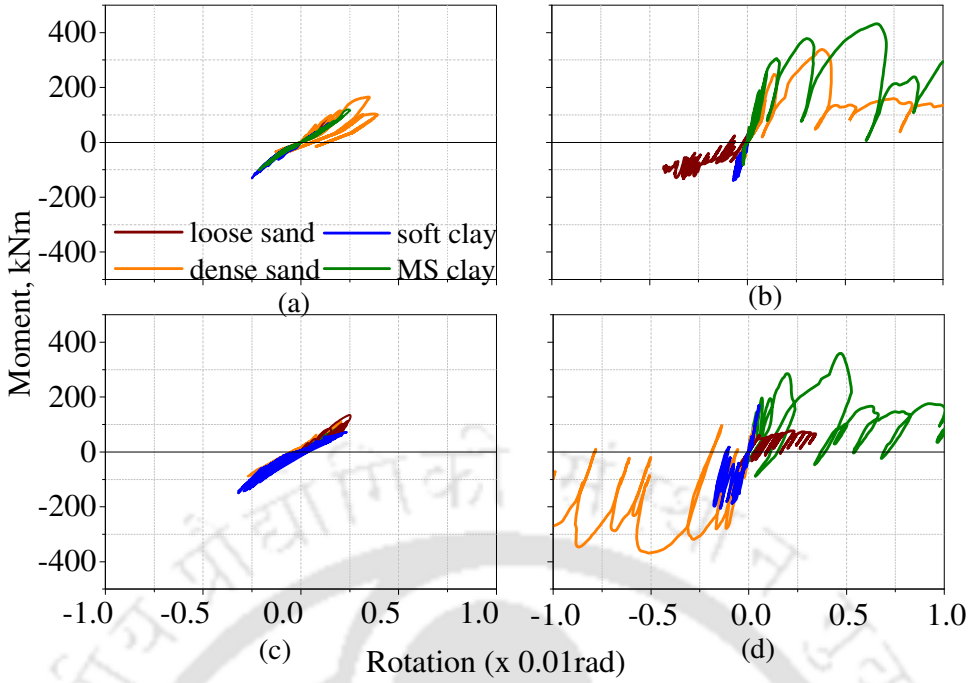

Fig. 7.5 Moment-rotation curves of M2 model for (a) abutment and (b) pier piles, and of M1 model for (c) abutment and (d) pier piles at the depth of 1.25 m, obtained under GM#1 (where, MS clay = medium stiff clay).

In Fig. 7.6, moment-rotation response in the 3rd pier are shown for a cross-section located at a depth of 1.2 m from the top of the pier. In loose sand, dense sand and soft clay (Figs. 7.6(a), 7.6(b) and 7.6(c)), insignificant nonlinear behaviour is observed in the cross-section for M1 and M2 models, though the pier response have reduced for the M2 model in those soils. In Fig. 7.6(d), in medium stiff clay foundation soil, pier is showing significant nonlinear behaviour in M1 model. But in M2 model, nonlinearity in pier has reduced with a reduction in moment-rotation response.

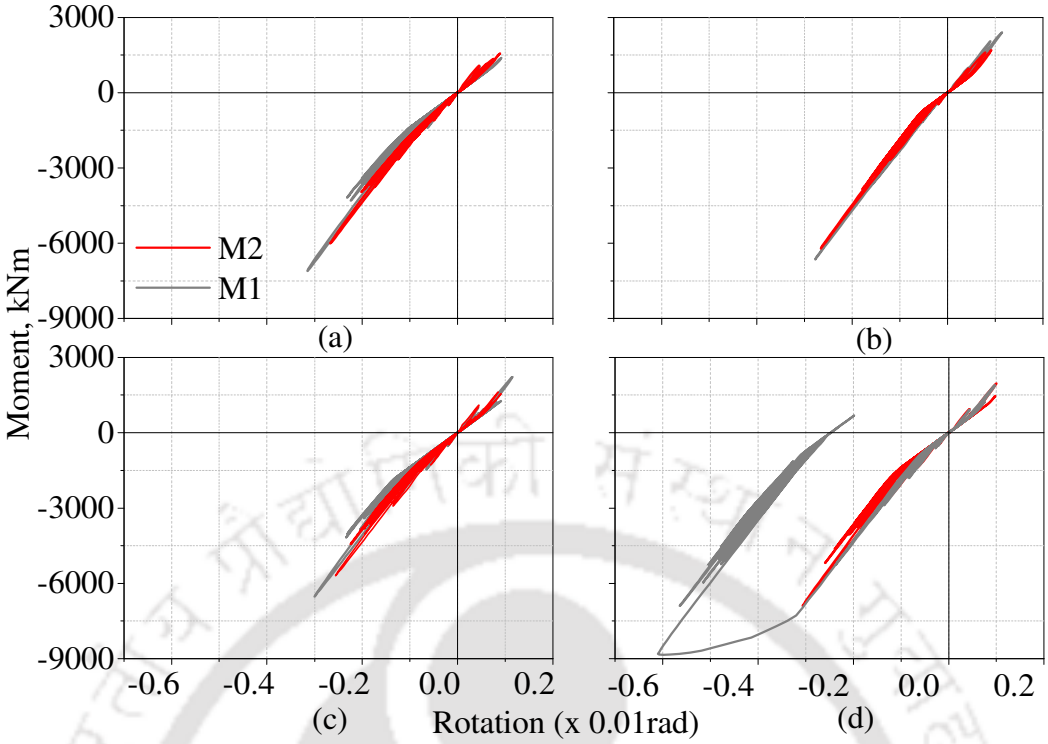

Fig. 7.6 Moment-rotation response in 3rd pier of M1 and M2 models for the cross-section located at 1.2 m depth from the top of the pier, in (a) loose sand, (b) dense sand, (c) soft clay and (d) medium stiff clay, obtained under GM#1.

Under GM#1, inelastic response is observed for the variation of axial force with axial displacement of the soil link elements at a depth of 2 m, in case of abutment piles of M1 model in loose sand (Fig 7.7(a)). However, the same gets reduced to linear elastic behaviour in case of M2 model. For the same soil at a depth of 4 m, linear elastic behaviour is observed for the link elements but with reduced response for M2 model (Fig. 7.7(c)). In dense sand, the response of soil link gets increased for the M2 model at the depth of 2m (Fig. 7.7(b)), as compared to the response of M1 model at the same depth. At the depth of 4 m in dense sand, the soil link response remains almost the same for both the models (Fig. 7.7(d)). Thus, the response of soil links gets modified in presence of encased piles for loose sand at the depth of 2 m due to higher lateral capacity of overall pile group and this effect is absent in case of dense sand. Similarly, for abutment piles in soft clay, the reduction in linear elastic response of the soil links is observed at the depths

of 2 m and 4 m (Figs. 7.8(a) and 7.8(c)). In case of medium stiff clay, marginal reduction in the linear axial force - axial displacement response is observed for the soil links at both the depths (Figs. 7.8(b) and 7.8(d)). Thus, the installation of new encased piles significantly affects the response of soil with lower lateral stiffness as compared to the response of soil with higher lateral stiffness.

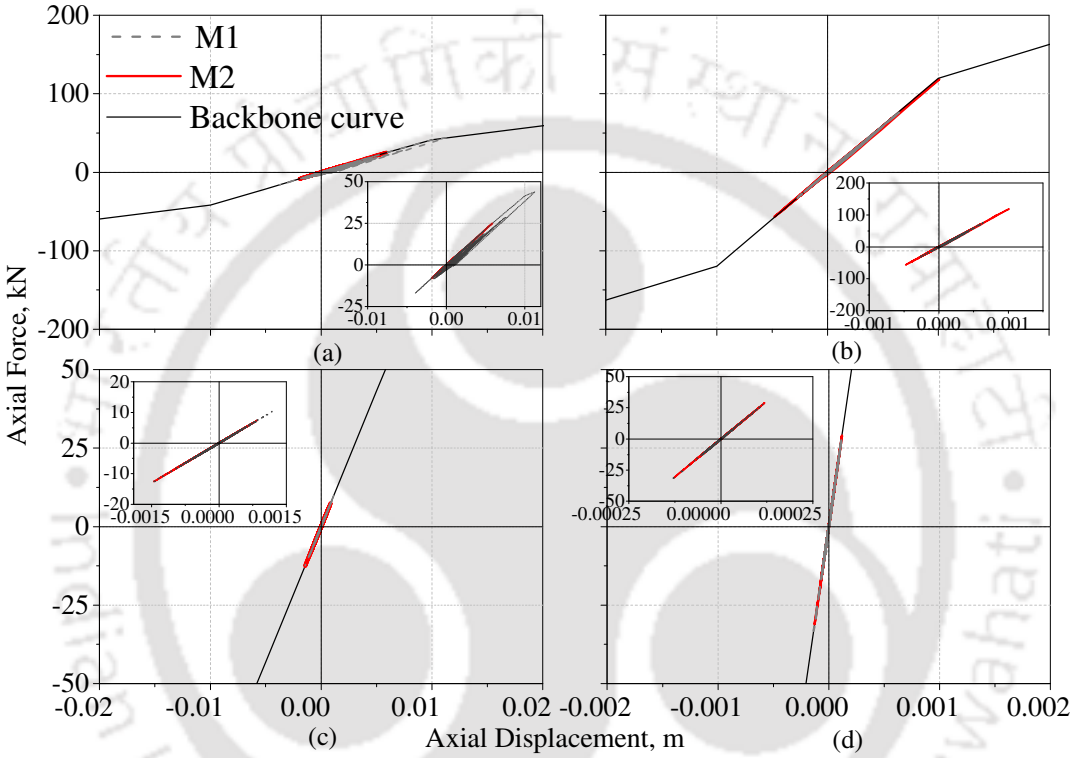

Fig. 7.7 Variation of axial force with axial displacement of the soil link elements at the depth of 2 m in (a) loose sand, (b) dense sand, and at the depth of 4 m in (c) loose sand and (d) dense sand for abutment pile under GM#1.

In Fig. 7.9, the variation of axial force with axial displacement of grout link elements is shown for different types of foundation soil at the depth of 1 m from the top of the encased pile. As observed, the grout link elements are subjected to very low axial strain levels, thus, low-level inelastic behaviour gets mobilized in the grout. The grout is expected to undergo cracking under very high tensile strain although the deformation of grout is very minimal in the present study. Among the soils, the maximum and the minimum response on the compression side are observed for encased piles in soft clay

and loose sand respectively. Similar to soil links, grout links have also very negligible effect on pile behaviour in terms of axial force-deformation. Grout links are modelled in series with soil links, thus grout and soil link behaviour interact with each other.

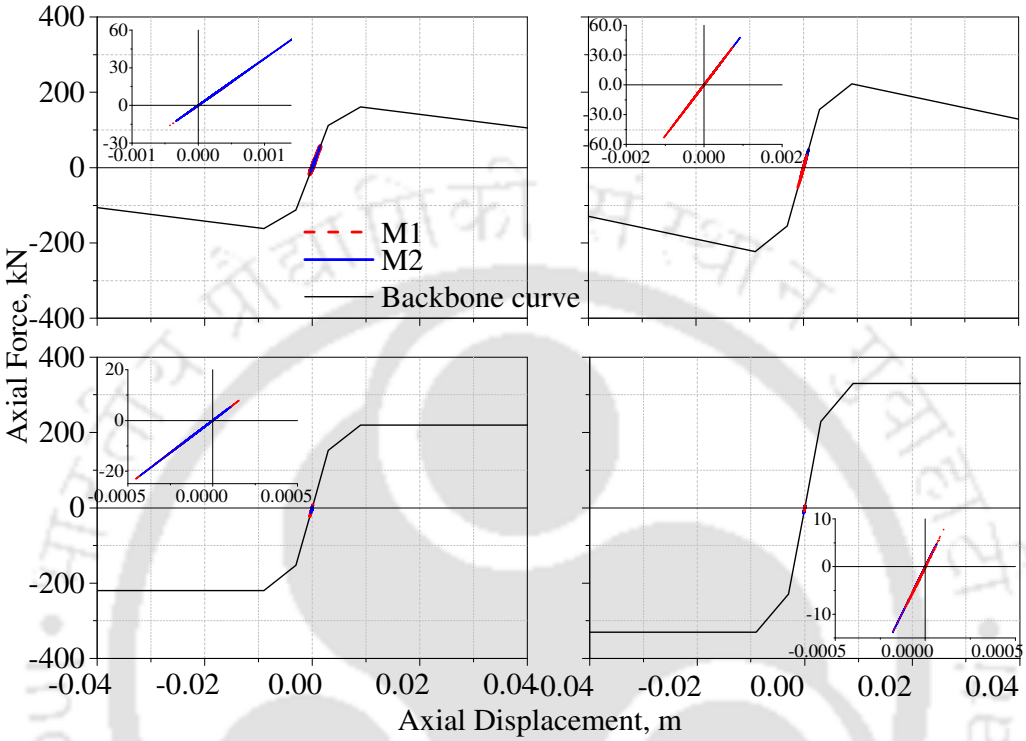

Fig. 7.8 Variation of axial force with axial displacement for the soil link elements at the depth of 2 m in (a) soft clay, (b) stiff clay, and at the depth of 4 m in (c) soft clay and (d) medium stiff clay for abutment pile under GM#1.

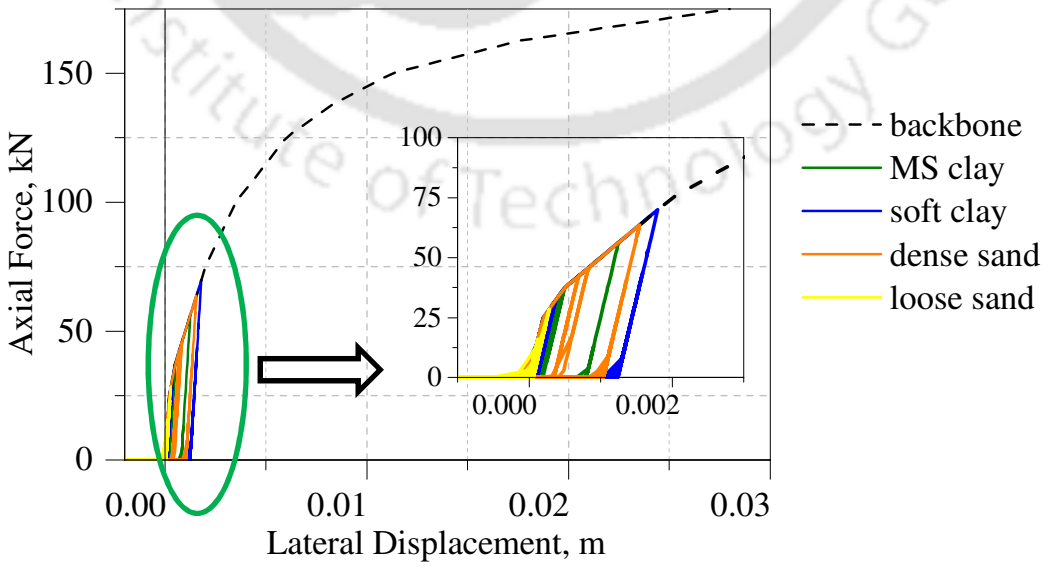

Fig. 7.9 Variation of axial force with axial displacement of grout link elements at the depth of 1 m of encased pile for M2 model (where, MS clay = medium stiff clay).

The displacement time histories (DTHs) at the top of 3rd pier (deck-pier junction) for M1 and M2 models are shown in Fig. 7.10. The residual displacements of M1 model in loose and dense sand are 0.10 m and 0.097 m, respectively (Fig. 7.10(a)). While in M2 model, the overall deck response gets reduced along with the values of residual displacements as 0.03 m and 0.075 m in loose sand and dense sand, respectively. A similar reduction in bridge deck response is observed for M2 model in soft clay and medium stiff clay as compared to the response of M1 model in the same soils (Fig. 7.10(b)). The M1 model is observed to have peak displacement response of 0.24 m and 0.28 m respectively, and residual response of 0.069 m and 0.15 m respectively in soft clay and medium stiff clay. For the same soils, the residual displacement response at the deck level of M2 model get reduced to 0.036 m and 0.10 m, respectively. The reduction in overall bridge deck response can be primarily attributed to the increased lateral stiffness of the abutment pile groups as well as that of the bridge through addition of the new encased piles. That also leads to the improvement of serviceability aspect of the bridge deck.

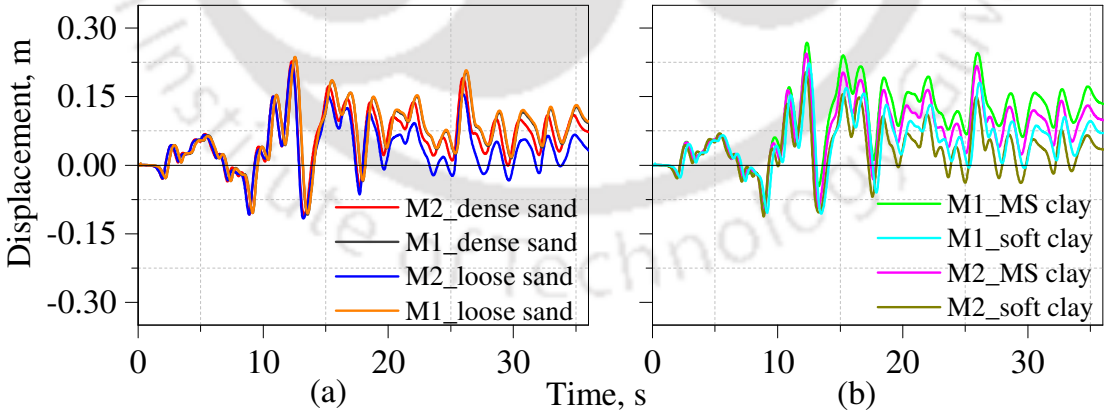

Fig. 7.10 Comparison of DTHs at the top of 3rd pier in (a) loose sand and dense sand, and (b) medium stiff clay and soft clay, for M1 and M2 models under GM#1 (where, MS clay = medium stiff clay).

7.4.2 Comparison between M2 and M3 models

Moment-rotation response in 3rd pier of M2 and M3 models for the cross-section located

at 1.2 m depth from the top of the pier in different types of foundation soil are shown in Fig. 7.11. In all the piers of M3 models, moment rotation response get reduced and piers are showing linear elastic behaviour for all the different types of soil. Thus, retrofitting at pier pile foundation is more effective than abutment pile foundation for this specific bridge as it reduces substructure response significantly.

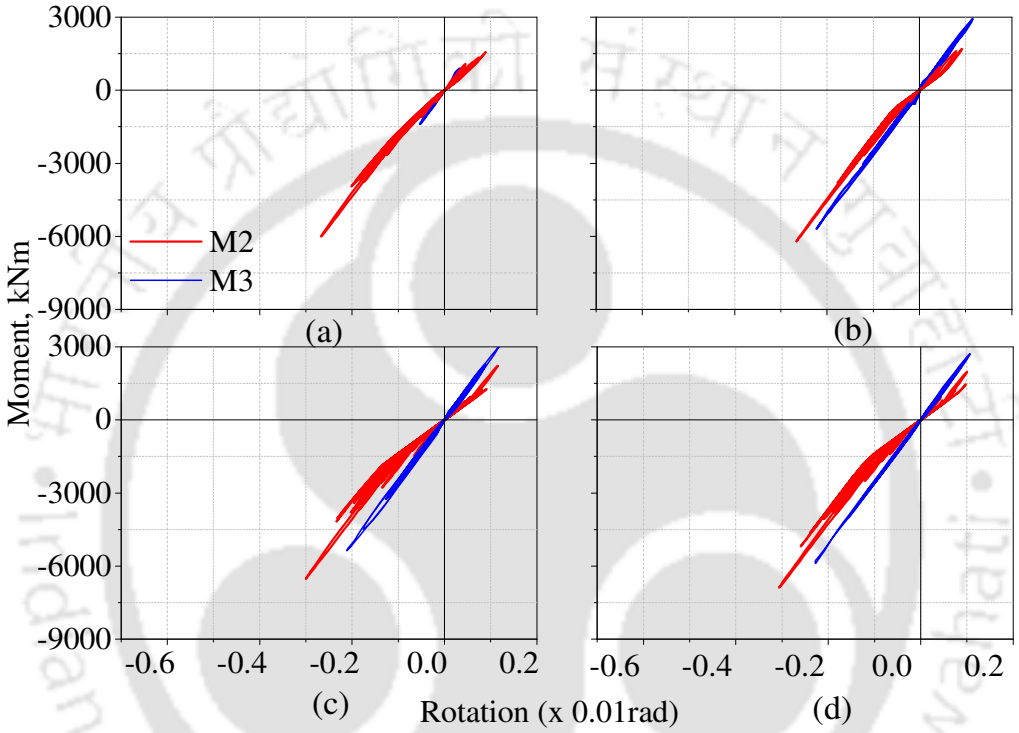

Fig. 7.11 Moment-rotation response in 3rd pier of M2 and M3 models for the cross-section located at 1.2 m depth from the top of the pier, in (a) loose sand, (b) dense sand, (c) soft clay and (d) medium stiff clay, obtained under GM#1.

The moment-rotation response of pier piles in M2 and M3 models are compared for cross-sections located at a depth of 1.25 m (Fig. 7.12). Between the depths of 1–2 m of pile length, monitored moment-curvature is found to be significant. In loose sand (Fig. 7.12 (a)) and soft clay (Fig. 7.12(c)), pier piles nonlinearity reduces in M3 model from M2 model. Pier piles rotation gets reduced with increase in moments for M3 model. In dense sand and medium stiff clay, nonlinear behaviour of pier piles gets reduced in M3 model significantly and the piles are forming narrow nonlinear loops at the same depth

of 1.25 m (Figs. 7.12(b) and 7.12(d)). For M3 models in different types of foundation soil, the response of the overall bridge is observed to be significantly reduced specially in medium stiff clay and dense sand.

For abutment piles in loose sand, linear elastic moment-rotation response is observed at the depth of 1.25 m from the ground level for M3 model and response has reduced from M2 model (Fig. 7.13 (a)). For all other soils, moment-rotation response is observed to be more for M3 models than M2 models at abutment piles (Figs. 7.13 (b), 7.13 (c) and 7.13(d)). So, special attention needs to be taken to achieve linear elastic response at abutment piles for M3 models.

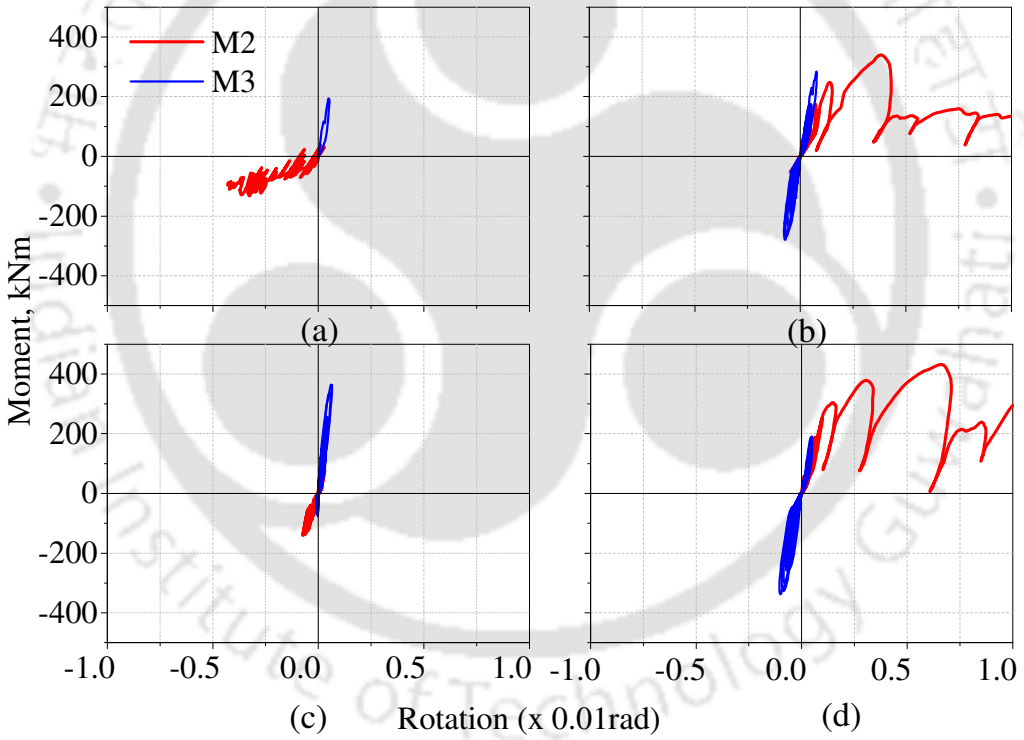

Fig. 7.12 Comparison of moment-rotation response for pier piles in M2 and M3 models at a depth of 1.25 m with (a) loose sand, (b) dense sand, (c) soft clay and (d) medium stiff clay under GM#1.

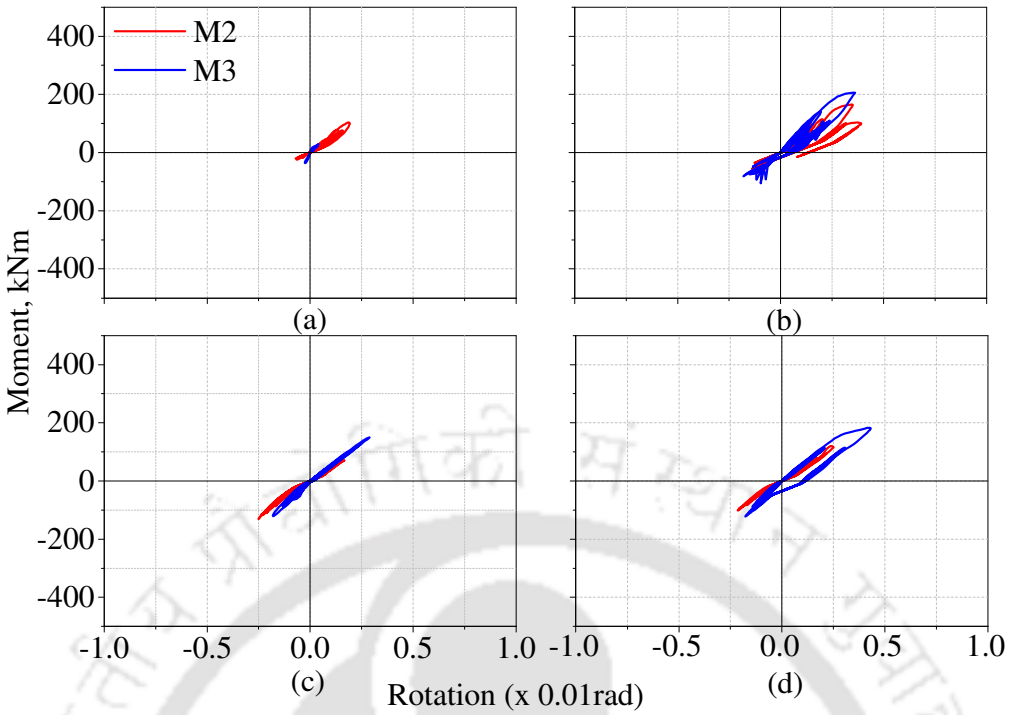

Fig. 7.13 Comparison of moment-rotation response for abutment piles in M2 and M3 models at a depth of 1.25 m with (a) loose sand, (b) dense sand, (c) soft clay and (d) medium stiff clay under GM#1.

Comparison of the DTHs at bridge deck level for the two models shows the reduction of deck displacement for stiff clay and dense sand foundation soils (Figs. 7.14(a) and 7.14(b)). The displacement response of M3 model in loose sand and soft clay are quite similar to that of the M2 model. With the presence of new encased piles at abutments and pier foundations, there is a significant increase in the lateral stiffness of the overall bridge that further leads to the observed reduction in bridge deck response. At deck level, the nonlinear behaviour of the piers has reduced significantly (Fig. 7.11), thus the displacement of the deck also gets reduced and ends up with insignificant residual deformation.

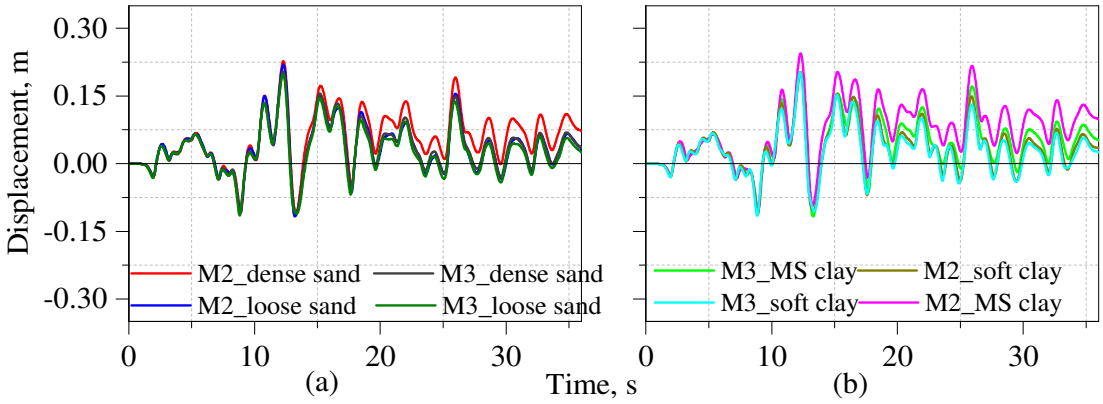

Fig. 7.14 Comparison of DTHs at the top of 3rd pier of M2 and M3 models in (a) loose sand and dense sand, and (b) medium stiff clay and soft clay under GM#1 (where, MS clay = medium stiff clay).

7.5 Discussion

In the present chapter, the effectiveness of retrofitting of pile foundation through encasement of new piles in jet grouting, is investigated on 9 span integral bridge model under GM#1 (with the similar bridge and soil parameters as mentioned in Chapter 6). The present study attempted to explore the possible implementation of jet grouting in strengthening of pile foundation. The force displacement curve for jet grout link is grout-pile interaction curve taken from experimentally established and numerically verified study (He *et al*., 2016). For more details, a parametric study is required to be carried out by varying grout properties like water-cement ratio or replacement ratio of cement. The lateral stiffness of pile increases partially due to increase of the apparent diameter of the pile under the extension of failure wedge and increased passive resistance during jet grouting. The jet-grouting provides additional confinement surrounding the new concrete pile, which reduces development of tensile stress in the pile. Thus, tension-induced nonlinearity in the RC pile gets reduced and degradation of stiffness and strength of the pile is lesser as compared to that of the original pile. Also, the effectiveness of the circumferential confinement is reduced by the grouting cracks because of the significant axial and circumferential tensile stress under dynamic loading. So, the lateral load

capacity of the encased pile is governed by passive resistance of soil and plastic damage of jet grouting.

The response of abutment piles are observed to get increased from M1 models to M3 models in all types of foundation soils except loose sand. However, the response of the pier piles gets reduced significantly from M2 to M3 models on implementation of the retrofitting technique. However, for the piers, response has reduced at all retrofitting stages. More studies need to be carried out regarding the strengthening of abutment piles for M3 models.

The effectiveness of the first stage of retrofitting (response of the M2 model) is reflected through the reduction of residual displacement at deck level by 67.1% and 53.2% as compared to the response of M1 model in medium stiff clay and soft clay, respectively. When further encased piles are added at pier pile foundation, the response of M3 models get reduced with reduction in deck-level displacement. Also, linear elastic response is observed in the bridge piers in all types of foundation soils of M3 models as compared to the nonlinear response of M1 models.

Chapter 8

Conclusions and Future Scope of Work

8.1 Conclusions

The significant contribution of the present study involves the comprehensive comparison of seismic response of an integral bridge on RC pile foundation using the detailed and simplified modelling approaches for soil-structure interaction. From the results, significant differences are observed in the response quantities using the two modelling approaches. Subsequently, the nonlinear behaviours of the substructure and foundation components of an integral bridge are also investigated by varying the overall length of the integral bridge model. Finally, with the possibility of extensive seismic damages in RC pile foundation below such bridge, the applicability of retrofitting of pile foundation using new encased piles in jet grout, is investigated for the considered 9 span integral bridge model.

Based on the present study, the following salient conclusions are drawn:

1. Consideration of soil domain and the foundation in the modelling of bridge-foundation-soil system (in absence of backfill soil) results in reduced overall response of the system under site specific ground motions, as compared to the response without the modelling of the soil domain (also in absence of backfill soil). Under strong earthquake shaking, differential settlement occurs at different location of bridge foundation. Abutment backfill itself may withstand high deformation and it reduces the amplification of bridge superstructure by confining it, along the length of the bridge, from both the ends.
2. The presence of abutment-backfill interaction tends to restrain the bridge deck during earthquake shaking, leading to a reduction in the displacement response at the deck level. During strong earthquake shaking, nonlinearity in structural components tends

to dominate the seismic response of integral bridge-foundation-soil system. However, during low intensity of earthquake shaking, nonlinearity of soil tends to govern the overall system response.

3. The simplified modelling of soil-structure interaction through nonlinear spring-dashpot system tends to overestimate the bridge-foundation response as compared to the integral bridge-foundation response obtained by modelling of soil as a continuum. This is attributed to the higher lateral stiffness and strength of soil as estimated by the conventionally used API curves (API, 2000) for foundation soil. The use of spring-dashpot model enhances the response at the deck level and results in higher forces and moments at pier-deck junctions.
4. In presence of backfill soil, the spring-dashpot modelling approach leads to higher nonlinear response of integral bridge-foundation system as compared to the response obtained by adopting the continuum soil model.
5. With increase in the overall length, seismic demand on an integral bridge with RC pile foundation increases due to the monolithic action of the bridge abutment-deck-pier system. During strong earthquake shaking, the pile foundation below such long integral bridge, particularly in clayey soil, is observed to become vulnerable to failure.
6. *Full SSI with BA* model shows lesser moment-curvature response compare to *FB_SD with BA* model so the overall imposed deformation on the bridge is also less. The residual deck displacement of *FB_SD with BA* model is also higher. Which results in elasto-plastic behaviour in bridge piers. From damping point of view, SSI models release more seismic energy than the *FB_SD* models in presence of continuum soil domain. Bridge piers structural response (moment and shear force) have been upto 10% higher in *FB_SD* models than *full SSI* models. So, from a designer point of view,

if engineers want to predict the piers designing forces from *FB_SD* models then they might be over predicting the results by 10% in reality for this specific local site condition, but, prior to that, proper site investigation analysis needs to be carried out.

7. The retrofitting method of pile foundation in an integral bridge through addition of new piles encased with jet grout, is found to be more effective for reducing the overall response of the bridge on medium stiff clayey soil.

8.2 New Contributions of the Present Study

The novelty of the present work is discussed as follows:

1. The seismic response of a multi-span integral bridge-soil system, with RC pile foundation, is compared with the different modelling approaches considering simplified and detailed soil-structure interaction aspects, along with site-specific ground motions. The relative performance of an integral bridge using commonly adopted spring-dashpot soil model with that of an integral bridge using detailed continuum soil model is investigated (absent in past studies).
2. The influence of overall length of an integral bridge-foundation-soil system on its response due to temperature loading, has been investigated in the past studies. However, the variation in seismic response of such an integral bridge-foundation-soil system with overall length, is attempted for the first time.
3. Effectiveness of seismic retrofitting of RC pile foundation below an integral bridge, using new piles encased in jet grout, is studied through numerical modelling of the bridge-pile-soil system. Past studies have carried out practical implementations of different methods, but the numerical modelling and analysis were absent for the different methods.

8.3 Scope of Future Work

1. The comparative seismic response of bridge-soil system using different modelling approaches can be studied for other types of bridges with bearings or shear keys. Particularly, the relative performances of bridge-soil system with spring-dashpot modelling and soil continuum modelling, under nonlinear time history analysis, need to be investigated.
2. The retrofitting method of pile foundation using new piles encased in jet grout, needs to be investigated in more detail for intermediate pier pile foundation in integral and other types of bridges. Detailed parametric study needs to be carried out by varying different bridge-specific parameters.
3. Further studies need to be conducted on the influence of ground motion parameters on the seismic response of an integral bridge-soil system, to identify the salient factors responsible for seismic vulnerability of such bridges.
4. API (2000) guidelines need reconsideration as it over predict the soil strength under dynamic analysis, which effects structural nonlinearities too. Correspondingly, foundation design should be rechecked if it's founded on softer soil and excess pore water pressure dissipation needs to be considered. Because over predicting foundation strength can be detrimental to overall bridge.
5. In case, the foundation soil is comparatively soft (mainly, sands) and soil liquefaction appears to be a major problem then it's better to consider interface elements to capture SSI in a more accurate manner. Because the present study is only limited to drained (or dry) condition of soil.
6. In the present study, varying the span length with no. of span of an integral bridge can be done in future to optimize the span length. With that, pier and pile configuration need to be arranged accordingly to complete the study.

★★★

References

AASHTO. (1989). *Guide Specifications - Thermal Effects in Concrete Bridge Superstructures*. Washington, DC: American Association of State Highway and Transportation Officials.

AASHTO. (1996). *Standard Specifications for Highway Bridges (16th ed.)*.Washington DC: American Association of State Highway and Transportation Officials.

AASHTO. (2002). *Standard Specifications for Highway Bridges (17th ed.)*. Washington DC: American Association of State Highway and Transportation Officials.

AASHTO LRFD. (2012). *Bridge Design Specifications (6th ed.)*. Washington, DC: American Association of State Highway and Transportation Officials.

Abendroth, R.E., & Greimann, L.F. (1988). Rational design approach for integral abutment piles. *Transportation Research Record,* 1233.

Abendroth, R. E., & Greimann, L. F. (2005). Field testing of integral abutments. Final Rep. HR-399, Iowa State University, Ames, IA.

Abendroth, R.E., Greimann, L.F., & Ebner, P.B. (1989). Abutment pile design for jointless bridges. *Journal of Structural Engineering, 115*, 2914–2929.

Abendroth, R. E., Greimann, L. F., & LaViolette, M. D. (2007). An integral abutment bridge with precast concrete piles. *Iowa Department of Transportation,* CTRE Project 99-48.

ACI. (1982). Prediction of creep, shrinkage, and temperature effects in concrete structures. *American Concrete Institute*, Tech. Rep. ACI 209R-82, Detroit, MI.

ADINA. (2017). Automatic Dynamic Incremental Nonlinear Analysis. *ADINA R & D, Inc*., Watertown, MA, www.adina.com.

AISC (1996). *Steel Construction Manual*. California: American Institute of Steel Construction. Inc., 13th edition, 1st print.

Anderson, D.G., Martin, G.R., Lam, I., & Wang, J.N. (2008). Seismic analysis and design of retaining walls, buried structures, slopes and embankments. *National Cooperative Highway Research Program*, NCHRP Report 611, Transportation Research Board, Washington, DC.

ANSYS. (2013). Mechanical APDL Introductory Tutorials, Release 15.0. ANSYS, Inc., PA, USA.

API RP2A-WSD. (2000). Recommended practice for planning, designing and constructing fixed offshore platforms-working stress design. American Petroleum Institute, 2000, Washington D.C, USA.

Argyroudis, S., Palaiochorinou, A., Mitoulis, S., & Pitilakis, D. (2016). Use of rubberised backfills for improving the seismic response of integral abutment bridges. *Bulletin of Earthquake Engineering*, *14*, 3573-3590.

Arockiasamy, M., Butrieng, N., & Sivakumar, M. (2004). State-of-the-art of integral abutment bridges: Design and practice. *Journal of Bridge Engineering*, *9*, 497–506.

Arockiasamy. M., & Sivakumar, M. (2005). Effects of restraint moments in integral abutment bridges. *The 2005FHWA Conference, Integral Abutment and Jointless Bridges (IAJB2005)* (pp. 185–198). Baltimore, MD.

Arsoy, S., Richard, M.B., & Duncan, J.M. (1999). *The behaviour of integral abutment bridges.* Virginia Tech. Research Counsel, VTRC 00-CR3, Blacksberg, VA.

Arsoy, S., Barker, R.M., & Duncan, M.J. (2002). *Experimental and analytical investigations of the piles and abutments of integral bridges.* Virginia Tech. Research Counsel, FHWA/NTRC 02-CR6, Charlottesville, VA.

Austroads. (2004). *Guide to the structural design of road pavements*. Austroads: Sydney, Australia.

BA 42/96 Amendment No. 1. (2003). *Design Manual for Integral Bridges: Design Manual for Road and Bridges.* Volume 1, Section 3, Part 12. The Highway Agency, UK.

Badoni, D., & Makris, N. (1996). Nonlinear response of single piles under lateral inertial and seismic loads. *Soil Dynamics and Earthquake Engineering*, *15(1),* 29–43.

Bahjat, R. (2014). *Short and Long-term Performance of a Skewed Integral Abutment Prestressed Concrete Bridge*, Master's Thesis. University of Massachusetts, Amherst, MA.

Baptiste, K.T., Kim, W., & Laman, J.A. (2011). Parametric study and length limitations for prestressed concrete girders integral abutment bridges. *Structural Engineering International, 21,* 151–156.

Barker, K.J., & Carder, D.R. (2001). Performance of an integral bridge over the m1- a1 link road at Bramham crossroads. *Transport Research Laboratory*, TRL Project Report 521, UK.

Barker, R.M., Duncan, J.M., Rojiani, K.B., Ooi, P.S.K., Tan, C.K., & Kim, S.G. (1991). Manual for the Design of Bridge Foundations. *National Cooperative Highway Research Program,* NCHRP Report 343, Transportation Research Board, Washington, DC.

Barr, P. J., Halling, M. W., Huffaker, C., & Boyle, H. (2013). Behaviour and analysis of an integral abutment bridge. *Department of Civil and Environmental Engineering, Utah State University,* Utah.

Bazant, Z.P., & Panula, L. (1980). Creep and shrinkage characterization for analysing prestressed concrete structures. *PCI Journal*, 86–121.

Bonczar, C., Brena, S., Civijan, S., DeJong, J., & Crovo, D. (2005). Integral abutment pile behaviour and design-field data and fem studies. *The 2005FHWA Conference, Integral Abutment and Jointless Bridges (IAJB 2005),* Baltimore, MD.

Boulanger, R.W., Curras, C.J., Kutter, B.L., Wilson, D.W., & Abghari, A. (1999). Seismic soil-pile-structure interaction experiments and analysis. Jr. of Geotech. Engg. ASCE, 125(9): 750-759.

Brødbæk, K.T., Møller, M., Sørensen, S.P.H., & Augustesen, A.H. (2009). Review of p-y relationships in cohesionless soil. Aalborg: *Department of Civil Engineering, Aalborg University*, DCE Technical Reports; No. 57.

Breña, S. F., Bonczar, C. H., Civjan, S. A., DeJong, J. T., & Crovo, D. S. (2007). Evaluation of seasonal and yearly behavior of an integral abutment bridge. *Journal of Bridge Engineering*, *12*, 296-305.

Briseghella, B., & Zordan, T. (2015). An innovative steel-concrete joint for integral abutment bridges. *Journal of Traffic and Transportation Engineering (English Edition)*, *2*, 209-222.

Broms, B. B. (1964). Lateral Resistance of Piles in Cohesive Soils. In *Proceedings of the American Society of Civil Engineers, Journal of the Soil Mechanics and Foundations Division*, *90*, SM2.

BSDC. (2017). *Bridge Structures Design Criteria.* Technical Standard Branch, Alberta Transportation, Canada.

BSI. (1998). Steel, concrete, and composite bridges. *British Standard Institution*, BS 5400-1: London, UK.

Burdette, E. G., Tidwell, J. B., Ingram, E. E., Goodpasture, D. W., Howard, S. C., Wasserman, E. P., and Deatherage, J. H. (2004). Lateral load tests on prestressed concrete piles supporting integral abutments. *PCI Journal*, 495, 70–77.

Burke, M.P.J. (1993). Integral bridges: attributes and limitations. *Transportation Research Record,* 1393.

Burke, M. P. J. (2009). *Integral and semi-integral bridges*. John Wiley & Sons.

Caltrans. (2004). *Seismic design criteria.* Version 1.3, California Department of Transportation, CA.

Caltrans. (2013). *Seismic design criteria*, California Department of Transportation Version 1.7.

CFEM. (2006). *Canadian Foundation Engineering Manual,* 4th edition. Canadian Geotechnical Society, Toronto, Canada.

Mander, J.B., Priestley, M.J.N. & Park R. (1984). Theoretical Stress-Strain Model for Confined Concrete. *Journal of Structural Engineering*, 114(3):1804-1826

Lopez-Caballero, F., Régnier, J., Bonilla, F. & Gélis, C. (2011). Site response analysis including earthquake input ground motion and soil dynamic properties variability. In: *Proceedings of the 15th World Conference on Earthquake Engineering*, Lisbon, Portugal.

CHBDC. (2014). *Canadian Highway Bridge Design Code*. Canadian Standards Association, CAN/CSA S6-14, Canada.

Chuhan, Z., Yanjie, X. & Feng, J. (1998) Effects of soil-structure interaction on nonlinear response of arch dams, Developments in Geotech Eng, 83:95-114, ISSN 0165-1250, http://dx.doi.org/10.1016/S0165-1250(98)80006-0.

Chung, Y. S., Park, C. K., & Lee, D. H. (2006). Seismic performance of RC bridge piers subjected to moderate earthquakes. *Structural Engineering and Mechanics*, *24*(4), 429-446.

Civjan, S. A., Bonczar, C., Brena, S. F., DeJong, J., & Crovo, D. (2007). Integral abutment bridge behavior: Parametric analysis of a Massachusetts bridge. *Journal of Bridge Engineering*, *12*(1), 64-71.

Civjan, S. A., Kalayci, E., Quinn, B. H., Breña, S. F., & Allen, C. A. (2013). Observed integral abutment bridge substructure response. *Engineering Structures*, *56*, 1177-1191.

Claugh, G.M., & Duncan, J.M. (1991). *Foundation engineering handbook*, Indian edition edn. CBS publisheres, New Delhi, India.

Comisu, C. C. (2005). Integral Abutment and Jointless Bridges. *The Bulletin of the Polytechnic Institute of Jassy, Construction. Architecture Section*, *51*, 107-117.

Conboy, D., & Stoothoff, E. (2005) Integral abutment design and construction: The New England experience. *The 2005FHWA Conference, Integral Abutment and Jointless Bridges (IAJB 2005)* (pp. 50-60). Baltimore, Maryland.

Connal, J. (2004). Integral Abutment Bridges–Australian and US Practice. In *5th Austroads bridge conference, Hobart, Tasmania*.

CSI. (2016). *Introduction to CSiBRIDGE*, v. 17. Computers and Structures, USA.

CSI. (2017). *Introduction to SAP2000*, v. 19.2.1. Computers and Structures, USA.

Cui, L., & Mitoulis, S. (2015). DEM analysis of green rubberised backfills towards future smart Integral Abutment Bridges (IABs). *Geomechanics from Micro to Macro, Vols I and II*, 583-588.

Darendeli, M.B. (2001). *Development of a new family of normalized modulus reduction and material damping curves*. Ph.D Thesis, University of Texas. Austin, Texas.

Darley, P., & Alderman, G.H. (1995). Measurement of thermal cyclic movements on two portal frame bridges on the m1. *Transport Research Laboratory*, TRL Project Report 165, UK.

Darley, P., Carder, D.R., & Barker, K.J. (1998). Seasonal thermal effects over three years on the shallow abutment of an integral bridge in Glasgow. *Transport Research Laboratory*, TRL Project Report 344, UK.

DeLano, J.G. (2002). *Behaviour of pile-supported integral abutments at bridge sites with shallow bedrock*. Master's thesis, Department of Civil Engineering, University of Maine.

Deng, Y., Phares, B. M., Greimann, L., Shryack, G. L., & Hoffman, J. J. (2015). Behavior of curved and skewed bridges with integral abutments. *Journal of Constructional Steel Research*, *109*, 115-136.

Dhar, S., Özcebe, A.G., Dasgupta, K., Dey, A., Paolucci, R. & Petrini, L. (2016). Nonlinear Dynamic Soil-Structure Interaction Effects on the Seismic Response of a Pile-Supported Integral Bridge Structure. In *6th International Conference on Recent Advances in Geotechnical Earthquake Engineering and Soil Dynamics.* Paper No. 141, New Delhi, India.

Dicleli, M. (2000). Simplified model for computer-aided analysis of integral bridges. *Journal of Bridge Engineering, 5,* 240–248.

Dicleli, M., & Albhaisi, S.M. (2003). Maximum length of integral bridges supported on steel h-piles driven in sand. *Engineering Structures, 25,* 1491–1504.

Dicleli, M., & Albhaisi, S.M. (2004). Performance of abutment-backfill system under thermal variations in integral bridge built in clay. *Engineering Structures, 26,* 949–962.

Douglas, B.M., & Reid, W.H. (1982). Dynamic test and system identification of bridges. *Journal of structural division, 108,* 2295–2312.

Duncan, J.M., & Arsoy, S. (2003). Effect of bridge-soil interaction on behaviour of piles supporting integral bridges. Transportation Research Record, 1849.

Duncan, M.J., & Mokwa, R.L. (2001). Passive earth pressure: Theories and tests. *Journal of Geotechnical and Geoenvironmental Engineering, 127*, 248–257.

Dunker, K. F., & Liu, D. (2007). Foundations for integral abutments. *Practice Periodical on Structural Design and Construction*, *12*(1), 22-30.

Dutta, T.K. (2010). *Seismic Analysis of Structures*. John Wiley & Sons (Asia) Pte Ltd.

Efretuei, E. O. (2013). *Thermal impact on soil-structure interaction for integral bridges* (PhD dissertation). School of Civil Engineering, University of Leeds, UK.

Elgamal, A., Yan, L., Yang, Z., & Conte, J.P. (2008). Three-dimensional seismic response of Humboldt bridge-foundation-ground system. *Journal of Structural Engineering, 134*, 1165–1176.

Emerson, M. (1976). Bridge temperatures estimated from the shade temperature. *Transportation Research Record*, TLR Project Report 696, Transport and Road Research Laboratory, UK.

EN 1998-2. (2005). *Eurocode 8: Design of structures for earthquake resistance*. Part 2: Bridges. Brussels, Belgium.

England, G.L., Tsang, N.C.M., & Bush, D.L. (2000). *Integral Bridges: A Fundamental Approach to the Time-Temperature Loading Problem.* Thomas Telford Ltd. UK.

Erhan, S., & Dicleli, M. (2017). Parametric study on the effect of structural and geotechnical properties on the seismic performance of integral bridges. *Bulletin of Earthquake Engineering*, *15*(10), 4163-4191.

Fan, C.C, & Long, J.H. (2005). Assessment of existing methods for predicting soil responses of laterally loaded piles in sand. *Computers and Geotechnics, 32,*274–289.

Far, N. E., Maleki, S., & Barghian, M. (2015). Design of integral abutment bridges for combined thermal and seismic loads. *Earthquakes and Structures*, *9*, 415-430.

Faraji, S., Ting, J.M., Crovo, D.S., & Ernst, H. (2001). Nonlinear analysis of integral bridges: finite element model. *Journal of Geotechnical and Geoenvironrnental Engineering, 127,* 454–461.

Figini, R & Paolucci, R. (2017). Integrated foundation–structure seismic assessment through non-linear dynamic analyses. *Earthquake Eng & Struct. Dyn.*, *46(3)*, 349-367. 10.1002/eqe.2790.

Fleming, W. G. K., Weltman, A. J., Randolph, M. F., & Elson, W. K. (1992). *Piling Engineering.* Blackie Academic & Professional, Glasgow, UK.

Filippou, F.C., Popov, E.P. & Bertero, V.V. (1983). Effects of Bond Deterioration on Hysteretic Behavior of Reinforced Concrete Joints. *Earthquake Engineering Research Center*, Report EERC 83-19, University of California, Berkeley.

Frangi, A., Collin, P., & Geier, R. (2011). Bridges with Integral Abutments: Introduction. *Structural Engineering International*, *21*, 144-150.

Frosch, R.J., Wenning, M., & Chovichien, V. (2005). The in-service behavior of integral abutment bridges: abutment-pile response. *The 2005FHWA Conference, Integral Abutment and Jointless Bridges (IAJB 2005)* (pp. 270-280). Baltimore, MD.

Fukada, H., Kato, K., Aoyagi, M., Inagawa, H., & Shioi, Y. (2005). Application of reinforcing methods for existing pile foundation on soft ground (in-cap method). In *Public Works Research Institute: The 23th US-Japan Bridge Engineering Workshop. Retrieved July* (Vol. 1, p. 2014).

Gazetas, G. (1991), Formulas and charts for impedances of surface and embedded foundations. *Jr. of Geotech. Eng. 117(9*), 1363-81.

Gazetas, G., & Dobry, R. (1984). Horizontal response of piles in layered soils. *Journal of Geotechnical Engineering, 110(1),* 20–40.

Gentela, S.R., & Dasgupta, K. (2012). Influence of soil-structure interaction on seismic design of reinforced concrete integral bridges. In: *Proceedings of the International Symposium on Engineering under Uncertainty: Safety Assessment ad Management (ISEUSAM-2012)* (pp. 743–756). Kolkata: Springer.

Gibbens, B., & McManus, A. (2011). Design of Peninsula Link Integral Bridges. In *Austroads Bridge Conference,* Sydney.

Girton, D.D., Hawkinson, T.R., & Greimann, L.F. (1991). Validation of design recommendations for integral-abutment piles. *Journal of Structural Engineering*, *117*, 2117–2134.

Granas, J.L. (2016). Undrained lateral soil response of offshore monopile in layered soil. M.Tech Thesis, *Dept. of Civ. & Transport Eng*., NTNU.

Greimann, L.F., & Wolde-Tinsae, A.M. (1988). Design model for piles in jointless bridges. *Journal of Structural Engineering, 114*, 1355–1369.

Greimann, L. F., Wolde-Tinsae, A. M., & Yang, P. S. (1983). Skewed bridges with integral abutments. *Transportation Research Record*, 903.

Greimann, L. F., Yang, P. S., Edmunds, S. K., & Wolde-Tinsae, A. M. (1984). Design of Piles for Integral Abutment Bridges: Final Report. *Department of Civil Engineering, Engineering Research Institute*, Iowa State University.

Greimann, L.F., Yang, P.S., & Wolde-Tinsae, A.M. (1986). Nonlinear analysis of integral abutment bridges. *Journal of Structural Engineering*, *112*, 2263–2280.

Greimann, L.F., Abendroth, R.E., Johnson, D.E., & Ebner, P.B. (1987). Pile design and tests for integral abutment bridges: Final report. *Iowa State University, Iowa Department of Transportation,* No. Iowa DOT Proj. HR-273.

Hansen, J. B. (1963). Discussion on Hyperbolic Stress-Strain Response, Cohesive Soils. *Journal for Soil Mechanics and Foundation Engineering*, *89*, 241- 242.

Hashash, Y.M.A., Musgrove, M.I., Harmon, J.A., Groholski, D.R., Phillips, C.A., & Park, D. (2016). *DEEPSOIL 6.1, User Manual*. Urbana, IL, Board of Trustees of University of Illinois at Urbana-Champaign

Hassiotis, S., Lopez, J.A., & Bermudez, R. (2005). Full scale testing of an integral abutment bridge. *The 2005FHWA Conference, Integral Abutment and Jointless Bridges (IAJB 2005).* Baltimore, MD.

Hassiotis, S., Khodair, Y., Roman, E., & Dehne, Y. (2006). Evaluation of integral abutments. *New Jersey Department of Transportation* and *U.S. Department of Transportation, Federal Highway Administration.* No. FHWA-NJ-2005-025.

He, B., Wang, L., & Hong, Y. (2016). Capacity and failure mechanism of laterally loaded jet-grouting reinforced piles: Field and numerical investigation. *Science China Technological Sciences*, *59*(5), 763-776.

Hibbitt, D., Karlsson, B., & Sorensen, P. (2014). *ABAQUS/CAE Standard User's Manual (Version 6.14).* Pawtucket, RI.: Hibbitt, Karlsson & Sorensen.

Holzer, T.L., Padovani, A.C., Bennett, M.J., Noce, E.T., Tinsley, J.C. (2005). Mapping NEHRP V_{S30} Site Classes. *Eq. Spectra, 21(2),* 1-18.

Horvath, J. S. (2000). Integral-abutment bridges: problems and innovative solutions using EPS geofoam and other geosynthetics. *Manhattan College, School of Engineering*, Research Report No. CE/GE-00, 2, NY.

Horvath, J. S. (2005). Integral-abutment bridges: Geotechnical problems and solutions using geosynthetics and ground improvement. *The 2005FHWA Conference, Integral Abutment and Jointless Bridges (IAJB 2005*) (pp. 281-291). Baltimore, MD.

Huang, J., Shield, C. K., & French, C. E. (2008). Parametric study of concrete integral abutment bridges. *Journal of Bridge Engineering*, *13*, 511-526.

Huckabee, P. (2005). Plastic design of steel HP-piles for integral abutment bridges. *The 2005FHWA Conference, Integral Abutment and Jointless Bridges (IAJB 2005)* (pp. 270-280). Baltimore, MD.

Husain, I., & Bagnariol, D. (2000). Design and performance of jointless bridges in Ontario: new technical and material concepts. *Transportation Research Record: Journal of the Transportation Research Board*, 1696, 109-121.

Hutchinson, T. C., Chai, Y. H., Boulanger, R. W., & Idriss, I. M. (2004). Inelastic seismic response of extended pile-shaft-supported bridge structures. *Earthquake Spectra*, *20*(4), 1057-1080.

IDOT. (2006). Bridge design manual. Iowa Department of Transportation, Ames, IA.

Imbsen, R.A., Vandershaf, D.E., Schamber, R.A., & Nutt, R.V. (1985). Thermal effects in concrete bridge superstructures, *National Cooperative Highway Research Program,* NCHRP Report 276, Transportation Research Board, Washington, DC.

Ingram, E.E., Burdette, E.G., Goodpasture, D.W., & Deatherage, J.H. (2003). Evaluation of applicability of typical column design equations to steel h-piles supporting integral abutments. *AISC Engineering Journal, 40*(1), 50–58.

IRC: 6. (2010). *Standard Specifications and code of practice for road bridge.* Section:II Load and Stresses (4th Rev.). New Delhi, IN.: The Indian Roads Congress.

IRC: 112 (2011). *Code of Practice for Concrete Road Bridges*. New Delhi, IN.: The Indian Roads Congress.

Itani, A. M., & Pekcan, G. (2011). Seismic performance of steel plate girder bridges with integral abutments. *U.S. Department of Transportation, Federal Highway Administration.* Report No. FHWA-HIF-11-043.

Jamieson, G. (2009). Towards practical modeling of integral-abutment bridges under longitudinal load. In *7th Austroads Bridge Conference,* Auckland, New Zealand.

JSCE. (1985). Dynamic Analysis and Earthquake Resistant Design. Japanese Society of Civil Engineers; Vol. 2, Methods of Dynamic Analysis, Oxford and IBH Publishing Co. Pvt. Ltd.

JRA. (2012). *Specifications for Highway Bridges. Part V: Seismic Design*. Japan Road Association: Tokyo, Japan.

Jayaraman, R., Merz, P. B., & McLellan. (2001). Integral bridge concept applied to rehabilitate an existing bridge and construct a dual-use bridge. In *26 th Conference on our World in Concrete and Structures* (pp. 26-28).

Jorgenson, J.L. (1983). Behaviour of abutment piles in an integral abutment in response to bridge movements. *Transportation Research Record*, 903.

Kagawa, T., & Kraft, L.M, (1980a). Seismic p-y response of flexible piles. *Journal of the Geotechnical Engineering*, *106*, 899–918.

Kagawa, T., & Kraft, L.M. (1980b). Lateral load-deflection relationship of piles subjected to dynamic loadings. *Soils and Foundations*, *20*, 19–36.

Kamel, M. R., Benak, J. V., Tadros, M. K., & Jamshidi, M. (1996). Prestressed concrete piles in jointless bridges. *PCI Journal,* 41, 56–67.

Kausel, E., & Tassoulas, J. L. (1981). Transmitting boundaries: a closed-form comparison. *Bulletin of the seismological society of America*, *71*(1), 143-159.

Kerokoski, O., & Laaksonen, A. (2005). Soil-structure interaction of jointless bridges. *The 2005FHWA Conference, Integral Abutment and Jointless Bridges (IAJB 2005*) (pp. 323-336). Baltimore, MD.

Khalili-Tehrani, P., Shamsabadi, A., Stewart, J. P., & Taciroglu, E. (2016). Backbone curves with physical parameters for passive lateral response of homogeneous abutment backfills. *Bulletin of Earthquake Engineering*, *14*, 3003-3023.

Khodabakhshi, P., Jahankhah, H., & Ghannad, M. A. (2011). A discrete model for response estimation of soil-structure systems with embedded foundations. *Earthquake Engineering and Engineering Vibration*, *10*(2), 263-276.

Knickerbocker, D., Basu, P.K., & Wasserman, E.P. (2005). Behavior of two-span integral bridges unsymmetrical about the pier line. *The 2005FHWA Conference, Integral Abutment and Jointless Bridges (IAJB 2005)* (pp. 244–256). Baltimore, MD.

Kong, B., Cai, C. S., & Zhang, Y. (2016). Parametric study of an integral abutment bridge supported by prestressed precast concrete piles. *Engineering Structures*, *120*, 37-48.

Kolay, C. (2009). *Seismic analysis of bridge abutment soil system.* Master's thesis. Department of Civil Engineering, IIT Kanpur, India.

Kontoe, S. (2006). *Development of time integration schemes and advanced boundary conditions for dynamic geotechnical analysis* (PhD dissertation). Imperial College London. England.

Kontoe, S., Zdravković, L., Potts, D.M., Salandy, N.E. (2007). The Domain Reduction Method as an advanced boundary condition. In: *4th International Conference on Earthquake Geotechnical Engineering*. Paper No. 1231. Greece.

Kramer, S. L. (1996). Geotechnical Earthquake Engineering Prentice Hall. New York.

Kumar, P.V. (2008.) *Behaviour of integral abutment bridges under temperature effect and seismic excavation* (PhD dissertation). Department of Civil Engineering, Indian Institute of Technology, Roorkee, India.

Lam, I. P., & Martin, G. R. (1986). Seismic design of highway bridge foundations. volume 2 and 3.

Laman, J.A., & Kim, W. (2010). Integral abutment bridge response under thermal loading. *Engineering Structures, 32*, 1495–1508.

Lampe, N., & Azizinamini, A. (2000). Steel bridge system, simple for dead load and continuous for live load. *Conference of High Performance Steel Bridge*, Baltimore,MD.

Lan, C. (2012). *On the performance of super-long integral abutment bridges-parametric analysis and design optimization* (PhD dissertation). Engineering of Civil and Mechanical structural Systems, University of Trento, Italy.

Lawver, A., French, F., & Shield, C.K. (2000). Field performance of an integral abutment bridge. Transportation Research Record 1740.

Li, Z. N., Li, Q. S., & Lou, M. L. (2005). Numerical studies on the effects of the lateral boundary on soil-structure interaction in homogeneous soil foundations. *Structural Engineering and Mechanics*, *20*(4), 421-434.

Liu, D., Magliola, R.A., & Dunker, K.F. (2005). Integral abutment bridges: IOWA and Colorado experience. *The 2005FHWA Conference, Integral Abutment and Jointless Bridges (IAJB 2005)* (pp. 136–147). Baltimore, MD.

Lu, J., Elgamal, A., & Yang, Z. (2011). *OpenSeesPL: 3D Lateral Pile-Ground Interaction User Manual* (Beta 1.0). Department of Structural Engineering, University of California, San Diego, CA.

LUSAS– Finite Element Analysis, (2014). LUSAS User Manual, Version 15.2.

Lysmer, J. & Kuhlemeyer, R.L. (1969). Finite dynamic model for infinite media. *J. Eng. Mech. Div. ASCE*, *95(EM4),* 859-877.

Maberry, J., & Camp, J.B. (2005). New York State Department of Transportation's experience with integral abutment bridges. *The 2005FHWA Conference, Integral Abutment and Jointless Bridges (IAJB 2005)* (pp. 125–135). Baltimore, MD.

Makris, N. & Gazetas, G. (1992), Dynamic pile-soil-pile interaction. Part II: Lateral and seismic response. *Earthquake Engng. Struct. Dyn., 21*, 145–162.

Maruri, R.F., & Petro, H. (2005). Integral abutments and jointless bridges (IAJB) 2004 survey summary. *The 2005-FHWA Conference, Integral Abutment and Jointless Bridges (IAJB 2005)* (pp. 12-29). Baltimore, MD.

Matlock, H. (1970). *Correlations for designs for laterally loaded piles in soft clay*. Second Annual Offshore Technology Conference, Houston, TX.

Matthewson, M.B., Wood, J.H., & Berrill, J.B. (1980). Seismic design of bridges: section 9: Earth retaining structures. *Bulletin of the New Zealand National Society for Earthquake Engineering, 13*, 280-293.

Mazzoni, S., McKenna, F., Scott, H.M. & Fenves, G.L. (2007). *The OpenSees Command Language Manual,* v6.0. Pacific Earthquake Engineering Research Center, University of California, Berkeley. *http://opensees.berkeley.edu*

McBride, K. C. (2005). *Thermal Stresses in the Superstructure of Integral Abutment Bridges.* West Virginia University Libraries, VA.

McClelland, B., & Focht, J.A. (1958). Soil modulus of laterally loaded piles. *Transactions of the American Society of Civil Engineers*, *123*(1), 1049-1063.

McKenna, F. & Fenves, G.L. (2008). Using the OpenSees interpreter in Parallel Computers. University of California, Berkeley. NEESit; TN-2007-16, v1.0

MIDAS Civil. (2017). Design of Civil Structures: Integrated Solution System for Bridge and Civil Engineering. v2.1.

Mistry, V. (2005). Integral abutment and jointless bridges. In *The 2005-FHWA Conference, Integral Abutment and Jointless Bridges (IAJB 2005)* (pp. 3-11). Baltimore, MD.

Mitoulis, S. A. (2016). Some open issues in the seismic design of bridges to Eurocode 8-2. *Challenge Journal of Structural Mechanics*, *2*(1), 7-13.

Mitoulis, S., Argyroudis, S., & Kowalsky, M. (2015). Evaluation of the stiffness and damping of abutments to extend direct displacement based design to the design of integral bridges. In *Proceedings of the Computational Methods in Structural Dynamics and Earthquake Engineering,* Crete,Greece.

Mitoulis, S. A., Palaiochorinou, A., Georgiadis, I., & Argyroudis, S. (2016). Extending the application of integral frame abutment bridges in earthquake-prone areas by using novel isolators of recycled materials. *Earthquake Engineering & Structural Dynamics*, *45*, 2283-2301.

Mokwa, R. L. (1999). *Investigation of the resistance of pile caps to lateral spreading* (PhD dissertation). Dept. of Civil Engineering, Virginia. Polytechnic Institute and State Univ., Blacksburg, Va.

Mokwa, R.L. & Duncan, J.M. (2000). Investigation of the Resistance of Pile Caps and Integral Abutments to Lateral Loading. Final Contract Report. *Virginia Transportation Research Council,* Virginia Tech, Blacksburg, VA.

Monkul, M.M. (2008). Validation of Practice Oriented Models and Influence of Soil Stiffness on Lateral Pile Response Due to Kinematic Loading. *Marine Geores. & Geotech, 26(3)*, 145-159.

Mourad, S., & Tabsh, S.W. (1998). Pile forces in integral abutment bridges subjected to truck loads. *Transportation Research Record*, 1633, 77-83.

Murchison, J.M. (1983). An evaluation of p-y relationships in sands. *American Petroleum Institute* (API), Research Report 41, USA.

Nielsen, R.J. & Schmeckpeper, E.R. (2001). Consistent Design of Integral Abutment, Bridges. *Department of Civil Engineering*, University of Idaho, Moscow, Idaho.

Novak, M., & Sheta, M. (1980). Approximate approach to contact effects of piles. In: *Proceedings on Session of Dynamic Response of Pile Foundations: Analysis Aspects* (pp. 53–79), ASCE.

NZTA. (2014). *Bridge manual*, (SP/M/022). New Zealand Transportation Authority, 3rd edition, amendment 1. Wellington: NZ Transport Agency.

Olson, S. M., Holloway, K. P., Buenker, J. M., Long, J. H., & LaFave, J. M. (2013). Thermal behavior of IDOT integral abutment bridges and proposed design modifications. *University of Illinois Urbana Champaign, Illinois Department of Transportation,* FHWA-ICT -12- 022.

Paraschos, A. (2016). *Effects of Wingwall Configurations on the Behaviour of Integral Abutment Bridges* (PhD dissertation). Department of Civil & Environmental Engineering, University of Maryland, MD.

Perkun, J., & Michael, K. (2005). Design and construction of dual 630-foot, jointless, three-span continuous multi-girder bridges in St. Albans, West Virginia, United States, carrying U.S. route 60 over the coal river. In *The 2005FHWA Conference, Integral Abutment and Jointless Bridges (IAJB 2005)* (pp. 97-112). Baltimore, MD.

Petursson, K., & Kerokoski, P. (2011). Monitoring and analysis of abutment-soil interaction of two integral bridges. *Journal of Bridge Engineering, 18(1),* 54–64.

Phares, B. M., Faris, A. S., Greimann, L., & Bierwagen, D. (2013). Integral bridge abutment to approach slab connection. *Journal of Bridge Engineering*, *18*, 179-181.

Prakash S, Sharma HD. Pile foundations in engineering practice. John Wiley & Sons, 1990.

Prevost, J.H. (1985). A Simple Plasticity Theory for Frictional Cohesionless Soils. *Soil Dyn. & Eq. Eng. 4(1)*, 9-17.

Puzey D.C. (2012). *Integral Abutment Bridge Policies and Details*. Memorandum, Illinois Department of Transportation, IL.

Quinn, B. H. (2016). *Detailed Study of Integral Abutment Bridges and Performance of Bridge Joints in Traditional Bridges* (PhD Dissertation). University of Massachusetts, Amherst, MA.

Quinn, B. H., & Civjan, S. A. (2016). Parametric Study on Effects of Pile Orientation in Integral Abutment Bridges. *Journal of Bridge Engineering*, 04016132.

Reese, L.C., Cox, W.R., & Koop, F.D. (1975). Field testing and analysis of laterally loaded piles in stiff clay. In *The 7th Offshore Technology Conference*, Houston, TX.

Rocha, L. P., & López, J. A. Procedure to account for non-linear effects in empirical transfer functions. In *Proceedings of the 14th Conference on Earthquake Engineering*, Beijing, China.

Roller, J.J., Russell, H.G., Bruce, R.N., & Martin, B.T. (1995). Long-term performance of prestressed, pretensioned high strength concrete bridge girders. *PCI Journal*, *40*, 48–59.

RP2A-WSD, A. P. I. (2000). *Recommended practice for planning, designing and constructing fixed offshore platforms–working stress design.* Washington, DC: American Petroleum Institute.

SCDOT. (2010). *Geotechnical Design Manual.* South Carolina Department of Transportation, Columbia, SC.

Scott, B.D., Park, R., & Priestley, M.J.N. (1982). Stress-strain behavior of concrete confined by overlapping hoops at low and high strain rates. *J. American Concrete Institute*, 79:13-27.

Shah, B. R., Perić, D., & Esmaeily, A. (2008). Effects of ambient temperature changes on integral bridges. *Kansas Department of Transportation*, Report No. K-TRAN: KSU-06-2, KS.

Shamsabadi, A. (2006). CT-FLEX Computer Manual. *Office of Earthquake Engineering*, California Department of Transportation, CA.

Shamsabadi, A., Rollins, K.M., & Kapuskar, M. (2007). Nonlinear soil abutment bridge structure interaction for seismic performance-based design. *Journal of Geotechnical and Geoenvironmental Engineering, 133,* 707–720.

Shamsabadi, A., Khalili-Tehrani, P., Stewart, J. P., & Taciroglu, E. (2010). Validated Simulation Models for Lateral Response of Bridge Abutments with Typical Backfills. *Journal of Bridge Engineering*, 15, 302-311.

Shia, H.C. (2005). *A study of the effects of slender ratio on the behaviour of piles in sands under cyclic lateral loading by laboratory model test.* MTech. Thesis. Feng Chia University, Taiwan, China.

Shiojiri, H., Irobe, M., Taguti, T., Goto, K., & Abudula, A. (2004). A method for nonlinear dynamic response analysis of structure considering soil structure interaction. In *Proceedings of the 13th World Conference on Earthquake Engineering*, Paper no. 1267, Vancouver, Canada.

Smerzini, C., Galasso, C., Iervolino, I. & Paolucci, R. (2014). Ground motion record selection based on broadband spectral compatibility. *Eq. Spectra, 30(4),* 1427-1448.

Smerzini, C., Paolucci, R., Galasso, C. & Iervolino, I. (2012). Engineering ground motion selection based on displacement-spectrum compatibility. In: *Proceedings of the 15th World Conference on Earthquake Engineering*, Paper no. 2354, Lisbon, Portugal.

Springman, S.M., Norrish, A.R.M., & Ng, C.W.W. (1996). Cyclic loading of sand behind integral bridge abutments. *Transport Research Laboratory*, TRL Report 146, UK

Sullivan, W.R., Reese, L.C., & Fenske, C.W. (1979). Unified method for analysis of laterally loaded piles in clay. *Numerical Methods in Offshore Piling* (pp. 135–146), London, UK.

Tatsuoka, F., Tateyama, M., Koseki, J., & Yonezawa, T. (2014). Geosynthetic-Reinforced Soil Structures for Railways in Japan. *Transportation Infrastructure Geotechnology*, *1*(1), 3-53.

Ting, J. M., & Faraji, S. (1998). Streamlined analysis and design of integral abutment bridges. *University of Massachusetts, Transportation Center*, Report UMTC, 97-13. Amherst, MA.

Torricelli, L. F., Marchiondelli, A., Pefano, R., & Stucchi, R. (2012). Integral bridge design solutions for Italian highway overpasses. In *Proceedings of the Sixth International IABMAS Conference*, Stresa, Italy.

Volz, R.G.O.J.S. (2005). Effective temperature and longitudinal movement in integral abutment bridges. *The 2005FHWA Conference, Integral Abutment and Jointless Bridges (IAJB 2005)* (pp. 302–311). Baltimore, MD.

Wang, E. (2015). Seismic Retrofit of Pile Group Foundation with Thickened Caps. *Open Construction and Building Technology Journal*, *9*, 248-254.

Wang, S., Kutter, B.L., Chacko, J.M., Wilson, D.W., Boulanger, R.W., & Abghari, A. (1998). Nonlinear seismic soil-pile-structure interaction. *Earthquake Spectra, 14*, 377–396.

Wang, S.T., & Reese, L.C. (1993). COM624P-Laterally Loaded Pile Analysis Program for the Microcomputer; Version 2.0. *U.S. Department of Transportation, Federal Highway Administration*, Washington, DC.

Wasserman, E. P. (2001). Design of integral abutments for jointless bridges. *Structure* (London), 85, 24–33.

Wasserman, E., & Walker, J. (1996). Integral abutments for steel bridges. *Tennessee Department of Transportation*, TN.

Weakley, K. (2005). VDOT integral bridge design guidelines. *The 2005FHWA Conference, Integral Abutment and Jointless Bridges (IAJB 2005)* (pp. 61-70). Baltimore, MD.

Wendner, R., & Strauss, A. (2013). Inclined Approach Slab Solution for Jointless Bridges: Performance Assessment of the Soil–Structure Interaction. *Journal of Performance of Constructed Facilities*, *29*, 04014045.

Wetmore, J., & Peterson, B. (2005). Case study jointless bridge Beltrami county state aid highway 33 over Mississippi river in ten lake township, Minnesota. *The 2005FHWA Conference, Integral Abutment and Jointless Bridges (IAJB 2005)* (pp. 84–96). Baltimore, MD.

White, H. (2007). Integral abutment bridges: Comparison of current practice between European countries and the United States of America. *Transportation Research and Development Bureau,* Special report 152, New York State Department of Transportation, NY.

White, H. (2008). Wingwall type selection for integral abutment bridges: Survey of current practice in the United States of America. *Transportation Research and Development Bureau*, Special report 154, New York State Department of Transportation.

White, H., Ptursson. H., & Collin. P. (2010). Integral abutment bridges: The european way. *Practice Periodical on Structural Design and Construction, 15*, 201–208.

Wood, J. H. (2015). Earthquake Design of Bridges with Integral Abutments. In *6th International Conference on Earthquake Geotechnical Engineering,* Christchurch, New Zealand.

Wood, J., Murashev, A., Palermo, A., Al-Ani, M., Andisheh, K. & Goodall, D. (2015). Criteria and guidance for the design of integral bridges in New Zealand November 2015. *NZ Transport Agency,* research report 577.

Wright, B., LaFave, J., Fahnestock, L., Jarrett, M., Riddle, J., & Jeffrey, S. (2015). Field Monitoring of Skewed Integral Abutment Bridges. *6th International Conference on Advances in Experimental Structural Engineering,* University of Illinois, Urbana-Champaign, USA.

Xue, J. (2013). *Retrofit of Existing Bridges with Concept of Integral Abutment Bridge: Static and Dynamic Parametric Analysis* (PhD dissertation). University of Trento, Italy.

Yannotti, A.P., Alampalli, S., & White, H.L. (2005). New York State Department of Transportation experience with integral abutment bridges. *The 2005-FHWA Conference, Integral Abutment and Jointless Bridges (IAJB 2005)* (pp. 41-49). Baltimore, MD.

Zhang, Y., Conte, J.P., Yang, Z., Elgamal, A., Bielak, J., & Acero, G. (2008). Two dimensional nonlinear earthquake response analysis of a bridge-foundation ground system. *Earthquake Spectra, 24,* 343–386.

Zhao, Q., Vasheghani-Farahani, R., & Burdette, E. G. (2011). Seismic Analysis of Integral Abutment Bridges Including Soil-Structure Interaction. In *Structures Congress 2011* (pp. 289-303).

Zornberg, J.G. (2007). New Concepts in Geosynthetic-Reinforced Soil. Keynote lecture, In *Proceedings of the Fifth Brazilian Symposium on Geosynthetics, Geossinteticos 2007, and of the Sixth Brazilian Congress on Environmental Geotechnics, REGEO 2007,* pp. 1-26, Recife, Brazil.

★★★

Appendix A

"Weak axis" bending and "strong axis" bending of an IAB has been illustrated in Fig. A1.

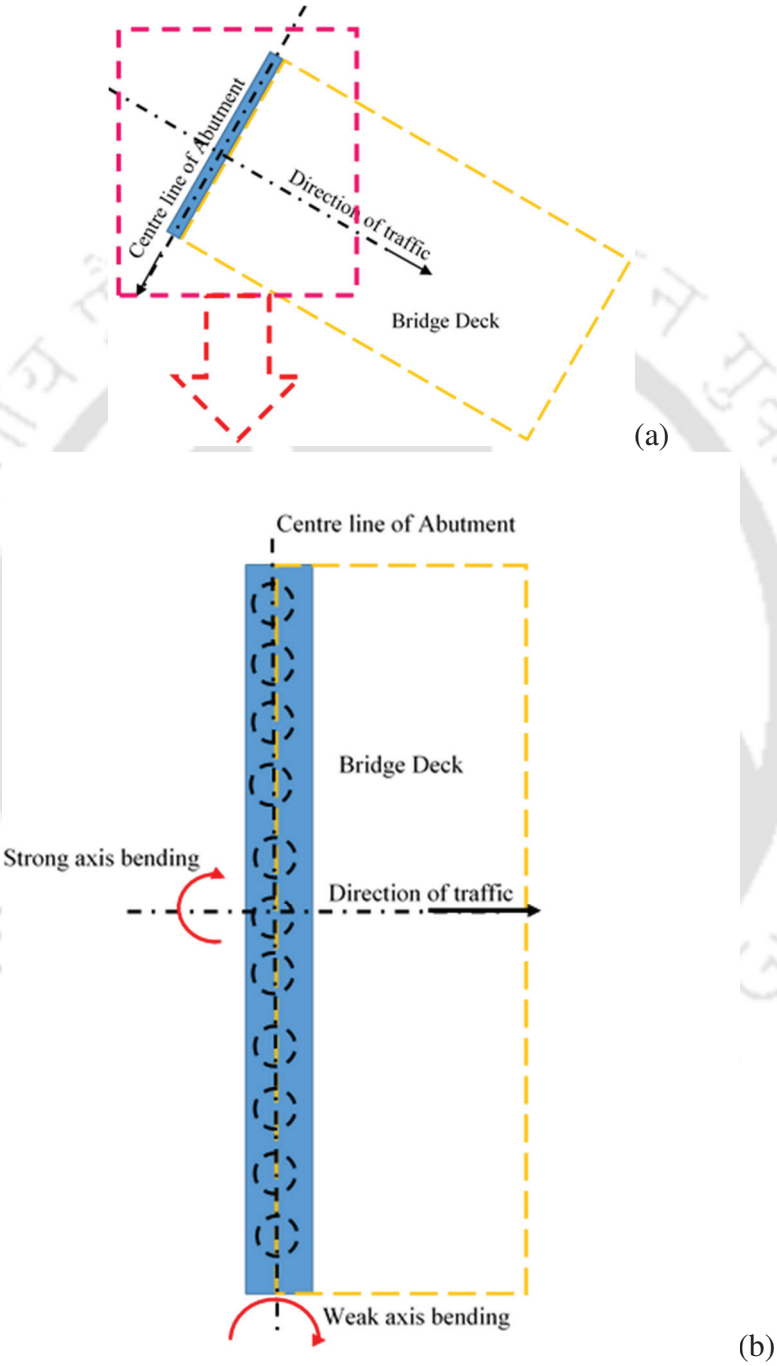

Fig. A1 (a) Orientation of bridge deck and abutment in plan and (b) weak and strong axis bending of an integral abutment.

Appendix B

Bridge Load Calculation

Bending Moment due to Dead Load (DL):

Density of Concrete = 25 kN/m^3

Average Length of Span = 36.43 m

Depth of the Slab = 165 mm

Weight per m^2 of slab = 0.165 × 25 = 4.125 kN/m^2

Weight of wearing Course per m of slab = 2 kN

Total DL = 6.125 kN/m^2

Total DL/span = 6.125 × 10 × 36.43 = 2231.4 kN

Shear Force at each support = 2231.4/2 = 1115.67 kN

Bending moment at the 1st interior support = 6.125 × 10 × 36.43^2/10 = 8128.76 kNm

Bending moment at other interior support moment = 6.125 × 10 × 36.43^2/12 = 6774 kNm

Deck Slab Design

Assuming, clear cover as 50 mm and diameter of the longitudinal bar as 10 mm.

Effective depth of slab = 165-(50+10) mm = 105 mm

Bending moment due to Live Load (LL): Class A wheeled vehicle with two-lane loading

2 axle loads of 114 kN each are to be placed on span to carry maximum BM. At support the

Maximum LL = 114 kN (according to IRC: 6, 2010)

Width of dispersion parallel to span = 250 + 2 × (105+56) mm = 572 mm [Depth of wearing course = 56 mm], which is less than the spacing of 1200 mm between the 114 kN axle loads. So, the dispersion areas will not overlap.

Impact factor = 4.5/ (6+34.43) = 0.094

Effective width of slab perpendicular to span, $b_{ef} = \alpha.\ a.\ (1-a/\ l_0) + b_1$ = 10.18 m ≈10 m,

[From, Eq. B3.1, (IRC: 112, 2011)]

where, α = 1.052; a = 17.615 m; b_1 = 0.612.

Intensity of loading/m width = 2 × 114 × 1.094 ≈ 25 kN/m

SF at support due to LL = 25 × 10 × 0.572 × 2/2= 143 kN

Max BM at midspan (X-Z Plane) = 25 × 10 × (1.2+0.572)/2 – 143 = 78.5 kNm

1.5 load factor [IRC: 6 (2010), Table 3.4] and 20% of LL [IRC: 6 (2010), Cl. 219.5.2] will be considered = 143 × 0.2 × 1.5= 42.9 kN

Total SF due to DL +LL = 1115.67+ 42.9 = 1158.5 kN

Vertical Load Calculation:

SF due to DL+LL = 1158.5 kN

DL from girders = 4 × 0.73 × 25 × 36.43 +10 × 1 × 0.73 × 25= 2841.89 kN

Design vertical load on each pier = 1158.5 + 2841.89 = 4001 kN

Assuming, factor of safety = 1.25

Designed axial load on pier = 5000 kN

Appendix C

Pier Detailing according to IRC: 112-2011

Axial force on pier = 5000 kN

According to cl 16.2.2. (3), $A_{s,\,min} = 0.10 \times N_{ed}/f_{yd} = 1204.82$ mm^2

$= 0.002\, A_c = 5507$ mm^2

So, $A_{s,\,min} = 5507$ mm^2

According to cl. 16.2.2. (4), $A_{max} = 4\%$ of A_c (without lap portion)

Assuming, $A_s = 0.5\%\, A_c = 13766$ mm^2

Providing, 24 Nos. 28 mm dia bar, longitudinal. $A_{s,\,pro} = 14770$ mm^2

Transverse reinforcement (according to Cl. 16.2.3)

Cl. 16.2.3 (2), dia of horizontal ties = min of (8mm or 28/4 = 7 mm)

So, dia of transverse r/f = 8 mm

Cl. 16.2.3 (4), Spacing min of (i) 12 × 28 = 336 mm

(ii) Least dimension of column= 1700 mm

(iii) 200 mm

So, spacing = 200 mm

According to 17.2.1.1(3), confined r/f:

$\eta_k = 0.049 < 0.08$; ***So, no need to provide confinement acc. to Cl 17.2.1.4***

According to cl. 17.2.1.1(4), $\omega_{\omega d} = 0.024$ mm^2, where, $\rho_\omega = 1.16\times10^{-3}$, A_{sw} = 7 × area of 8mm dia. ties in a breadth of 1516mm.

So, minimum confined r/f should be provided according to Cl. 17.2.1.2

According to cl. 17.2.1.2 (2), $\rho_L = A_{st,\,pro}/A_c = 0.00536$, $\eta_k = 0.049$, $\omega_{\omega,\,req} = 0.022$

$\omega_{\omega d} = \max(0.022; 0.12) = 0.12$

Spacing of the Ties:

According to cl. 17.2.1.3 (1), S_L = min ($5D_b$; 1/5th of the smallest dimension of concrete core concrete) = min (140; 303.2) = *140mm*

According to Cl. 17.2.1.3 (2), S_T = min (1/3rd of the smallest dimension of concrete core concrete; 200mm) = min (505.34 mm; 200 mm) = *200 mm*

According to design potential hinges are not forming through the column. If it's forming then the buckling of longitudinal reinforcement will be taken care by Cl. 17.2.2.

Vertical and horizontal detailing of pier column (2000 mm × 1700 mm) are shown in Figs. C.1 and C.2.

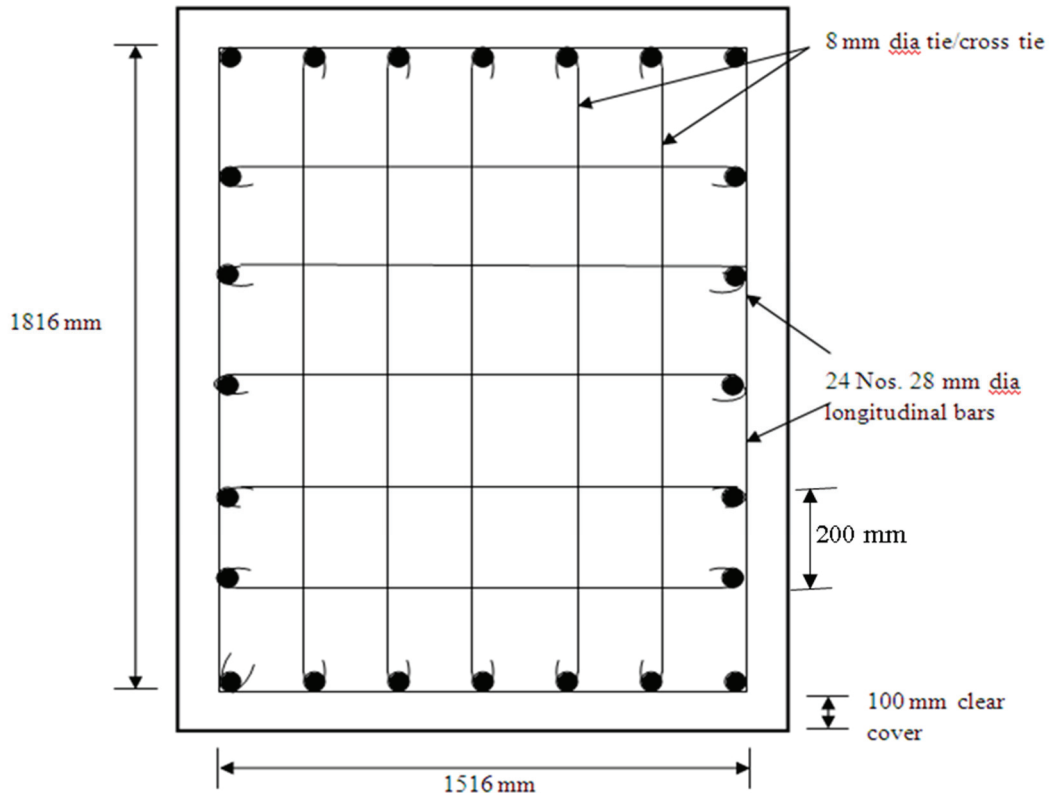

Fig. C.1 Cross section of reinforcement detailing in pier

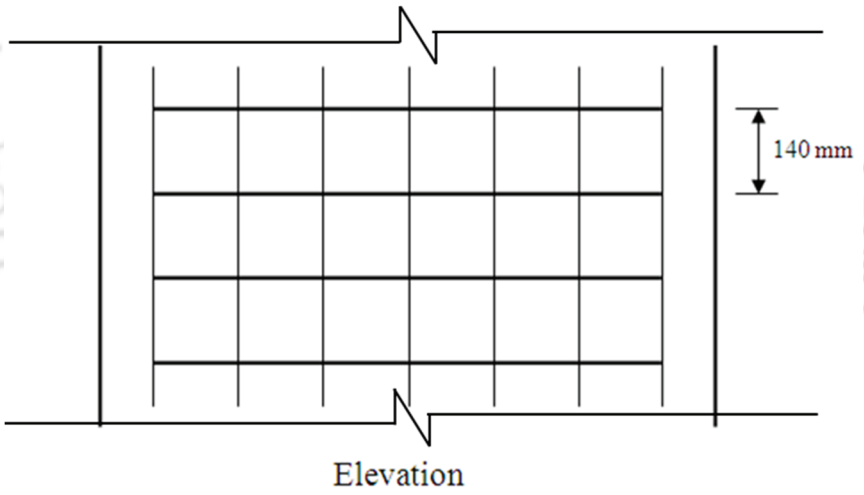

Fig. C.2 Elevation of reinforcement detailing in pier

Appendix D

Equivalent stiffness of pile group in *OpenSees*

From Ariyarathne *et al*. (2013), equivalent stiffness of pile group has been derived to model the piles in *OpenSees*.

Equivalent stiffness of two pile in a row (Fig. D.1), $E_{eq} \times A_w = (E_p \times A_p) + E_s\,(A_w - A_p)$; where,

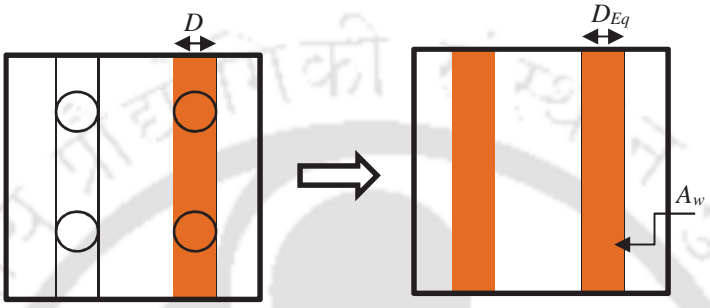

Fig. D.1 Equivalent pile stiffness calculation

$A_w = 5 \times 1.372 = 6.86$ m

$E_p = 28E6$ kN/m^2

$A_p = \frac{\pi}{4} \times (1.372)^2$ m^2= 2.955 m^2

$E_s = 200440$ kN/m^2

$E_{eq} \,.\, A_w = E_p \times 2A_p + E_s\,(A_w - 2A_p)$

$E_{eq} = 12.188E6$ kN/m^2

Equivalent stiffness of one pile in a row:

$E_{eq} \,.\, A_w = E_p \,.\, A_p + E_s \,.\, (A_w - A_p)$

$E_{eq} = 6.20\times10^6$ kN/m^2

To consider the soil between the piles, the overall pile's efficiency decreases by considering *p*–multiplier.

For piles on soft clay, *p*–multipliers are as following according to Mokwa (1999):

Leading Row	0.80
1st trailing row	0.50
2nd trailing row	0.45

During the cyclic loading, leading and 2nd trailing row pile efficiency get interchanged.

So, final stiffness of both the side rows $E_1 = E_3 = 9.75\times10^6$ kN/m^2

Middle row equivalent stiffness $E_2 = 3.1\times10^6$ kN/m^2

$\frac{1}{Eeq} = \frac{1}{E1} + \frac{1}{E2} + \frac{1}{E3}$; $E_{eq} = 1.65\times10^6$ kN/m^2

As these three stiffnesses are in series in 2D plane, so equivalent pile group stiffness = 1.65×10^6 kN/m^2

Appendix E

Pile length calculation in soft clay

Assume, length of pile l

Pier pile diameter, D = 1.372 m

Cross sectioned area of pile, A_p = 1.49 m^2

Perimeter of pile, p = 4.31 m

Cohesion, c = 18 kN/m^2

N_c = 9.0

The axial load carrying capacity of the pier piles is 500 kN.

Assuming, factor of safety (FOS) = 2.0, Ultimate load capacity $(Q_v)_{ult} = Q_p + Q_f$ (E.1)

End bearing capacity, $Q_p = A_p\, c\, N_c$ = 239.7 kN

Shaft friction, $f_s = c + \sigma'_h\, tan\, \delta$ = 18 kN/m^2 [for, cohesive soil, $\delta = 0$]

Friction capacity, $Q_f = p\, f_s \sum_{l=0}^{l=l} l$ = 77.54l kN

So, equation D.1 becomes,

⇨ 500×2 = 239.7 + 77.54l

⇨ l = 10 m

So, length of the pier pile in soft clay is calculated as 10 m.

Appendix F

Calculations of API Curves in Medium Stiff Clay for Pier Pile

In medium stiff clay, soil cohesion c = 27 kN/m^2

Unit density, γ = 0.019 kN/m^3

Pile diameter, D = 1372 mm

Perimeter of pile, p = 4.31E6 mm^2

Strain at which half of maximum stress occurring, ε_c = 0.002

Actual lateral deflection = y

$y_c = 2.5\ \varepsilon_c\ D =$ 6.86 mm

Where, ε_c = strain which occurs at one-half the maximum stress on laboratory undrained compression tests of undisturbed soil samples.

$$X_R = \frac{6D}{(\gamma D/c)+J} \quad \text{(F.1)}$$

[Dimensionless empirical constant, J= 0.5]

$\therefore X_R$ is obtained as 5621 mm.

$$\text{Ultimate resistance, } p_u \text{ (in kPa)} = 3c + \gamma X + \frac{JcX}{D} \quad \text{(F.2)}$$

Where, X= depth below soil surface

Applied force on a certain depth of pile, $F = (P_u \times p)$ kN

Using all the parameters, lateral force-displacement curve for pier piles at the depths of 1 m and 4 m are shown in Table F.1.

Table F.1 Lateral force displacement curves for pier pile in medium stiff clay

1 m depth		4 m depth	
Force (F), kN	Displacement (y), m	Force (F), kN	Displacement (y), m
0	0	0	0
236.82	0.007	423.25	0.007
341.02	0.021	609.48	0.021
60.66	0.103	433.69	0.103
60.66408	∞	433.6897	∞

Appendix G

Calculations of API curves in loose sand for pier pile

Pile diameter, D = 1372 mm,

Perimeter of pile, $p = 4.31 \times 10^6$ mm^2,

Coefficients are determined from Figure 6.8.6-1 of API (2000) as function of φ´,

$C_1 = 1.6$; $C_2 = 2.6$; $C_3 = 23$;

Effective unit weight of soil, γ = 16 kN/m^3,

Angle of internal friction of sand, $\phi = 29°$,

Initial modulus of subgrade reaction, k = 2170 kN/m^3,

A factor to account for cyclic or static loading condition, A = 0.9 (for cyclic loading),

y = lateral deflection in m.

H = depth in m.

Ultimate lateral resistance at depth H, p_u (in kN/m) = smallest of (p_{us}, p_{ud});

Where, $p_{us} = (C_1 \times H + C_2 \times D) \times \gamma \times H$ (G.1)

and $p_{ud} = C_3 \times D \times H$ (G.2)

At the depth of 6 m from soil surface, the lateral force-displacement curves in loose sand are derived below from API (2000) (section 6.8.6) for pier piles.

At 6 m depth, p_{us} = 1264.051 kN and p_{ud} = 3029.376 kN

Then, the lateral soil resistance-deflection (p-y) relationship for sand at any specific depth H, is approximated by the following expression:

$$P = A \times p_u \times \tanh \frac{k \times H}{A \times pu} \times y \quad \text{(G.3)}$$

The values of p-y curves at the depth 6 m in loose sand are shown in Table. G.1